SPECTROSCOPIC STUDIES OF ANTIMONY III AND V HALIDE COMPLEXES

TO MY MOTHER AND FATHER

SPECTROSCOPIC STUDIES OF ANTIMONY III AND V HALIDE COMPLEXES

By

JACK GEORGE BALLARD, (B.Sc.)

A Thesis

Submitted to the Faculty of Graduate Studies

in Partial Fulfilment of the

Requirements for the Degree

Doctor of Philosophy

McMaster University

July 1977

DOCTOR OF PHILOSOPHY (1977)
(Chemistry)

McMASTER UNIVERSITY
Hamilton, Ontario

TITLE: Spectroscopic Studies of Antimony III and V Halide Complexes

AUTHOR: Jack George Ballard, B.Sc. (Brandon University)

SUPERVISOR: Professor T. Birchall

NUMBER OF PAGES: xvi, 195

ABSTRACT

Antimony-121 Mössbauer spectra have been recorded at liquid-helium temperatures for a number of complex anions derived from SbF_3: $M_2[SbF_5]$ (M_2 = Na_2, K_2, or N_2H_6); $NaSbF_4$; $M[SbClF_3]$ (M = K or NH_4); $Na[SbClF_3]\cdot H_2O$; $M[Sb_3F_{10}]$ (M = Na, Tl, or NH_4); $M[Sb_4F_{13}]$ (M = K or Cs); and $[NH_4]_4[Sb_5F_{19}]$. The data were consistent with the known stereochemistry of these compounds in which the antimony 5s electron pair is stereochemically active in a distorted AX_6E environment with a 3:3:1 arrangement or monocapped octahedron, the lone pair in the 1 position.

The ^{121}Sb Mössbauer spectra of a number of $[SbX_4^-]$ (X = Cl, Br, or I) and $[Sb_2X_9^{3-}]$ (X = F, Cl, Br, or I) salts have been reported. Only $[Sb_2F_9^{3-}]$ shows a significantly large quadrupole splitting with the 5s electrons being stereochemically active.

The nature of the compounds of the series $SbCl_{5-x}F_x$ have been in dispute in the literature for several years, but only $SbCl_4F$, which has been identified as a cis-fluorine bridged tetramer, and "$SbCl_2F_3$", which has been shown to exist with the ionic formulation $[SbCl_4^+][Sb_2Cl_2F_9^-]$, are well characterized. It was found in this work that a fluorine bridged $[SbCl_4^+][Sb_2Cl_2F_9^-]$ species in the solid state is more consistent with the chemistry of this compound. The previously unknown $Sb_3Cl_{10.75}F_{4.25}$ was prepared and found from X-ray crystallography to exist as a disordered cis-fluorine bridged trimer in the solid state. $SbCl_3F_2$ was prepared and characterized as a cis-fluorine bridged tetramer in the solid state. An attempt to prepare $SbClF_4$ always resulted in the formation of $[SbCl_4^+][Sb_2F_{11}^-]$, which previously had been little studied. These

$SbCl_{5-x}F_x$ compounds have been characterized using Mössbauer and Raman spectroscopy, and Mass spectrometry. The reaction of $SbCl_4F$ with strong Lewis acids was also investigated. $SbCl_4F$ was found to form $[AsCl_4^+][SbF_6^-]$ with AsF_5, $[SbCl_4^+][Sb_2Cl_2F_9^-]$ with SbF_5, and a polymeric complex of the type $[SbCl_4F\cdot(NbF_5)_x]$ (x = 1, or 2) with NbF_5.

The reaction of alkali metal halides with antimony(V) halides in liquid SO_2 at room temperature yielded the salts: $M[SbCl_6]$ (M = Na or K); $Na[SbCl_4F_2]$; $Na[SbCl_2F_4]$; and $M[SbF_6]$ (M = K or Cs). The variation of ^{121}Sb Mössbauer isomer shifts and quadrupole coupling constants are discussed in terms of molecular geometry. The salt $Na[SbCl_4F_2]$ has been shown by Raman spectroscopy to exist as the trans isomer in the solid state.

Mössbauer data are reported for pure SbF_5 and $SbCl_5$, and when intercalated into graphite the spectra show that these halides do not enter the graphite lattice without some reduction to Sb(III) occurring.

Data are reported for a number of $SbF_5\cdot X$ adducts, where X represents SbF_3, AsF_3, or SO_2 at 4°K. The Mössbauer parameters of $SbF_5\cdot SbF_3$ (type A), and the SbF_5-SbF_3 1:1 adduct, $[Sb_2F_4^{2+}][SbF_6^-]_2$, do not support the contention that these forms are identical.

The complex anions of $[Te_2Se_2^{2+}][Sb_3F_{14}^-][SbF_6^-]$ and $[Te_{3.3}Se_{0.7}^{2+}]$-$[Sb_3F_{14}^-][SbF_6^-]$ have also been investigated by the Mössbauer method. The magnitude of the η values calculated for the Sb(III) sites are interpreted in terms of the varying asymmetry about the principle axis, which passes through the lone pair of electrons.

ACKNOWLEDGEMENTS

The author wishes to thank his research director, Professor T. Birchall, for his sincere interest, patience, and encouragement during the course of this work.

Special thanks are also due to Dr. D. R. Slim, who determined the single crystal X-ray structures of $SbCl_3F_2$ and $Sb_3Cl_{10.75}F_{4.25}$, and to Dr. J. Miller, who recorded the mass spectra discussed in this thesis. Thanks is also due to Dr. L. H. Bowen, who provided the subroutine "calfun" for fitting ^{121}Sb resonances with large asymmetry parameters.

Thanks are due to the technical staff of McMaster University for their assistance and maintenance of the instrumentation. Much appreciation is also extended to F. Ramelan and D. Hodgson, who drew the diagrams, and to Mrs. Jan Gallo, who typed this thesis.

The author wishes to thank Dr. Khin Mar Tun for her friendship and helpful advice. The author also wishes to thank his colleagues and many friends, who made his stay at McMaster University both stimulating and enjoyable.

Financial assistance from the National Research Council of Canada, which provided a bursary for 1970-71, and McMaster University, which provided financial support from 1971-1976, is gratefully acknowledged.

Finally, the author thanks his wife, Frances, for her patience, encouragement, and support.

TABLE OF CONTENTS

LIST OF TABLES

LIST OF FIGURES

CHAPTER ONE

INTRODUCTION

A. GENERAL

There are upward of 114 minerals in nature containing antimony. The sulfide of antimony, stibnite, forms the predominant ore; next come the oxides; then, of less importance, the hydroxides and oxysulfides. Pure antimony metal is produced by first roasting the stibnite to form the oxide and then reducing the oxide with hydrogen or carbon. Antimony exists in nature in both the (III) and (V) oxidation states.

B. ANTIMONY(III) HALIDES

The antimony(III) binary halides, SbF_3, $SbCl_3$, $SbBr_3$ and SbI_3, are best obtained by direct halogenation of the pure metal with the antimony being in excess. The antimony(III) halides are strong halide ion acceptors forming a variety of complex anions.

(i) Fluoroantimonates(III)

All of the fluoroantimonates(III) are prepared by mixing either Sb_2O_3 in aqueous HF or SbF_3 with an appropriate quantity of a fluoride salt such as NaF, CaF_2, or a suitable amine or ammonium salt, etc.[1-12] The stoichiometry of the reaction can vary, producing a number of different types of anions. Equation 1.1 outlines an example of a fluoroantimonate which can be prepared from a 1:2 mixture of SbF_3 and an appropriate fluoride salt. The ratio 1:2 is the highest ratio reported

$$SbF_3 + 2KF \rightarrow 2K^+[SbF_5^{2-}] \quad \ldots \quad (1.1)$$

for the antimony(III) fluoroanions. Binuclear anions, $[Sb_2F_9^{3-}]$, can be prepared in a similar fashion, that is, from a stoichiometric mixture of Sb_2O_3 and $[Co(NH_3)_6]F_3$ in aqueous HF.[13]

Mixed antimony(III) chloride fluoride anions have recently been prepared by substituting the fluoride salt of the previous reactions with a similar chloride salt.[15,16] Complex anions including $[SbClF_3^-]$, $[Sb_2ClF_6^-]$, and $[SbCl_3F_2^{2-}]$ are known, with structural information available only for the complex anion, $[SbClF_3^-]$.[17]

(ii) Structures of the Fluoroantimonates(III)

The geometry about the antimony atom of the fluoride, SbF_3,[18] and the fluroanions of antimony(III) is profoundly influenced by the 5s "lone pair" of electrons. Recent crystallographic evidence[6,7,10,11] for a number of the antimony fluoroanions has suggested that the most prevalent geometry is AX_6E. This is especially true of SbF_3 and complex anions where the ratio of $SbF_3 \cdot MF$ is less than 1:1.5, where M represents alkali metal, thallium, ammonium, or hydrazinium cations. The only exception known is the Sb_1 site of $K[Sb_2F_7]$ which has the geometry AX_4E.[8] In each of the anions mentioned above which have a geometry AX_6E, three of the Sb-F bonds are longer than the other three, and the F-Sb-F' angles about the longer Sb-F bonds are greater than 90°, presumably providing space for the lone pair, E. The geometries of all the known fluoroanions are listed in Table 1.1. When the $SbF_3 \cdot MF$ ratio is 1:2 or 1:1.5 the geometry is AX_5E (M represents a suitable cation).[11,12,14] The stereochemical activity of the "lone pair" of electrons in these anions implies

an involvement of the 5s electrons in the bonding to a considerable degree.

(iii) Chloro, Bromo and Iodoantimonates(III)

There are fewer anion salts reported for the chloro, bromo, and iodoantimonates than in the case of the fluoroantimonates(III). The anions prepared from 1:1 and 1:2 molar ratios of SbX_3 and MX, where MX represents an alkali metal halide, for example, are known for each of $SbCl_3$, $SbBr_3$, and SbI_3.[19-23] They are prepared in much the same way as the analogous fluoroantimonates(III). Complex anions can be prepared from a 1:3 molar ratio of $SbCl_3$, $SbBr_3$, or SbI_3 and a respective halide salt. They are formulated as $[SbX_6^{3-}]$.[22-24,29] A binuclear anion, formulated as $[Sb_2X_9^{3-}]$, is also known for each of the antimony halides mentioned above, (i.e., X = Cl, Br, I).[23,25-27]

(iv) Structures of Chloro, Bromo, and Iodoantimonates(III)

According to the V.S.E.P.R. theory of Gillespie,[28] the geometry about the central antimony atom of the chloro, bromo, and iodoantimonates(III) should be strongly influenced by the lone pair of electrons. Although these structural predictions are borne out in practice with respect to the fluoroantimonates(III), this simple theory does not account for the near regular octahedral structures of the $[SbX_6^{3-}]$ [29,30] and $[Sb_2X_9^{3-}]$ [25,26,27] (X = Cl, Br, I) anions. It appears that in these cases the involvement of the 5s electrons in the bonding is somewhat less than in the $[Sb_2F_9^{3-}]$ anion, for example. These electrons presumably remain in a spherical orbital. The chloro, bromo, or iodoantimonates(III), whose geometries are known from crystallographic data, are summarized in Table 1.2. The

Mössbauer data reported in this thesis suggest that the geometries about the antimony atoms of the iodoantimonates(III) parallel the analogous chloro- and bromoantimonates. The $[SbCl_4^-]$ anion of pyridinium tetrachloroantimonate has an octahedral arrangement of six chlorine atoms about the antimony.[33] Two chlorine atoms about each antimony atom are bridging and subsequently have longer Sb-Cl bonds. The Cl-Sb-Cl' angles about these bonds are slightly greater than 90°. The geometries about the antimony of $[SbBr_4^-]$ and $[SbI_4^-]$ are probably similar to the tetrachloroantimonate(III) anion. The geometry about the antimony atom of $[SbCl_5^{2-}]$ [31,32] is AX_5E, as in the case of $[SbF_5^{2-}]$, and a similar geometry is expected for the bromide and iodide anions.

C. ANTIMONY(V) HALIDES

(i) Antimony(V) Chloride Fluorides

The known geometries about each antimony of the chloride fluoride molecules are listed in Table 1.3. The molecules contain antimony in three distinct geometries, AX_4, AX_5, and AX_6, where X = Cl or F.

At the outset of the work presented in this thesis, many antimony chloride fluoride molecules had been reported in the literature,[34,35-40] but they were very poorly characterized. $SbCl_4F$ had been reported as a cis-fluoride bridged tetramer.[41] The other chloride fluoride molecules, $SbCl_3F_2$, $SbCl_2F_3$, $SbClF_4$, were assumed to have a trigonal bipyramidal arrangement, like the analogous phosphorous chloride fluorides.[42] However, at that time, some doubt had been expressed about these structures. For example, ^{19}F n.m.r. studies strongly suggested the presence of a fluorine bridged polymer for $SbCl_2F_3$.[43] During the completion of the work reported

in this thesis, the structure of $SbCl_2F_3$ was determined and was reported to contain an $[SbCl_4^+]$ cation and an $[Sb_2Cl_2F_9^-]$ anion.[44] More recently, another compound was prepared which also contained the $[SbCl_4^+]$ cation in the molecule, $Sb_3Cl_4F_{11}$.[45] These are the only tetrahedral antimony(V) halide species identified in the solid state.

(ii) Antimony(V) Chloride Fluoride Anions

Antimony(V) halides, for example, SbF_5 and $SbCl_5$, are strong halide ion acceptors forming octahedrally coordinated anions such as $[SbF_6^-]$,[47] and $[SbCl_6^-]$,[48] respectively. A number of octahedrally coordinated chloride fluoride anions such as $[SbCl_5F^-]$,[49] $[SbCl_4F_2^-]$,[50] and $[SbCl_2F_4^-]$ [51] have been reported. Only the $[SbCl_4F_2^-]$ anion has been characterized to any great extent.[50]

(iii) Antimony(V) Chloride and Fluoride Adducts and Complex Anions

The pentafluoride and pentachloride of antimony are both highly reactive liquids, hydrolysing rapidly in air. In the solid state, $SbCl_5$ has been reported to have a trigonal bipyramidal geometry.[46] Others have suggested that $SbCl_5$ undergoes a phase change at lower temperature to $[SbCl_4^+][SbCl_6^-]$, or to a dimeric structure in which two octahedra have an edge in common.[53,54] Antimony pentafluoride in the solid state is a cis-fluorine bridged tetramer.[52] The geometry about the antimony in this molecule is AY_6 (Y = F). $SbCl_5$ and SbF_5 are easily intercalated into graphite,[55] and this media appeared to provide an excellent means for recording their ^{121}Sb Mössbauer spectra. Mössbauer spectra of frozen samples of SbF_5 and $SbCl_5$ have been reported previously in the literature.[56,57]

As pointed out earlier, antimony pentafluoride is a strong fluoride ion acceptor and will react with other halides such as SbF_3 and AsF_3 forming a number of adducts. The structure of the 1:1 adduct $AsF_3 \cdot SbF_5$ suggests some contribution from the ionic formulation $[AsF_2^+][SbF_6^-]$.[58] A completely ionic structure would result in a regular octahedral coordination about the antimony atom similar to the analogous $[M^+][SbF_6^-]$ salts.[47] A number of adducts of SbF_5 and SbF_3 have been reported in the literature.[59-63] Antimony pentafluoride in the presence of antimony trifluoride and fluoride anions form the complex anion, $[Sb_3F_{14}^-]$, in conjunction with a number of mixed selenium-tellurium polyatomic cations.[64] Antimony pentafluoride also reacts with SO_2 forming a 1:1 adduct[65] which has a pseudo-octahedral coordination about the antimony, that is, five fluorine atoms and one oxygen atom.[65]

D. MÖSSBAUER EFFECT

(1) Theory

Emission or absorption of a low energy gamma-ray photon with no loss of energy due to recoil of the nucleus and with no thermal broadening is known as the Mössbauer effect. It was discovered in 1957 by Rudolph L. Mössbauer[67] and since that time has had a significant influence on the field of chemistry. Its use to chemistry arises from its ability to detect slight variations in the energy of interaction between the nucleus and the extranuclear electrons. This is brought about by its production of monochromatic radiation with a narrowly defined energy spectrum which is used to resolve exceedingly small energy differences.

For a hypothetical situation where a nucleus is not rigidly

bound in a lattice, a nuclear transition from the excited state, E_e, to the ground state, E_g, by the emission of a gamma-ray of energy, E_γ, would result in the nucleus recoiling in one direction. The conservation of momentum requires that this recoil is equal and opposite to the momentum of the gamma-ray emitted in the opposite direction. The gamma-ray energy, E_γ, would not equal the total energy of the transition, E_o (equation 1.2), due to the recoil energy.

$$E_o = E_e - E_g \ldots \tag{1.2}$$

For a system at rest, the recoil energy, E_R, at the time of the transition can be given by[68]

$$E_R = \frac{(h\nu)^2}{2m_{eff}C^2} \approx \frac{E_o^2}{2m_{eff}C^2} \ldots \tag{1.3}$$

where m_{eff} is the effective mass of the recoiling system, E_R is the recoil energy, and C is the velocity of light. The gamma-ray energy, E_γ, then equals

$$E_\gamma = E_o - E_R \ldots \tag{1.4}$$

The recoil energy is also involved in the absorbing system in a similar manner. The total energy lost in the emission-absorption system is then $2E_R$ and the energy required for resonance absorption is $E_\gamma + 2E_R$.

The gamma-ray is also deficient in energy by a thermal or Doppler energy,[68] which is dependent on the thermal motion of the nucleus. A mean value, E_D, can be defined by

$$E_D = E_\gamma \frac{2\bar{E}_K}{m_{eff}C^2} \tag{1.5}$$

where $\bar{E}_K$ is the mean kinetic energy per translational degree of freedom. The statistical distribution in energy of the emitted gamma-ray is displaced by $-E_R$ and broadened by E_D into a Gaussian distribution of width $2E_D$. The distribution for absorption has the same shape. Nuclear resonant absorption will only have a significant probability if the two energy distributions overlap strongly.

For nuclei bound in a solid, the coupling between the atoms of the crystal lattice must be considered. For the nucleus, the recoil momentum is transferred to the centre of mass of the whole crystal. The effective mass of equations (1.3) and (1.5) can be very large and the energy lost to recoil and to Doppler broadening may be negligible. In these cases, the entire crystal recoils rather than the single nucleus. Hence, both the recoil energy and the Doppler broadening become very small and much less than the line width at half maximum, Γ. The energy distribution is then dictated by the Heisenberg uncertainty principle defined by

$$\Gamma = \frac{\bar{h}}{\tau} \qquad (1.6)$$

where τ is the lifetime of the excited state, and $h = (2\pi\bar{h})$ is Planck's constant.

The recoil energy is similar in magnitude to the lattice vibration energy and since the Debye theory of solids[70] requires that lattice vibrations are quantized, the recoil energy cannot be transferred in an arbitrary manner to the lattice. The fraction of emissions which do not excite the lattice vibrations, and where recoiless gamma-ray emissions

occur, are described as the recoiless free fraction, f. It is possible to relate the recoiless free fraction to the vibrational properties of the crystal lattice[70,71,72] by the equation

$$f = \exp\left(\frac{-E_\gamma^2 \langle x^2 \rangle}{(hc)^2}\right) \qquad (1.7)$$

where $\langle x^2 \rangle$ is the mean-square vibrational amplitude of the nucleus in the direction of the gamma-ray emission. f is large for small mean-square displacements and for small gamma-ray energies. The mean-square vibrational amplitude of the nucleus is dependent on the temperature and hence the recoiless free fraction is inversely proportional to the temperature. The precise form of the temperature dependence is discussed elsewhere.[73]

(ii) Isomer Shift

The isomer shift results from the electrostatic interaction between the charge distribution of the nucleus and the electrons, which have a finite probability of being found in the vicinity of the nucleus. This interaction results in slight relative shifts of the ground and excited nuclear energy levels with varying electron density. Although the interaction between the nucleus and the electrostatic environment cannot be measured directly, it is, however, possible to compare the energy differences between two nuclei, which are the absorber and the source in the Mössbauer experiment. A Doppler velocity is supplied to the source to observe resonance, since the shifts may be different in the source and the absorber. This comparison is referred to as the isomer shift and is represented by the equation[74]

$$\text{I.S.} = \delta = \frac{4\pi}{5} Ze^2R^2\left(\frac{\Delta R}{R}\right)\left(|\psi_s(0)_{abs}|^2 - |\psi_s(0)_{source}|^2\right) \qquad (1.8)$$

where R represents the radius of the nucleus, and ΔR represents the change of the nucleus during its transition from the excited state to the ground state. $|\psi_s(0)|^2$ is the non-relativistic Schrödinger wavefunction at r = 0 and represents the s-electron density at the nucleus. A negative $\frac{\Delta R}{R}$ means that the nucleus swells on de-excitation. The isomer shift, δ, is then a product of a chemical term, i.e., the electron density, and a nuclear term, $\frac{4\pi}{5}Ze^2R^2(\frac{\Delta R}{R})$. The latter is constant for a particular nucleus and hence isomer shifts can be related directly to changes in electron density about the nucleus.

The term, $|\psi_s(0)|^2$ in the above equation, represents the occupied s orbitals in the antimony atom in this thesis. $|\psi_s(0)|^2$ includes contributions from both the core s-electrons as well as the valence electrons. The values of $|\psi(0)|^2$ for the p, d, and f electrons are zero and consequently these orbitals have no direct effect on the isomer shift; however, they serve to shield the s electrons from the nucleus, which ultimately affects the isomer shift. The $\frac{\Delta R}{R}$ term for the ^{121}Sb nucleus is negative, which implies that an increase in s electron density results in a more negative isomer shift. For this reason, the isomer shifts of compounds of antimony(III) are much more negative than those of compounds of antimony(V) because of the presence of the 5s electrons in the former. In the antimony(III) compounds, the isomer shift varies with the involvement of the 5s electrons in the bonding, and the electronegativity of the ligands bonded to the antimony. The variations in the isomer shift of antimony(V) compounds are related to changes in the electronegativity of the ligands. Of course, any changes in the electron density of the p, d, and f orbitals

will also result in a change in s electron density at the nucleus. Consequently, the isomer shift is a measure of the overall electronic environment of the ^{121}Sb Mössbauer nucleus.

The isomer shift is temperature dependent upon two factors; one is known as the second-order Doppler shift, which is a consequence of the temperature dependence of the lattice vibration term, $\langle X^2 \rangle$. This results in a small change in the gamma-ray energy of the form[74]

$$\delta E_\gamma = \frac{-\langle X^2 \rangle}{2C^2} E_\gamma \qquad (1.9)$$

Since C^2 is considerably greater than $\langle X^2 \rangle$, this term is very small. The second-order Doppler shift will be essentially zero for a series of similar compounds recorded at the same temperature, since $\langle X^2 \rangle$ will be essentially constant. The second temperature dependent effect arises from chemical or physical changes in the system itself, such as, a phase change in the crystal without a subsequent chemical change.

(iii) Quadrupole Splitting

Another way in which nuclear energy levels interact with the chemical environment is via the nuclear electric quadrupole moment. Nuclei which have a nuclear spin number, I, greater than 1/2 have a non-spherical nuclear charge distribution. The magnitude of this charge distribution is governed by Q, the nuclear quadrupole moment. ^{121}Sb has an oblate charge distribution about the spin axis, hence Q is negative. The distorted nucleus interacts with the extranuclear electric field gradient, e.f.g., giving rise to a splitting of the nuclear energy levels. The

nuclear quadrupole coupling Hamiltonian for a nucleus of spin I may be expressed as[75]

$$H_Q = \frac{eQV_{ZZ}}{4I(2I+1)}[3\hat{I}_Z - \hat{I}^2 + \frac{\eta}{2}(\hat{I}_+ + \hat{I}_-)] \qquad (1.10)$$

where V_{ZZ} is the electrostatic potential in the direction of the principle axis and η, the asymmetry parameter, is given by

$$\eta = \frac{V_{XX} - V_{YY}}{V_{ZZ}} (0 \leq \eta \leq 1) \qquad (1.11)$$

$\hat{I}_Z$ is the spin operator and $\hat{I}_+$ and $\hat{I}_-$ are the shift operators. For axial symmetry, $\eta = 0$, the $I = \pm \frac{5}{2}$ ground state is split into three degenerate levels, and the excited state, $I = \pm \frac{7}{2}$, is split into four degenerate levels, as outlined in Figure 1.1. The relative energies of the degenerate levels are included in the Figure where $A = \frac{eQV_{ZZ}}{40}$ and $B = \frac{ReQV_{ZZ}}{84}$.[76] The relative energies of the transitions between the ground and the excited state are then determined by the quadrupole moment of the ground state (-0.28 ± 0.1 barn),[77] and the ratio of the quadrupole moments of the excited and ground states, $R = \frac{Q_{ex}}{Q_g} = 1.34 \pm 0.01$.[78] The intensities of the transitions are in the ratios of the squares of the Clebsch-Gordan coefficients of each transition.[79] The selection rules restrict the number of lines to eight when $\eta = 0$, the energies of which are the differences between those of the ground and the excited states.

If the electrostatic field is not axially symmetric about the principle axis, $\eta \neq 0$, then all 12 transitions between the excited state and the ground state are allowed because the quantum numbers, which determine the nuclear spin states, are no longer applicable and the states

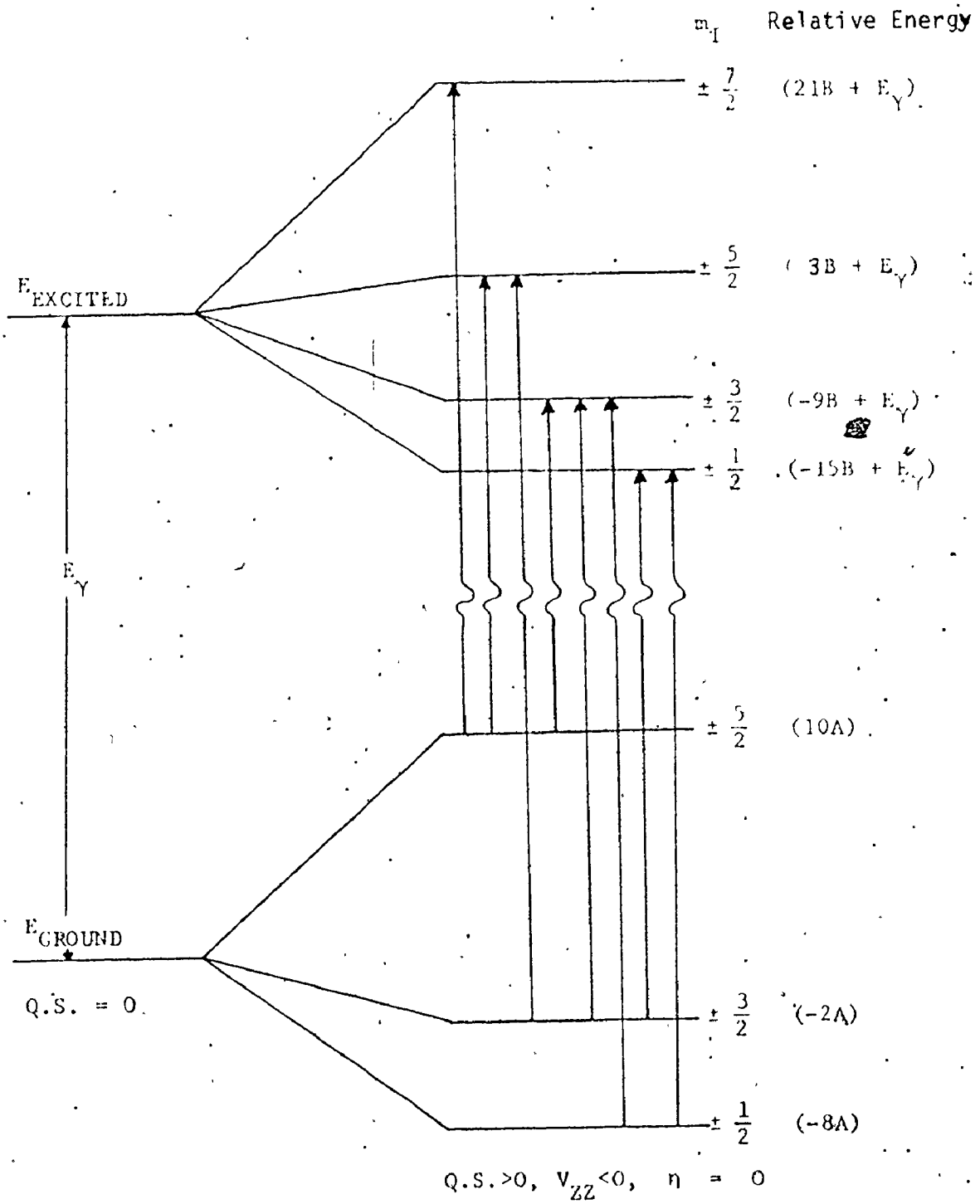

Figure 1.1. Energy Diagram for an ^{121}Sb Nucleus Subjected to an Non-zero Axially Symmetric Electric Field Gradient.

$A = \frac{eQ_g V_{ZZ}}{40}$, $B = \frac{ReQ_g V_{ZZ}}{84}$, $R = \frac{Q_e}{Q_g}$, and Q.S. is Quadrupole Splitting.

are mixed. If $\eta > 0$, the ratios of the intensities of all the lines are modified. Some of the transitions may be accidentally degenerate. Examples of simulated ^{121}Sb Mössbauer spectra reported by Donaldson et al.[76] for the cases where $\delta = 0$ mm/sec, $\eta = 0$, and $eQV_{ZZ} = 4$, 6, and 10 mm/sec are shown in Figure 1.2. The bars indicate the intensities and positions of the individual peaks. The spectra were convoluted with Lorentzian line-shapes assuming a natural line width of 2.1 mm/sec at half peak height. The sign of eQV_{ZZ} can be obtained from the spectra, since it is reversed if high and low energy regions of the spectra are interchanged. A simulated spectrum with the $\delta = 0$, $eQV_{ZZ} = 10$ mm/sec, and with $\eta = 1$ is also shown in Figure 1.2. The quadrupole spectra of ^{121}Sb therefore contains information not only on the sign and magnitude of the quadrupole splitting, eQV_{ZZ}, and indirectly the nature of the electric field gradient, but also on the size of the asymmetry parameter, η.

(iv) Line Width

As mentioned previously, the natural line width is given from the uncertainty principle. The ideal source would emit radiation with a Lorentzian distribution of energy and, assuming an ideally thin absorber, the resonant absorption would have a line width at half maximum, Γ_{exp}, which is $2\Gamma_{nat}$. However, in practice, the line-shape departs from the simple Lorentzian, and it is seldom possible to observe resonance lines as narrow as $2\Gamma_{nat}$ due to several possible broadening effects such as; non-homogeneity of chemical environments of the resonant atoms in the source and/or absorber, geometric effects, thermal effects, the presence of hyperfine structure due to extranuclear field effects, and finite

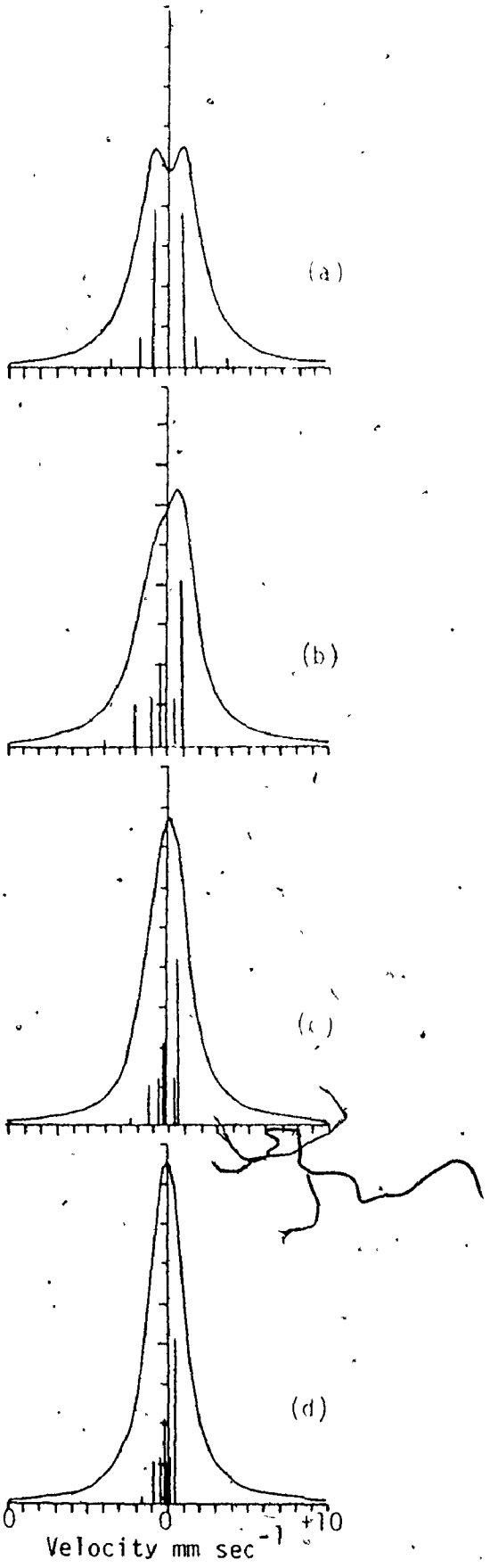

Figure 1.2. Simulated ^{121}Sb Mössbauer spectra:
(a) eQV_{ZZ} = 10 mm/sec η = 1,
(b) eQV_{ZZ} = 10 mm/sec η = 0,
(c) eQV_{ZZ} = 6 mm/sec η = 0,
(d) eQV_{ZZ} = 4 mm/sec η = 0.
(Reproduced from Reference 76).

source and absorber thickness effects.

In the case of ^{121}Sb Mössbauer, the hyperfine interactions are small compared to the resonance line width and, as a result, the individual hyperfine components are not separable. Thus, the absorption spectra appear as a single broad envelope, the shape of which is primarily dependent on the magnitude and sign of the quadrupole interaction, as indicated earlier. Therefore, the individual line positions can be fitted to a sum of Lorentzian lines with suitable constraints[80] using an iterative technique.

The intensities of the different hyperfine transitions in a quadrupole spectrum of a powder sample have been reported to vary, in some instances, from those prescribed by the Clebsch-Gordan coefficients. Stevens and Ruby[78] reported deviations in the intensities of certain hyperfine components and attributed this effect to the presence of the Goldanskii-Karyagin effect,[81] which is the non-angularly dependent asymmetry in the hyperfine components due to anisotropy of the recoiless free fraction. More recently, this asymmetry has been attributed to absorber thickness effects.[80,82]

Although, for very thin absorbers, the absorption envelope can be represented as a summation of Lorentzian lines, this is not valid in samples of finite thickness because of saturation effects on the absorption intensity. The transmission integral,[80] which has been shown to be useful to deal with this problem,[83,84] is given by

$$I(v) = I_0\{1 - \frac{1}{\pi}\int_{-\infty}^{\infty} \frac{(\Gamma/2)dE}{[E + (vE_0/C)]^2 + (\Gamma/2)^2} \times \exp[-\sum_k \frac{A_K T_A (\Gamma/2)^2}{(E - E_K)^2 + (\Gamma/2)^2}]\} \qquad (1.12)$$

and can be used in the fitting procedure replacing the summation of Lorentzian formulation. N_0 is a scaling parameter to include background effect: $I(v)$ is the absorption intensity at a Doppler shift from the emitted gamma-ray energy E_0: 2Γ is the full width at half maximum of the resonance at zero thickness: E_K is the energy, and A_K the fractional ideal intensity of the Kth hyperfine line: T_A is the effective absorber thickness (which is a dimensionless parameter).

E. PURPOSE

The purpose of the work presented in this thesis was to extend the knowledge of the structures and chemistry of antimony(III) and antimony(V) halides.

An extensive study by ^{121}Sb Mössbauer spectroscopy was undertaken to examine the electronic environment about the antimony atom in various antimony(III) complexes and complex anions. These complexes were examined with particular reference to the stereochemical activity of the 5s electrons and consequently some conclusions may be drawn concerning their involvement in the bonding.

At the outset of this work, very little information was available on the structures and the chemistry of antimony(V) chloride fluoride compounds, $SbCl_xF_{5-x}$ ($x = 1, 2, \ldots, 5$); most of these compounds had been previously suggested in the literature, but very poorly characterized. Therefore, attempts were made to prepare and characterize all of these compounds and other possible intermediate species, such as $Sb_3Cl_{11}F_4$. Also, preparations of the analogous series of anions, $[SbCl_xF_{6-x}^-]$ ($x = 1, 2, \ldots, 6$), were attempted. An extensive study was undertaken

to study the structures and the electronic environments about each antimony atom of these series.

Mössbauer spectroscopy was used to examine the electron density and electric field gradients about the antimony atom in a number of antimony(V) adducts in order to obtain more information about the nature of the bonding in these systems.

TABLE 1.1

KNOWN MOLECULAR GEOMETRIES OF SOME ANTIMONY(III) FLUORO ANIONS

Total No. of Bonds and Lone Pairs	Arrangement About Sb	Geometry	SbF_3:MF	Example	Ref.
5	Trigonal Bipyramid	AX_4E	2:1	Sb_1 of $K^+[Sb_2F_7^-]$	8
6	Octahedron	AX_5E	1:2	$[SbF_5^{2-}]$	11,12
			2:3	$[Sb_2F_9^{3-}]$	14
7	Monocapped Octahedron, Pentagonal Bipyramid, Monocapped Trigonal Prism	AX_6E	1:0	SbF_3	18
			4:1	$[Sb_4F_{13}^-]$	6
			3:1	$[Sb_3F_{10}^-]$	7
			2:1	$[Sb_2F_7^-]$	8,9
			1:1	$[SbF_4^-]$	1,2
			1:1	$[SbF_3Cl^-]$	17

TABLE 1.2

KNOWN MOLECULAR GEOMETRIES OF SOME ANTIMONY(III) CHLORIDE, BROMIDE AND IODIDE ANIONS

Total No. of Bonds and Lone Pairs	Arrangement About Sb	Geometry	SbX_3:MX	Examples	Ref.
6	Octahedron	AX_5E	1:2	$[SbCl_5^{2-}]$	31,32
6	Octahedron	AX_6	1:3	$[SbCl_6^{3-}]$	29,30
			2:3	$[Sb_2Cl_9^{3-}]$	27
			2:3	$[Sb_2Br_9^{3-}]$	25,26
7	Monocapped Octahedron, Pentagonal Bipyramid, Monocapped Trigonal Prism	AX_6E	1:1	$[SbCl_4^-]$	33

TABLE 1:3

KNOWN ANTIMONY(V) CHLORIDE FLUORIDE MOLECULES AND RELATED CATIONS AND ANIONS

Total No. of Bonds	Arrangement About Sb Site	Site Geometry	Molecular F:Cl Ratio	Example	Ref.
4	Tetrahedron	AX_4	3:2	$[SbCl_4^+](SbCl_2F_3)$	44
			3 2/3:1 1/3	$[SbCl_4^+](Sb_3Cl_4F_{11})$	45
5	Trigonal Bipyramid	AX_5	0:5	$SbCl_5$	46
6	Octahedron	AX_4Y_2	1:4	$SbCl_4F$	41
		AXY_5	3:2	$[Sb_2F_9Cl_2^-](SbCl_2F_3)$	44
		AY_6	3 2/3:1 1/3	$[Sb_2F_{11}^-](Sb_3Cl_4F_{11})$	45
		AY_6	5:0	SbF_5	52
		AX_6	0:6	$[SbCl_6^-]$	48
		AX_4Y_2	2:4	$[SbCl_4F_2^-]$	50*
		AY_6	6:0	$[SbF_6^-]$	47

* Infrared Analysis

CHAPTER TWO

EXPERIMENTAL

A. GENERAL PREPARATIVE TECHNIQUES

(i) Vacuum System

The majority of the preparative work presented here was performed using a pyrex vacuum system. The vacuum line was divided into a highvacuum all-pyrex section and a greaseless pyrex section with teflon stopcocks. Both sections were accessible to a rotary pump and a two-stage mercury diffusion pump. Connections were made to the high-vacuum section by 9 mm I.D. ball joints and connections were made to the teflon stopcocks by 1/4" O.D. pyrex fitted by a straight Swagelock union or a teflon valve with Swagelock fittings.

(ii) Dry Atmosphere System

All of the samples, which hydrolyze in air, were handled in a dry-nitrogen filled Labconco glove-box fitted with an external constant-circulation liquid nitrogen drying system. The glove-box was filled with "extra-dry nitrogen", supplied by Specialty Gases. An evacuable port provided access to the glove-box.

(iii) Reaction Vessels

Where it was necessary for samples to be prepared in the absence of air, or in liquid SO_2 as a solvent, a vessel of the kind shown in Figure 2.1.a was used. A vessel, shown in Figure 2.1.b, was used for reactions where reactants were refluxed for a long period of time. The stopcocks used in both vessels were either 10 mm I.D. pyrex or teflon

Figure 2.1. Reaction Vessels for Preparations in Liquid SO_2.

[a] = Vessel for Room Temperature Reactions

[b] = Reflux Vessel

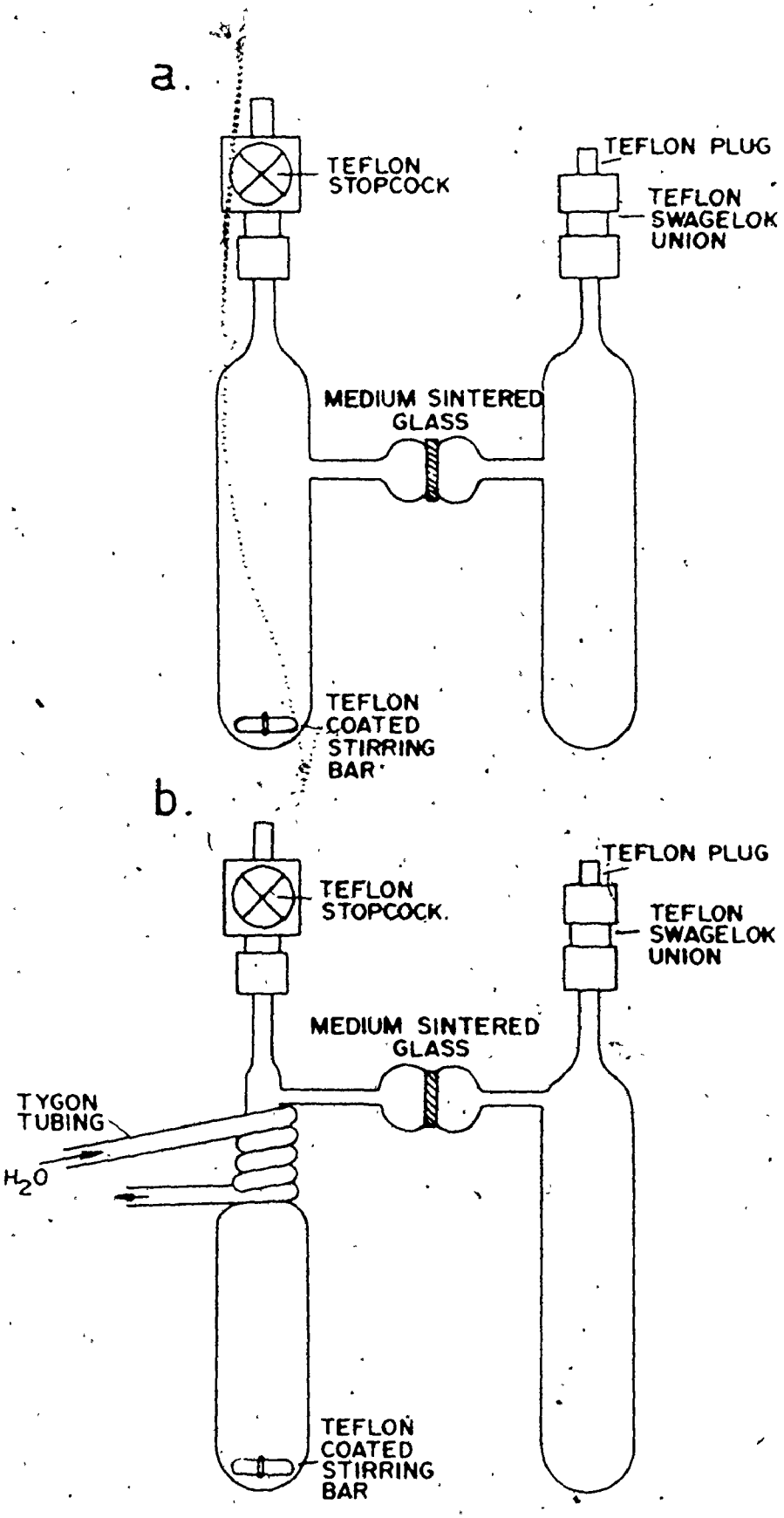
a.
TEFLON STOPCOCK
TEFLON PLUG
TEFLON SWAGELOK UNION
MEDIUM SINTERED GLASS
TEFLON COATED STIRRING BAR
b.
TEFLON STOPCOCK.
TEFLON PLUG
TEFLON SWAGELOK UNION
MEDIUM SINTERED GLASS
TYGON TUBING
H_2O
TEFLON COATED STIRRING BAR

as described earlier.[85] The vessels were carefully dried by repeated flamings on the highvacuum system before use. The reactions involving chlorine were performed in a pyrex vessel, which was inserted into a 150 ml stainless steel bomb. The pyrex vessel was heated in an oven and stored in a dry atmosphere for several days before use. The stainless steel bomb was pumped on the vacuum line for several days. The bomb was equipped with a 0-2000 psig stainless steel gauge and a 1000 psig blow-out valve. The input connector was 1/4" O.D. stainless steel.

B. EXPERIMENTAL TECHNIQUES AND APPARATUS

(i) Mössbauer Spectrometer

The Mössbauer spectra were recorded using an Austin Science Associates (A.S.A.) model S3 drive system and an A.S.A. model K3 linear motor. Constant acceleration motion was used and the sense of the acceleration was controlled by a multichannel analyzer operating in the multiscalar mode. A triangular waveform motion was used. The velocity, and hence the gamma-ray energy, varied linearly with time. Either a PIP 400 Victoreen multichannel analyzer or a Northern-900 series multichannel analyzer were employed. Both systems were comprised of a preamp/amplifier, single channel analyzer, analog-to-digital converter, a complete core memory package, readout drives and a cathode ray tube display. The Northern-900 series multichannel analyzer was used in conjunction with a Northern-458 dual input multichannel scaling controller. The external address advance was produced by an Austin Science Associates TU 100A crystal controlled time-base generator powered by an Ortec Model 401A power amplifier. The block diagram, Figure 2.2, illustrates the

Figure 2.2. Schematic of the Mössbauer Spectrometer used to record ^{121}Sb Mössbauer Spectra.

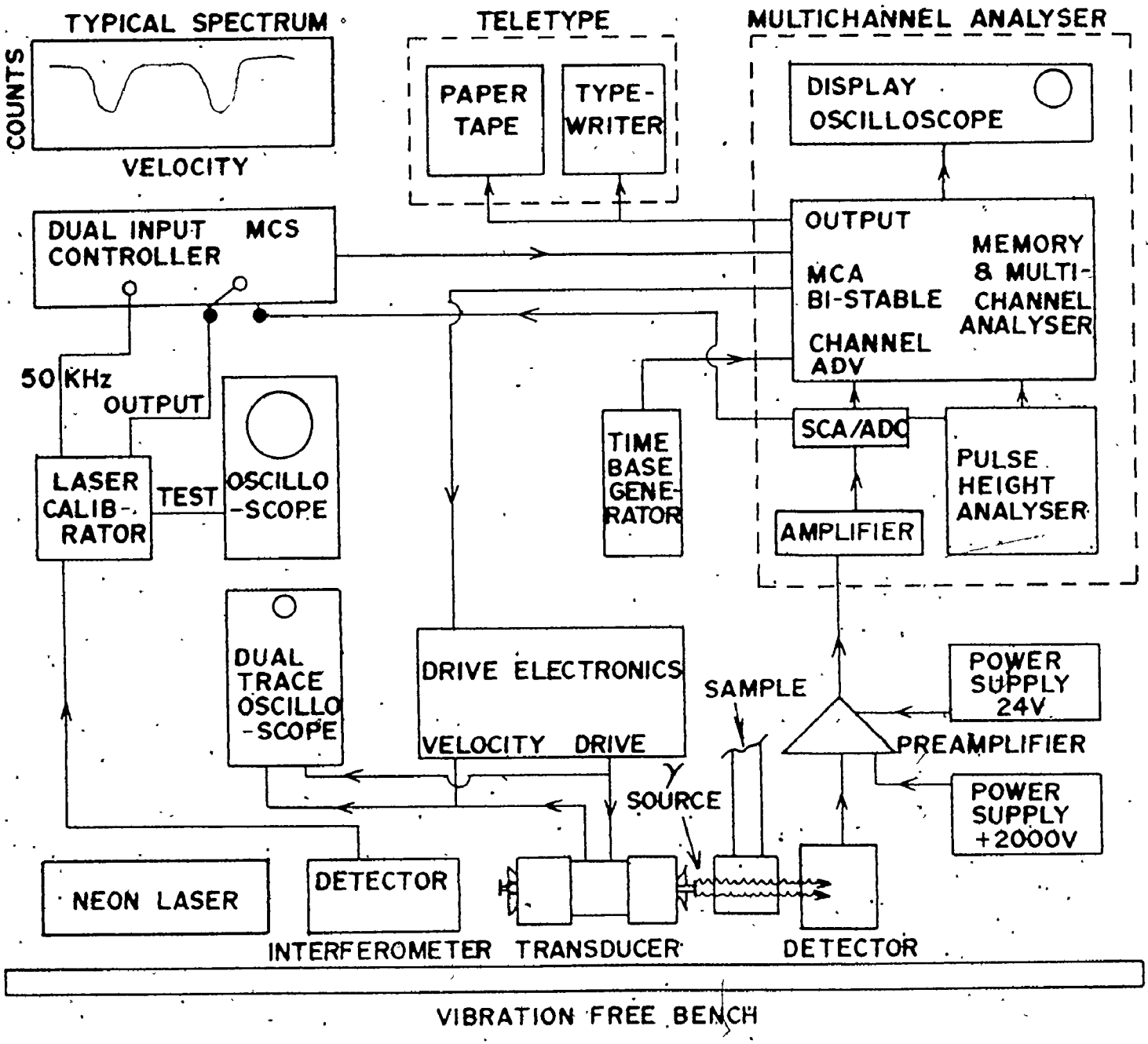
TYPICAL SPECTRUM
COUNTS
VELOCITY
TELETYPE
PAPER TAPE
TYPE-WRITER
MULTICHANNEL ANALYSER
DISPLAY OSCILLOSCOPE
DUAL INPUT MCS CONTROLLER
OUTPUT
MCA BI-STABLE
MEMORY & MULTI-CHANNEL ANALYSER
CHANNEL ADV
50 KHz OUTPUT
LASER CALIB-RATOR
TEST
OSCILLO-SCOPE
TIME BASE GENE-RATOR
SCA/ADC
PULSE HEIGHT ANALYSER
AMPLIFIER
DUAL TRACE OSCILLO-SCOPE
DRIVE ELECTRONICS
VELOCITY DRIVE
SAMPLE
POWER SUPPLY 24V
PREAMPLIFIER
SOURCE
POWER SUPPLY +2000V
NEON LASER
DETECTOR
INTERFEROMETER
TRANSDUCER
DETECTOR
VIBRATION FREE BENCH

elements of the Mössbauer spectrometer.

The gamma-ray source was a 0.5 mCi $Ba^{121}Sn(Sb)O_3$ emitter supplied by the New England Nuclear Corporation and the single channel analyzer was set on the escape peak of the 37.15 keV gamma-ray. The detector was a $Xe\text{-}CO_2$ filled proportional counter and the desired energy was selected by adjusting the upper and lower input voltage of the single channel analyzer. The signal from the single channel analyzer was amplified, counted, and stored in the core memory.

The Mössbauer spectra consisted of a plot of count rate vs. velocity. The constant acceleration motion has opposite signs in alternate halves of the memory. As a result, a mirror image appears in the memory halves, with one spectrum being counted during acceleration and the other during deceleration of the drive.

Data were recorded onto a teletypewriter, T/T 33, which included a typewriter and a paper tape punch. The data were then transferred to computer cards for processing.

The drive velocity was calibrated after each spectrum using either ^{57}Co in Pd supplied by the New England Nuclear Corporation and a standard iron foil, or by using the Austin Science Associates laser absolute velocity calibrator equipped with a Metrologic Neon Laser supplied by Edmund Scientific. The laser absolute velocity calibrator was used in conjunction with the Northern-458 dual input multichannel scaling controller. When calibrating, two multiscaling spectra were recorded for equal lengths of time: a velocity which represents the number of fringes produced by the interferometer; and a 50 KHz crystal oscillator. The crystal oscillator provided a measurement of the live time per channel.

All isomer shifts were recorded with respect to InSb at the same sample temperature as zero isomer shift.

Spectra were recorded with the source at room temperature and the absorber cooled to either 77°K or 4°K with a model LT-3-110 Liquid Helium transfer Refrigerator from Air Products and Chemicals Incorporated, Figure 2.3, which was equipped with a model 3610 Temperature Controller. The temperature was continuously monitored with a chromel vs. gold (0.07% atomic Fe) thermocouple. The sample was mounted into a copper holder with a window of cross-section 2.5 cm^2 which was securely fastened into the copper holder of the cryotip. The sample was covered by a vacuum shroud as shown in Figure 2.4. The shroud was furnished with beryllium windows for gamma-ray irradiation and ports for introduction of volatile samples. The solid samples contained 8-10 mg/cm^2 of antimony and were finely powdered, mixed with Apiezon grease and packed into the copper sample holder. Any samples which reacted with Apiezon grease were finely powdered and compressed between two teflon discs coated with a thin film of halocarbon grease or oil. The liquid samples were distilled through the ports onto the cold copper holder fitted with a thin aluminum disc. Typical spectra were recorded for 40-50 hours and when folded gave 70,000-80,000 counts per channel.

A number of fitting routines were applied to the data points. When the data were fitted to a single Lorentzian, a program using an iterative least squares method[86] was used to find the best parameters. Data, computer fitted to eight or more lines, were calculated using the program originating from Shenoy and Dunlap[87] which basically took multi-

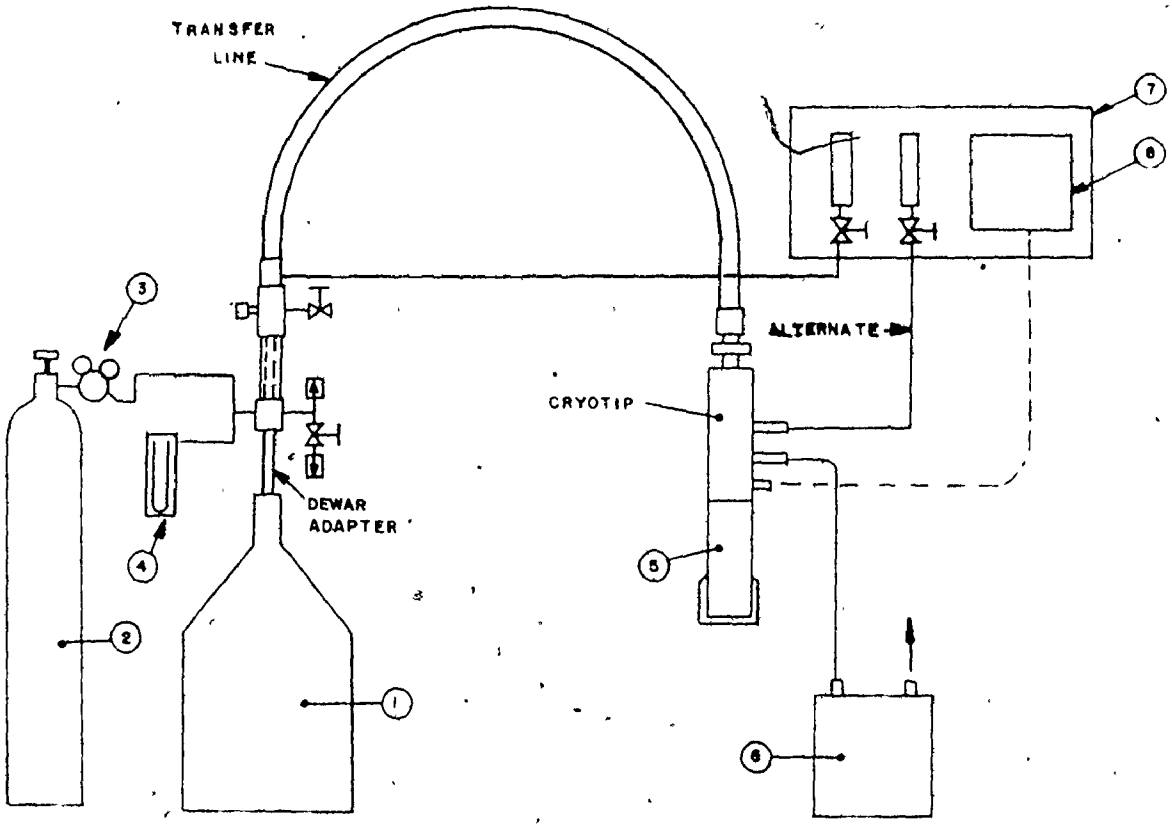

1. Helium Dewar
2. Helium Cylinder
3. Pressure Regulator
4. Mercury Manometer, 0 to 20" Hg
5. Vacuum Shroud (detail Fig. 2.4)
6. Vacuum Shroud Pump
7. Accessory Flow Control Panel
8. Temperature Controller, Automatic

Figure 2.3. Low Temperature Transfer Refrigerator used to Cool Absorbers to 77°K and 4°K.

Figure 2.4. Schematic of Sample Holder and Cryo-Tip Assembly used on Low Temperature Transfer Refrigerator.

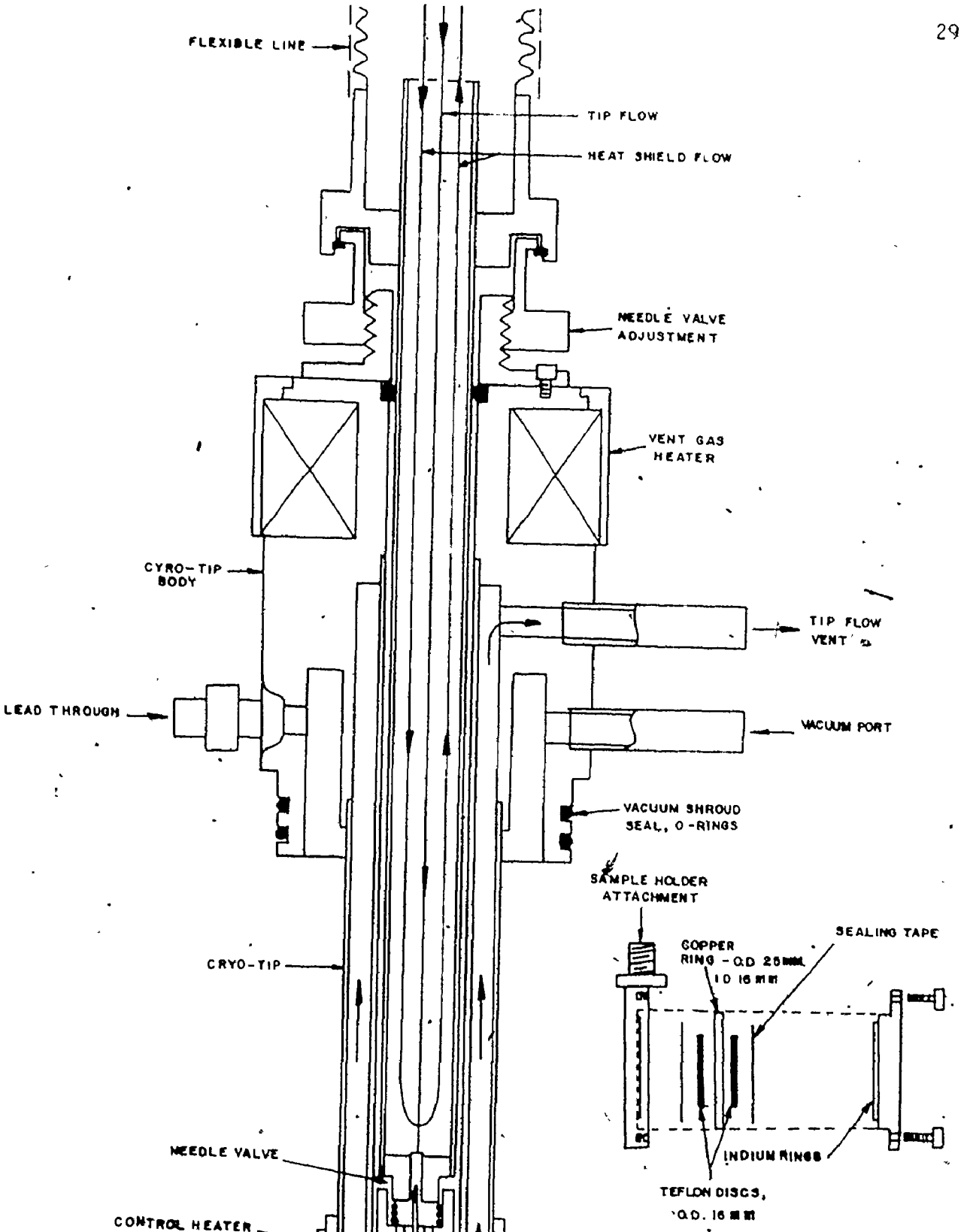
FLEXIBLE LINE
TIP FLOW
HEAT SHIELD FLOW
NEEDLE VALVE ADJUSTMENT
VENT GAS HEATER
CYRO-TIP BODY
TIP FLOW VENT
LEAD THROUGH
VACUUM PORT
VACUUM SHROUD SEAL, O-RINGS
SAMPLE HOLDER ATTACHMENT
CRYO-TIP
NEEDLE VALVE
CONTROL HEATER
SAMPLE HOLDER ATTACHMENT
TEMP SENSOR HOLE
SEALING TAPE
COPPER RING - O.D 25mm I.D 16 mm
INDIUM RINGS
TEFLON DISCS, O.D. 16 mm

channel counting data, folded it if necessary, and found the best parameters to fit the data to an appropriate function. Two functions were used throughout this work. In the majority of cases, the absorbers were suitably thin powders and appropriate sums of Lorentzians were evaluated. All spectra were first calculated assuming axial symmetry, i.e., $\eta = 0$, and non-zero quadrupole splitting. The relative intensities of the eight allowed transitions were the appropriate combinations of Clebsch-Gordan coefficients[88] which were expressed as constraints. The ratio of the nuclear quadrupole moments, $R = \frac{Q_{ex}}{Q_{gr}} = 1.34$,[89] was used in the calculations. The parameters were varied for the best least-squares fit.

For spectra which gave poor fits for $\eta = 0$, a function was used which allowed η to vary.[90] For $\eta \neq 0$ the selection rule, $\Delta m = \pm 1, 0$, no longer applies and intensity ratios were calculated for all possible transitions using combinations of Clebsch-Gordan coefficients.[88] A least-squares minimization routine was used to find the best value for the parameters.

A number of spectra were not suitably fitted with the sum of Lorentzian functions. This may have been due to sample thickness broadening. A function devised by T.E. Cranshaw,[91] which accounted for broadening due to absorber thickness, based on the transmission integral developed by M. Celia Dibar Ure and P.A. Flinn,[92] was employed. For spectra with $\eta \neq 0$, a fitting routine briefly outlined by Shenoy and Friedt,[83] was incorporated into the transmission integral which allowed for η and eQV_{ZZ} as variables. The transmission integral calculated a spectrum allowing for the finite thickness of the sample.

In addition to the usual goodness of fit criterion, χ^2, the

misfit criterion of Ruby[108] was employed in some of the fitting routines. In each Table of Mössbauer Data, the χ^2 is presented as a fraction of the degrees of freedom with a value close to one representing an acceptable computer fitted spectrum. The misfit is represented as M, with a value < 0.1 indicating an acceptably fitted spectrum.

(ii) Laser Raman Spectrometer

The instrumentation has been described previously.[93] For temperature variations, a cylindrical pyrex dewar was mounted perpendicular to the scattered beam. The appropriate temperature was controlled by passing a continuous stream of air into the dewar. The air was warmed or cooled to the desired temperature before entering the dewar. The temperature of the sample was recorded using a copper-constantan thermocouple.

Samples were prepared in either a 5 mm O.D. medium-walled polished glass n.m.r. tube glass blown to a 1/4" pyrex tube, or a melting point tube. Melting point tubes were previously heated under vacuum and stored in a glove-box. The samples were added to the melting point tubes in the glove-box and sealed before recording the spectrum. N.m.r. tubes were flame-dried under vacuum and the samples were introduced in the glove-box. The n.m.r. tubes were sealed with a Swagelock union and a teflon 1/4" plug. Liquid samples were prepared in a similar fashion except that they were sealed off under vacuum before the spectra were recorded.

The Raman spectra occasionally contained lines due to the glass sample tube. These lines occurred at 235(18), 246(6) broad, 333(100) cm^{-1}. In this work the glass lines were subtracted from the spectra in the tables, but are shown in the figures.

(iii) Mass Spectrometer

The spectra were recorded on an A.E.I. MS30 double beam, double focusing mass spectrometer. PFK was admitted into beam II via a gas/liquid probe to serve as a chemical mass marker, recorded simultaneously, but not interferring with the system under investigation. A consistently strong ion current was achieved with the electron voltage kept at 20 ev and the sample temperature at 50-60°C.

The samples were placed in previously dried melting point tubes and a dry nichrome wire was inserted into the tube to spread a thin layer of sample onto the walls of the tube. All this work was performed in the glove-box. The sample tubes were sealed and subsequently opened inside a dry-bag which enclosed the inlet port. The section of the tube containing the sample was inserted into the sample chamber using a direct insertion probe and the chamber was subsequently evacuated. Spectra were recorded to approximately 1200 m/e.

(iv) Chemical Analysis

Analytical determinations of antimony(III) in the antimony(III) complexes were performed using the standard iodine titration described in Vogel.[94] Antimony(V), fluorine, and chlorine analyses were performed by Mikroanalytisches Laboratorium.[95]

C. PURIFICATION OF STARTING MATERIALS

(i) Antimony Pentafluoride

Antimony pentafluoride (Ozark-Mahoning) was doubly distilled in an all-pyrex apparatus described previously.[96] The fraction boiling at 142-143°C was collected. A third distillation was performed using the

vacuum line and the distillate was collected in a pyrex flask which was stored in the glove-box for subsequent use in the dry atmosphere.

(ii) Antimony Pentachloride

Antimony pentachloride (J.T. Baker Co. Reagent) was distilled initially under reduced pressure. The fraction boiling at 110°C was collected. The distillate was then transferred to the vacuum line where it was distilled from a 21°C trap and collected at 0°C. The collection trap had a small necked flask glass-blown onto the bottom and the pure $SbCl_5$ was isolated by sealing off this flask. The flask was wrapped with aluminum foil to restrict the light and stored in the glove-box until required.

(iii) Niobium Pentafluoride

Niobium pentafluoride (Ozark-Mahoning) was sublimed at 20°C under vacuum and stored in the dry box until required. The sample purity was checked by Raman spectroscopy.[97]

(iv) Antimony Trihalides

Antimony trifluoride (Alfa Inorganics) was sublimed at 319°C under vacuum and stored in a dry nitrogen atmosphere until required. The purity of the sample was checked by Raman spectroscopy.[98]

Antimony trichloride (Allied Chemical) was sublimed at 50°C under vacuum and stored in the glove-box until required.

Antimony tribromide (Alfa Inorganics) was sublimed at 200°C under vacuum and stored in the glove-box until required.

Antimony triiodide (Alfa Inorganics) was used without further purification.

(v) Arsenic(V) and (III) Fluorides

Arsenic pentafluoride (Ozark Mahoning Co.) was used without further purification.

Arsenic trifluoride (Alfa Inorganics) was distilled under vacuum and stored in a stoppered vessel over sodium fluoride.

(vi) Alkali Metal Halides

All alkali fluoride and chloride salts used were reagent-grade and were placed in a platinum crucible and dried by heating to 300°C for 2-3 days under vacuum. The dry salts were stored in the dry nitrogen atmosphere of the glove-box.

Sodium fluoride was obtained from Shawinigan Chemical Co., sodium chloride and potassium fluoride from B.D.H. Chemical Co., caesium fluoride from K & K Laboratories Ltd., and potassium bromide from J.T. Baker Co.

(vii) Alkali Metal Carbonates

Caesium carbonate (Ventron Alfa Products), and sodium and potassium carbonates (J.T. Baker Chemical Co.) were used without further purification.

(viii) Halogens

Iodine (Fischer Scientific Co.) was freshly sublimed before use.

Bromine (McArthur Chemical Co.) was used without further purification.

Chlorine (Matheson Co.) was purified by passing the gas through a drying system described in Figure 2.5. The system was initially flushed

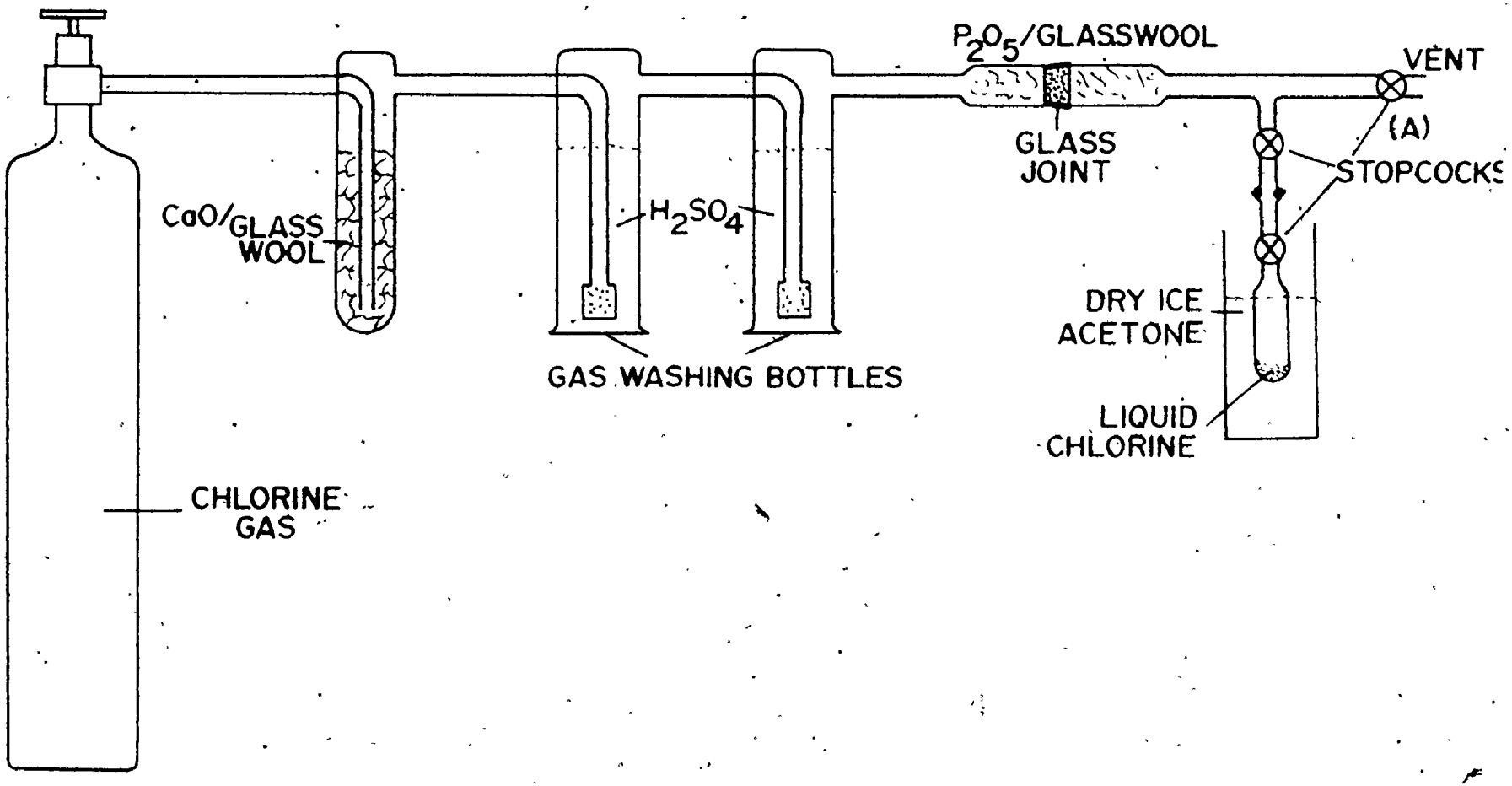

Figure 2.5. Diagram of Chlorine Gas Purification System.

out with dry nitrogen and then chlorine. The stopcock (A) was then closed and liquid chlorine was collected in the collection flask immersed in a dry-ice acetone slush bath. The liquid chlorine was then degassed several times on the vacuum line and finally trap-to-trap distilled through a vessel cooled in a methylene chloride slush bath (-96.7°C) and into a vessel cooled in an n-pentane slush bath (-130°C). The pure pale yellow chlorine was then stored in a glass vessel at -78°C. The presence of moisture was checked by infrared spectroscopy.

(ix) Solvents

Sulfur dioxide (Matheson Co.) was dried and stored over P_2O_5 before use. When required, it was distilled into the reaction vessel.

Aqueous hydrofluoric acid (J.T. Baker Chemical Co., 48%), analytical reagent hydrochloric acid (Mallinckrodt, 37%), hydrobromic acid (Fisher Scientific, 48.1%), and hydroiodic acid (J.T. Baker, 50.3%) were used without further purification.

Graphite (Fischer Scientific Co., Grade #38) was dried by heating to 300°C under vacuum for three days. The dry gray powder was then stored in the glove-box until used.

(x) Antimony(III) Oxide

Sb_2O_3 was supplied by General Chemical Co. (Analytical Reagent) and was used without further purification.

(xi) Indium Antimonide

Pure indium antimonide (99.99%), supplied by Alfa Inorganics, was finely ground, made into a paste with apiezon grease and pressed

into a copper ring between two discs of plastic (teflon) for a standard zero isomer shift.

(xii) Antimony Metal

Pure antimony metal (United Mineral and Chemical Corp., 99.9999) was used without further purification. The metal was finely ground and a Mössbauer sample was prepared as an apiezon grease paste with 8-10 mg of antimony per cm^2 of sample holder.

(xiii) Amines

The majority of the amines used in the preparations were supplied by Eastman Organic Chemical Co. and were used without further purification.

D. PREPARATION OF FLUOROANTIMONATES(III)

(i) $[Sb_5F_{19}^{4-}]$, $[Sb_4F_{13}^{-}]$, $[Sb_3F_{10}^{-}]$, $H_6N_2[SbF_5^{2-}]$, and $[SbClF_3^{-}]$

The salts containing the fluoroantimonate anions $[Sb_5F_{19}^{4-}]$, $[Sb_4F_{13}^{-}]$, $[Sb_3F_{10}^{-}]$, $H_6N_2[SbF_5^{2-}]$, and $[SbClF_3^{-}]$ were prepared and supplied by Robert Fourcade and Guy Mascherpa.[10] All of these compounds have been characterized by chemical analysis, infrared and Raman spectroscopy, and X-ray crystallography.[6,7,10,15,17]

(ii) $M_2[SbF_5]$, where M = Na or K

The sodium[11] and potassium[5] salts were prepared by first dissolving Sb_2O_3 in a minimum amount of aqueous HF and slowly adding Na_2CO_3 or K_2CO_3 to this hot solution. More HF was added to dissolve the solid material formed. The solution was left to digest on a steam bath, and eventually evaporated to dryness. The products were recrystallized three

times from water at 100°C.

[$Na_2[SbF_5]$. Calc: Sb, 46.34; found: Sb, 46.59.]

[$K_2[SbF_5]$: Calc: Sb, 41.28; found: Sb, 41.43.]

(iii) $Na[SbF_4]$

This salt was prepared earlier by B. Della Valle.[99]

E. PREPARATION OF CHLORO, BROMO, AND IODOANTIMONATES(III)

(i) $[R_4N][SbX_4]$, where X = Cl, Br, I, and R = C_2H_5 or C_4H_9

The chloro, bromo and iodoantimonates(III) were prepared by mixing stoichiometric amounts of SbX_3 and R_4NX in solutions of HX as described by Ahlijah and Goldstein.[20] The products were characterized by their melting points, and Raman spectroscopy.

[$[(C_2H_5)_4N][SbCl_4]$: m.p., 149-151°; major Raman bands, 330(s), 294(m).]

[$[(n\text{-}C_4H_9)_4N][SbBr_4]$: m.p., 111-113°; major Raman bands, 220(s), 180(m).]

(ii) $[C_5H_5NH][SbCl_4]$

This compound was prepared by the same procedure as described by Ahlijah and Goldstein.[20] The white product was characterized by its melting point and Raman spectroscopy.

[$[C_5H_5NH][SbCl_4]$: m.p., 174-176°; major Raman bands, 331(s), 300(m).]

(iii) $[(nC_4H_9)_2NH_2][SbI_4]$

This compound was prepared by the method outlined by Whealy and Blackstock.[23] Sb_2O_3 dissolved in a minimum amount of HI was added to $(n\text{-}C_4H_9)_2NH$ dissolved in a minimum amount of HI resulting in the formation of a yellow precipitate. The precipitate was washed with isopropanol and diethyl-ether and recrystallized from a 1:1 acetone-isopropanol solution.

It was characterized by chemical analysis and its melting point.

[$[(n\text{-}C_4H_9)_2NH_2][SbI_4]$: m.p., 125.5-127°; calc.; Sb, 16.03; found, Sb, 15.73.]

(iv) $[n\text{-}C_4H_9NH_3]_3[SbI_5]$

A similar procedure was used to prepare this compound.[23] The yellow product was characterized by chemical analysis and its melting point.

[$[n\text{-}C_4H_9NH_3]_3[SbI_5]$: calc., Sb, 13.45; found, Sb, 13.45; m.p. ~ 210°C (decomposition).]

(v) $[Co(NH_3)_6][Sb_2F_9]$

This compound was prepared and supplied by Moffat and Milne.[13] The sample was characterized by chemical analysis and X-ray crystallography.[29]

(vi) $Cs_3[Sb_2X_9]$, where X = Cl, Br and I

The chloro,[100] bromo and iodo[101] compounds were prepared by mixing stoichiometric amounts of SbX_3 and Cs_2CO_3 in concentrated HX solution. The mixtures were stirred for 18-20 hours and the precipitates were separated and washed with diethyl-ether. The products were characterized by chemical analysis.

[$Cs_3[Sb_2Cl_9]$: calc., Sb, 25.33; found, Sb, 25.62.]

[$Cs_3[Sb_2Br_9]$: calc., Sb, 17.89; found, Sb, 17.82.]

[$Cs_3[Sb_2I_9]$: calc., Sb, 13.65; found, Sb, 13.54.]

(vii) $[i\text{-}C_4H_9NH_3]_3[Sb_2Cl_9]$

A stoichiometric amount of $SbCl_3$ dissolved in concentrated HCl

was mixed with 1-butylamine dissolved in concentrated HCl. A vigorous reaction resulted in the formation of a white product. Diethyl-ether was added to dissolve the precipitate and the vessel was left overnight on a steam bath. The product was identified by chemical analysis. [$[i\text{-}C_4H_9NH_3]_3[Sb_2Cl_9]$: calc., Sb, 31.02; found, Sb, 30.86.]

(viii) $\underline{[C_5H_5NH]_5[Sb_2Br_9]Br_2}$

The compound was prepared by addition of pyridine to a solution of $SbBr_3$ dissolved in concentrated HBr as outlined by Porter and Jacobson.[19] The product melted at 219-220°C which was the same as the literature value.

(ix) $\underline{[(CH_3)_4N]_3[Sb_2Br_9]Br_2}$

This compound was prepared by the method described by Hubbard and Jacobson[26] which involved the reaction of $SbBr_3$ and $(CH_3)_4NBr$ dissolved in concentrated HBr with Br_2 (10:1). The red product which had been previously characterized by X-ray crystallography[26] was stored over H_2SO_4 with a partial pressure of Br_2.

(x) $\underline{[i\text{-}C_4H_9NH_3]_3[Sb_2I_9]}$

The procedure described by Whealy and Blackstock[23] was used. The product decomposed before melting and was characterized by chemical analysis.

[$[i\text{-}C_4H_9NH_3]_3[Sb_2I_9]$: calc., Sb, 15.14; found, Sb, 14.91.]

F. PREPARATION OF ANTIMONY(V) CHLORIDE FLUORIDES

(i) $\underline{SbCl_4F}$

In a typical experiment, $SbCl_5$ was reacted with an excess of AsF_3.[37]

The mixture was refluxed for 30 minutes at 70-80°C. When the excess AsF_3 and the $AsCl_3$ produced by the reaction were removed, a colourless oil remained. Dry SO_2 (~ 20 mls) was condensed into the vessel and a solid precipitate was produced by rapidly distilling the SO_2 at a reduced temperature from the reaction vessel. The solid product was vacuum sublimed at 40°C. The sublimate was a pale yellow powder which melted at 80-81.5°C. The sample was identified by its Raman spectrum[97] and by chemical analysis.

[$SbCl_4F$: calc., Sb, 43.06; F, 6.72; Cl, 50.22; found, Sb, 43.92; F, 7.14; Cl, 42.42.]

(ii) $SbCl_3F_2$

0.719 gms of $SbCl_4F$ were added to one side of the reaction vessel, shown in Figure 2.1.a, which had been previously dried on the vacuum line. 0.206 gms of SbF_5 were added to the other side of the reaction vessel. All manipulations were performed in the glove-box. SO_2 was distilled onto the SbF_5 at -196°C. All the SbF_5 dissolved when the vessel was warmed to room temperature. The solution of SbF_5 in SO_2 was then added to the $SbCl_4F$ which slowly dissolved and the resultant solution was stirred overnight. A solid, which resulted on evaporation of the SO_2, was washed with SO_2, dried, then vacuum sublimed at 40°C to yield a white powder melting at 62-64°C. A quantity of the product was sealed in an evacuated quartz capillary tube. Single crystals were prepared by sublimation following application of a temperature gradient. The product was characterized by X-ray crystallography and Raman spectroscopy (Chapter Five).

(iii) $\underline{Sb_3Cl_{10.75}F_{4.25}}$

In another attempted preparation of SbF_2Cl_3, 6.73 gms of SbF_5 and 6 ml of $SbCl_5$ were added to opposite sides of the same reaction vessel. This yielded a reaction mixture ratio of $SbCl_5/SbF_5$ of slightly greater than 3/2. All manipulations, except the weighings, were carried out in the glove-box. SO_2 was condensed onto the SbF_5 at -196°C and, when allowed to warm, the SbF_5 dissolved completely. The SbF_5/SO_2 solution was slowly added to the $SbCl_5$ and the mixture was stirred overnight. A white precipitate, partially soluble in SO_2, appeared. This precipitate was isolated and washed with SO_2. The white powder was dried and vacuum sublimed at 20°C. Single crystals were prepared by subliming the material in a quartz capillary tube. The sublimate melted at 64-69°C. The analytical data were as follows: found: Sb, 45.71%; F, 11.57%; Cl, 41.11%.

[$Sb_3Cl_9F_6$: calc., Sb, 45.73; Cl, 40.00; F, 14.27.

$Sb_3Cl_{10}F_5$: calc., Sb, 44.80; Cl, 43.54; F, 11.65.

$Sb_3Cl_{11}F_4$: calc., Sb, 43.91; Cl, 46.95; F, 9.14.]

Neutron activation analysis yielded an antimony:chlorine ratio of 1:3.04.

(iv) $\underline{SbCl_2F_3}$

A reaction first studied by Kolditz and Leith[38] was used to prepare $SbCl_2F_3$. The SbF_3 was transferred to a reaction vessel in the glove-box. The reaction vessel was then placed in a stainless steel bomb, previously dried on the vacuum line. An excess of pure chlorine was added and the bomb was heated to 110-120°C for two hours with occasional shaking. The oily product slowly crystallized at room temperature.

The crystalline material was sublimed at 50°C yielding a white solid which melted at 49-53°C. A portion of the sublimed material was sealed in a quartz capillary and single crystals were grown by application of a temperature gradient.

[$SbCl_2F_3$: calc., Sb, 48.75; F, 22.82; Cl, 28.43; found, Sb, 49.89; F, 21.71; Cl, 26.35.]

Neutron activation analysis gave a Sb:Cl ratio of 1:2.0.

(v) $Sb_3Cl_4F_{11}$

A weighed amount of $SbCl_4F$ (0.656 gms) was transferred to a dry reaction vessel in the glove-box. A stoichiometric amount of SbF_5 was added to the other half of the reaction vessel in the glove-box. A method similar to that outlined earlier for $SbCl_3F_2$ was employed. All the $SbCl_4F$ appeared to have reacted after several minutes. When SO_2 was distilled from the reaction vessel, the resultant white powder was sublimed at 80°C. The sublimate melted at 81-82°C.

[$Sb_3Cl_4F_{11}$: calc., Sb, 51.00; F, 29.18; Cl, 19.83; found, Sb, 50.38; F, 28.92; Cl, 20.90.]

(vi) Attempted preparation of $SbClF_4$

Two separate attempts were made to prepare $SbClF_4$, both of which were carried out in liquid SO_2. The first reaction used a stoichiometric mixture of SbF_5 and $SbCl_5$ which produced a white product when the SO_2 was removed by distillation. Raman analysis of the white solid showed significant bands at 661 cm^{-1}, 643 cm^{-1} and 1085 cm^{-1} which suggested the presence of $SbF_5 \cdot SO_2$ (Chapter Seven), indicating that SbF_5 was in excess. When the SbF_5 was washed out of the white product, the Raman and Mössbauer

spectra, and the melting point indicated that the remaining product was $Sb_3Cl_4F_{11}$. A second attempt involving a stoichiometric mixture of $SbCl_4F$ and SbF_5 gave the same result. It appears that, in the SO_2 system described, $Sb_3Cl_4F_{11}$ is preferentially formed along with the excess SbF_5.

(vii) $\underline{SbCl_4F \cdot MF_5 \ (M = Sb, As, Nb)}$

$SbCl_4F$ was reacted with three Lewis acids in an attempt to prepare 1:1 adducts. $SbCl_4F$ (≈ 1.0 gms) was added to a previously dried reaction vessel in a glove-box. A stoichiometric amount of the appropriate Lewis acid was added. The acid was first dissolved in SO_2 and this solution was added to the $SbCl_4F$. The reaction was left stirring overnight. SO_2 was distilled from the vessel and the resultant white products were washed several times and dried. The SbF_5 and NbF_5 were weighed out during additions in a glove-box, but the AsF_5 was added on a calibrated vacuum line and distilled onto the weighed $SbCl_4F$. The melting point of the adducts $SbCl_4F \cdot SbF_5$ and $SbCl_4F \cdot NbF_5$ were 48-52°C and 55-57°C, respectively. The adduct, $SbCl_4F \cdot AsF_5$, decomposed before melting. The compounds were examined by Raman and Mössbauer spectroscopy (Chapter Five).

G. PREPARATION OF CHLORIDE FLUORIDE ANTIMONATES(V)

(i) $\underline{M[SbCl_6], \text{ where } M = Na \text{ or } K}$

The sodium and potassium hexachloride salts were prepared by reacting stoichiometric mixtures of $SbCl_5$ with the appropriate alkali metal chloride in SO_2. The mixture was allowed to stir at room temperature for twelve hours. The soluble product was separated, washed with SO_2, and dried. The resultant white solid was characterized by Raman spectroscopy.[48]

(ii) $Na[SbCl_4F_2]$

The sodium salt was prepared by reacting NaF with a stoichiometric amount of $SbCl_4F$. All manipulations were carried out in the glove-box except for the weighings. The $SbCl_4F$ was dissolved in SO_2 and the solution was added to the NaF. The product was soluble in SO_2 and was isolated by first filtering off any unreacted NaF and then removing the SO_2 by distillation. The white powder which remained was washed with SO_2 and the sample was pumped to dryness. A small impurity of $Na[SbCl_6]$ was often found in the sample as was demonstrated from its characteristic Raman spectrum, ν_1 = 331 cm^{-1}. It was usually not possible to separate all the $Na[SbCl_6]$ from the sample, but most was removed by extraction with SO_2.

(iii) $Na[SbCl_2F_4]$

This salt was prepared by the method of Müller et al.[50] in which SbF_5 was reacted with NaCl in liquid SO_2 at -10°C to -15°C. After SbF_5 had dissolved in the SO_2, a stoichiometric amount of NaCl was added and a white precipitate formed immediately. The mixture was allowed to stir for 24 hours. The white precipitate was removed and washed several times. This precipitate was later identifed as $Na[SbF_6]$ by Raman[102] and Mössbauer spectroscopy.[103] When SO_2 was distilled from the remaining solution, a white precipitate which was soluble in SO_2 remained. This product was washed several times with small amounts of SO_2 and subsequently dried. The precipitate was deduced to be a mixture of $Na[SbCl_2F]$ and $Na[SbCl_4F_2]$ from the Raman and Mössbauer spectra (Chapter Six).

(iv) $M[SbF_6]$, where M = K or Cs

The hexafluoroantimonates of potassium and caesium were prepared by reaction of SbF_5 and a stoichiometric amount of the appropriate fluoride in liquid SO_2. The white insoluble product was filtered, washed several times with SO_2, and dried. The samples were characterized by Raman spectroscopy.[102]

(v) Attempted Preparations of $Na[SbCl_5F]$, $Na[SbCl_3F_3]$ and $Na[SbClF_5]$.

Stoichiometric mixtures of the appropriate antimony chloride fluoride and the alkali metal salt in liquid SO_2 resulted in a mixture of the salts identified earlier. None of the above salts could be obtained by the method prescribed.

H. PREPARATION OF ANTIMONY(V) CHLORIDE AND FLUORIDE ADDUCTS AND COMPLEX ANIONS

(i) $SbF_5 \cdot SO_2$

This complex was prepared by the method previously described by Peacock et al.[65] The product was soluble in SO_2 and it was isolated by removing the excess SO_2 by distillation. The white crystalline product was then sublimed to a side arm, Figure 2.6, and the product was dried by removing the excess SO_2 at 0°C. The white crystalline material which melted at 65-68°C was then sealed off under a vacuum at 0°C.

(ii) $SbF_5 \cdot AsF_3$

The preparation was previously described by Woolf and Greenwood.[59] Since the complex decomposed on pumping at room temperature, a similar procedure was used to separate the product from the unreacted starting

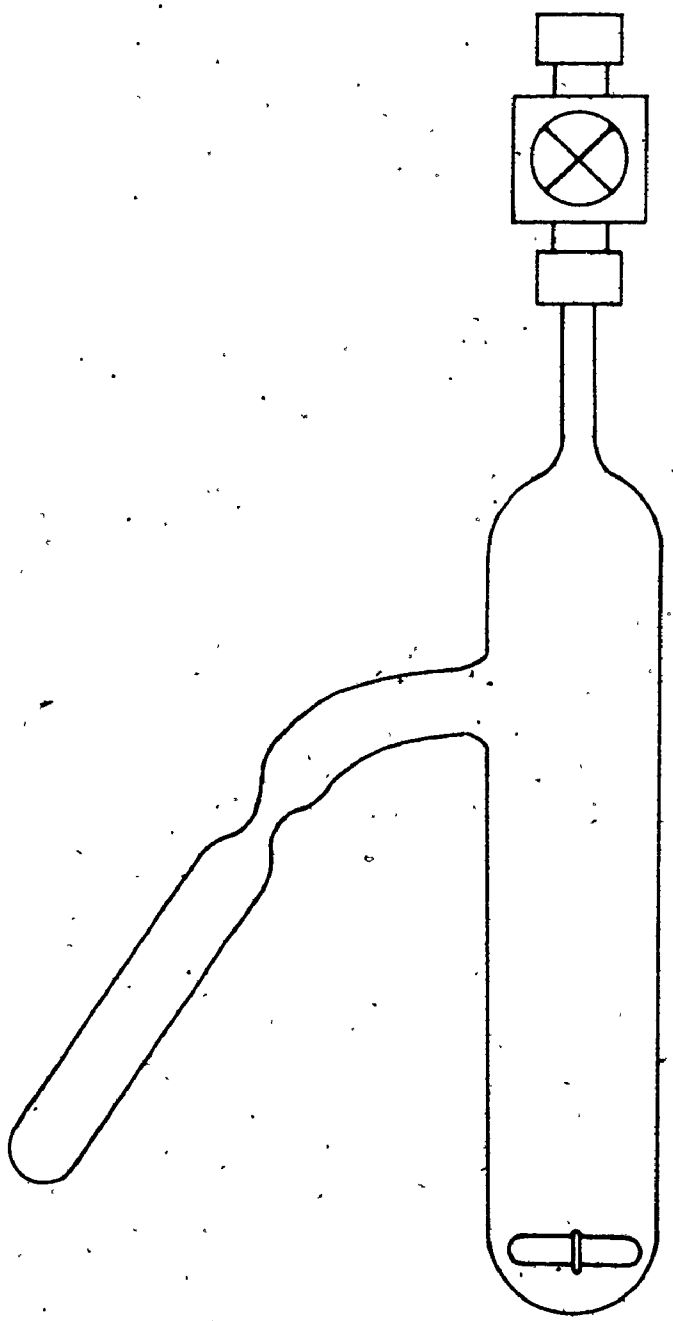

Figure 2.6. Reaction Vessel used to Prepare $SbF_5 \cdot SO_2$ and $SbF_5 \cdot AsF_3$ Adducts.

materials as described in 2.H(i). The excess AsF_3 was distilled from the arm of the vessel, Figure 2.6, at 0°C. The white product decomposed at 36°C. The product was identified by Raman spectroscopy.[60]

(iii) $SbF_5 \cdot SbF_3$

The complex described earlier by Birchall et al.[60] prepared from SbF_3 and a large excess of SbF_5 in SO_2 was reprepared. The product was insoluble in liquid SO_2 and easily separated, washed, and dried. The white powder was identified by Raman spectroscopy as $SbF_5 \cdot SbF_3$(A).[60]

(iv) $[Sb_2F_4][SbF_6]_2$

This compound, supplied by Gillespie et al., was identified by X-ray crystallography.[63]

(v) Complexes containing the $[Sb_3F_{14}^-]$ ion

Two compounds, $[Te_2Se_2][Sb_3F_{14}][SbF_6]$ and $[Te_{3\ 1/3}Se_{2/3}][Sb_3F_{14}][SbF_6]$ were supplied by Gillespie et al.[64] These compounds were identified by X-ray crystallography.

(vi) SbX_5/graphite, where X = F or Cl

Both SbF_5 and $SbCl_5$ were heated in the presence of dry graphite in a sealed pyrex flask as described by Lalancette and Lafontaine.[55] The products were dry graphite-like powders which contained 65% and 20% by weight SbX_5. Although the Lewis acids, SbF_5 and $SbCl_5$, hydrolyze rapidly in air, the SbX_5/graphite adducts were unaffected on exposure to the atmosphere for several hours.

CHAPTER THREE

^{121}Sb MÖSSBAUER STUDIES OF FLUOROANTIMONATES(III)

A. INTRODUCTION

Fluoroantimonate(III) anions are now known for the following $SbF_3 \cdot MF$ ratios: 4:1, $[Sb_4F_{13}^-]$; 3:1, $[Sb_3F_{10}^-]$; 2:1 $[Sb_2F_7^-]$; 5:4, $[Sb_5F_{19}^{4-}]$; 1:1, $[SbF_4^-]$; and, 1:2, $[SbF_5^{2-}]$, where M represents a variety of alkali metal, thallium, ammonium, or hydrazinium cations. The structures of most of these antimony(III) salts have been reported in the literature.[1-12,17] Byström and coworkers[1-5] were the first group to examine the structures of these fluoroantimonates(III) by X-ray crystallography. Since these early investigations, the structures of several more fluoroanions were reported by Ryan et al.[8,9,12] More recently, Mascherpa et al.[10,11] re-examined a number of these earlier structures, isolated a number of new compounds containing more complex anions such as $[Sb_3F_{10}^-]$ and $[Sb_4F_{13}^-]$, and reported their crystal structures.[6,7,10] Ryan et al.[8,9] discovered that the geometry of the $[Sb_2F_7^-]$ anion was dependent upon the counter ion. Mascherpa et al.[15,104,105] concluded from their infrared and Raman investigation that the structure obtained for a given $SbF_3:F^-$ ratio was often dependent on the cation. Representations of the structures of some of the fluoroanions discussed in this chapter are depicted in Figure 3.1. Some of the significant bond lengths and bond angles are included to more clearly demonstrate the geometries of these anions.

Crystallographic evidence has recently been reported for a number

Figure 3.1. Structural Representations of the Antimony Environments in SbF_3 and the Fluoroantimonate(III) Salts.

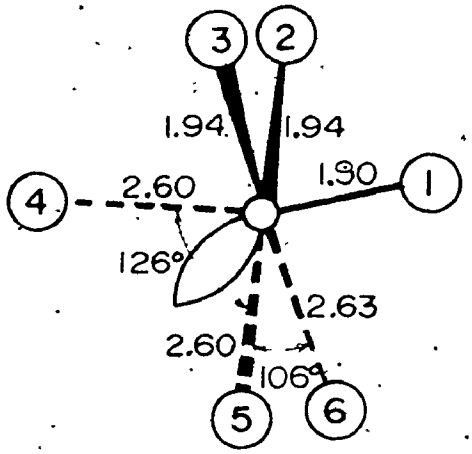

SbF_3

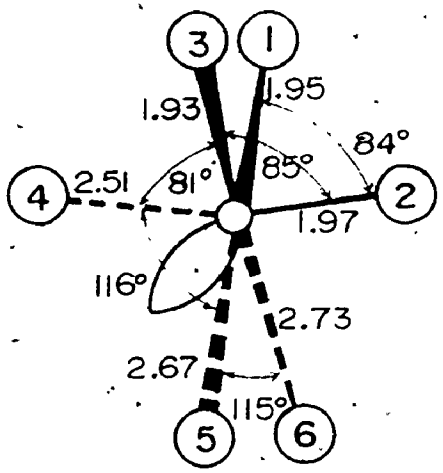

KSb_4F_{13}

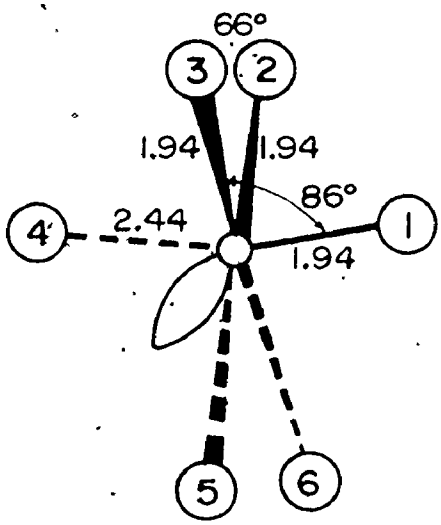

$NH_4Sb_3F_{10}$

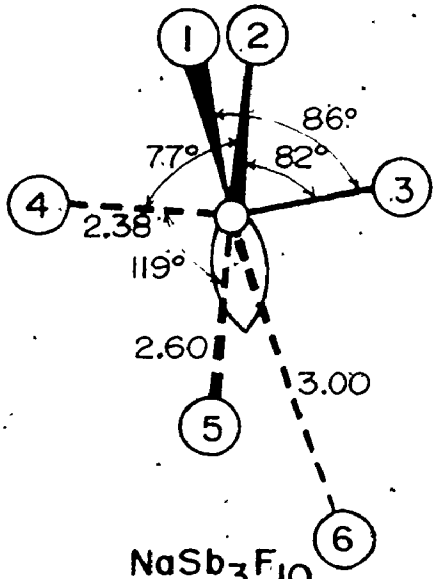

$NaSb_3F_{10}$

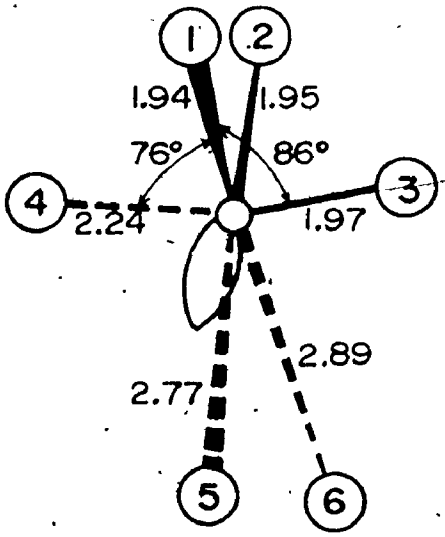

$CsSb_2F_7$

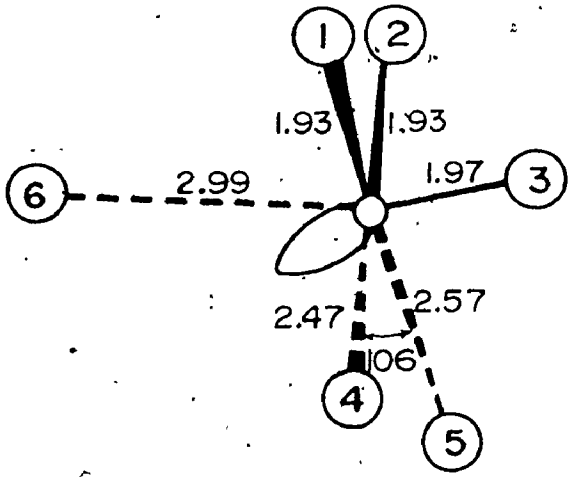

$Sb_{(2)}$ of KSb_2F_7

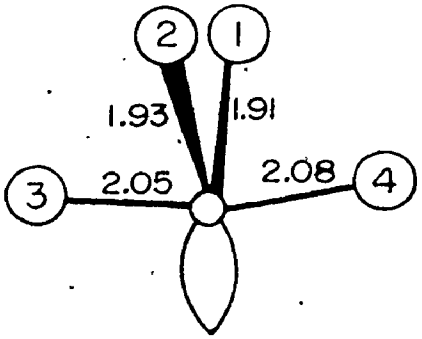

$Sb_{(1)}$ of KSb_2F_7

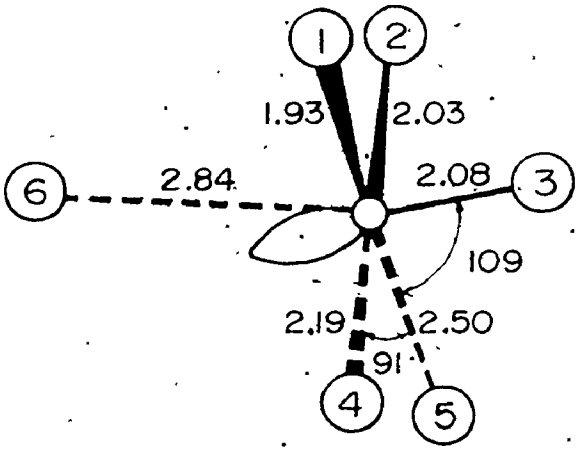

$NaSbF_4$

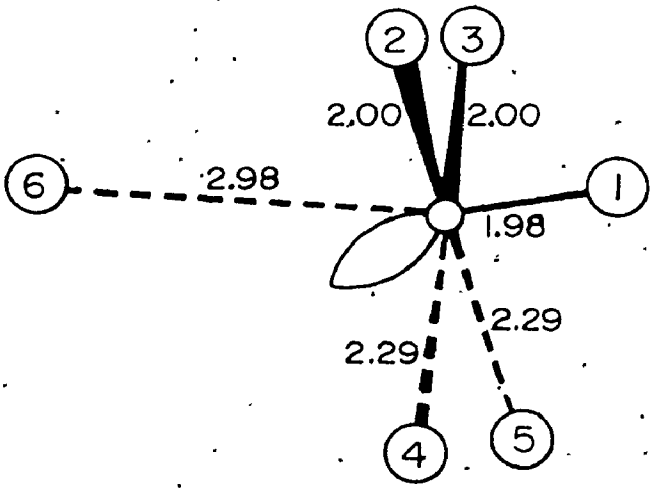

$Sb_{(1)}$ of $KSbF_4$

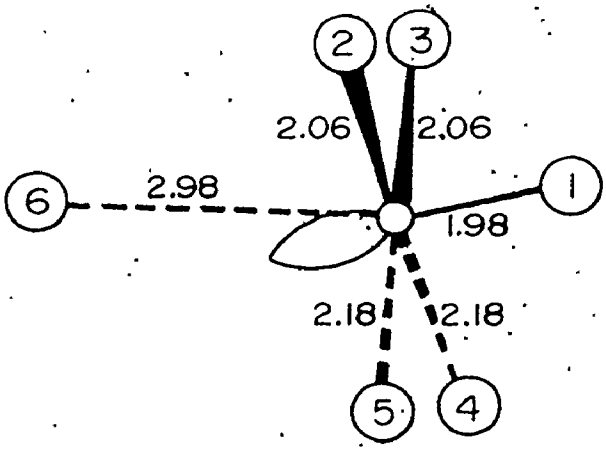

$Sb_{(2)}$ of $KSbF_4$

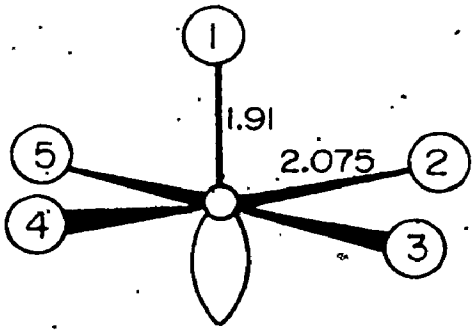

$(NH_4)_2SbF_5$

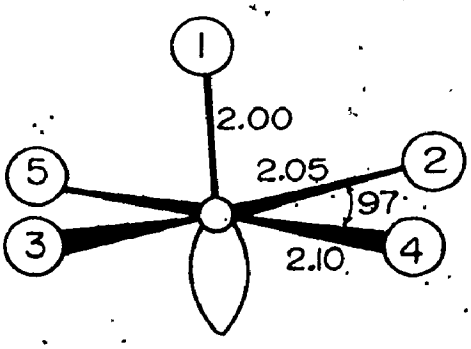

Na_2SbF_5

of analogous mixed chloride fluoride anions.[10,17] A structural representation of the environment of the antimony atom of $K[SbClF_3]$ is presented in Figure 3.2.

^{121}Sb Mössbauer data have been previously reported for salts of $[Sb_2F_7^-]$, $[SbF_4^-]$ and $[SbF_5^{2-}]$,[99,106] and attempts were made to interpret these results in terms of known structures. The interpretations of isomer shift data for these fluoroantimonates(III) were based on the assumption that, apart from SbF_3, the antimony is six coordinate or lower; the geometry being described as AX_5E, or AX_4E according to V.S.E.P.R. theory.[28] Recently published crystallographic data have prompted this re-examination of some of the earlier Mössbauer results, and the investigation of the salts containing complex fluoride anions. ^{121}Sb Mössbauer data are also presented for a number of $[SbClF_3^-]$ salts. Attempts are made to correlate the isomer shift and quadrupole coupling data for the fluoroantimonates(III) presented in this chapter with available structural data.

B. RESULTS AND DISCUSSION

The Mössbauer data for these fluoroantimonates(III) are listed in Table 3.1. This Table includes data for the new fluoroanions and chloride fluoride anions recorded at 4°K. In addition, this Table contains data for SbF_3, $M[SbF_4]$, $M[Sb_2F_7]$, and $M[SbF_5]$, which have already been reported,[106,77] together with our data for SbF_3, $Na[SbF_4]$, $Na_2[SbF_5]$, and $K_2[SbF_5]$. Examination of these results reveals a general increase in isomer shift from $[Sb_4F_{13}^-]$ through to $[SbF_5^{2-}]$, the latter having the most positive isomer shift. Within this series there are exceptions to

Figure 3.2. Structural Representation of the Antimony Environment in $KSbClF_3$.

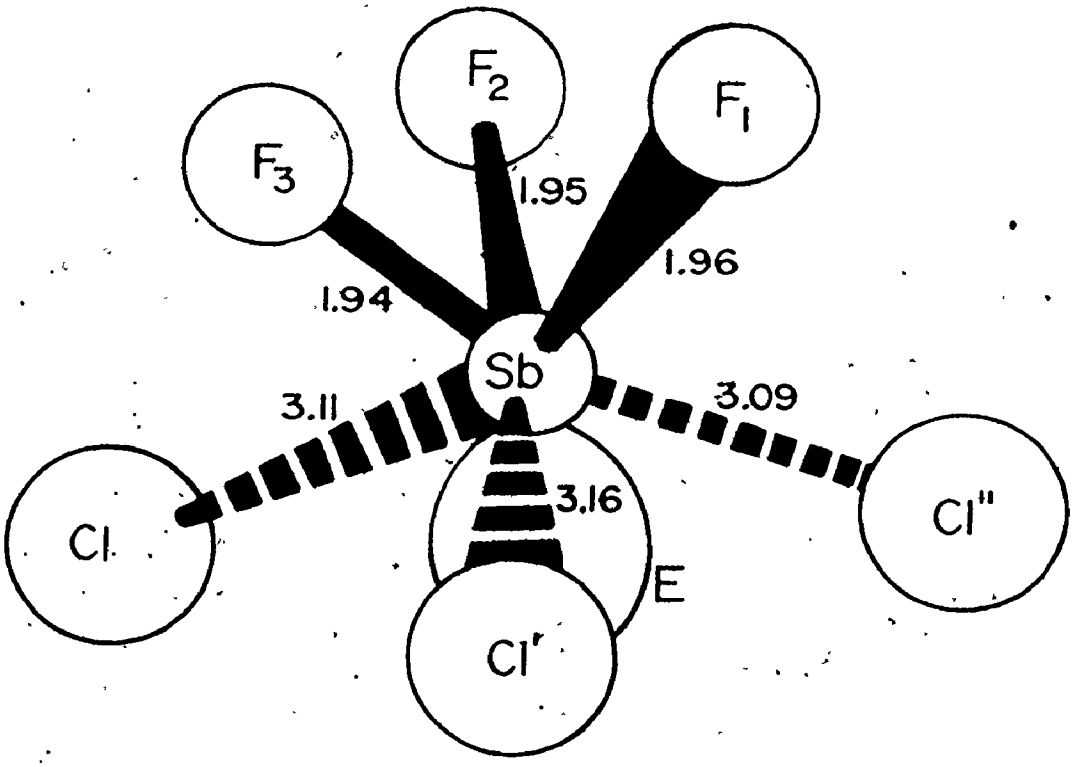
F2
F1
F3
1.95
1.96
1.94
Sb
3.11
3.09
3.16
Cl
Cl''
E
Cl'

this trend. These are discussed in more detail in relation to the specific structure of the fluoroanion.

The antimony atom in SbF_3 is surrounded by six fluorine atoms, three of which are at 1.92 Å and three at 2.64 Å [18] forming a distorted octahedral arrangement. The three nearest fluorine atom neighbours have mean F-Sb-F' angles of 87.3°. Edwards[18] suggested that the distortion from octahedral coordination can be correlated with the presence of a lone pair of electrons on antimony occupying a seventh coordination site. This environment has been described as AX_6E, a monocapped octahedron (3.3.1),[28] and is shown in Figure 3.1.

In the recently reported crystallographic data[6-12] for the fluoroantimonates(III), strong evidence was presented which indicated that the AX_6E, monocapped octahedral, configuration is the predominant geometry in these fluoroanions. It can be seen from Figure 3.1 that only two of these fluorine salts contain anions with a geometry other than AX_6E. The $[SbF_5^{2-}]$ anion provides an excellent example of a distorted octahedral arrangement involving a lone pair and five bond pairs, or AX_5E geometry. In addition, one antimony site of $K[Sb_2F_7]$ has distorted AX_4E geometry with four fluorines, and a lone pair which occupies the equatorial position of the trigonal bipyramid.

All of the anions depicted in Table 3.1 involve a stereochemically active lone pair of electrons implying participation of the 5s electrons in the bonding. The isomer shift of the Sb(III) complexes is strongly influenced by these electrons. Since the $\frac{\Delta R}{R}$ term in the isomer shift expression (Chapter One) is negative, an increase in isomer shift indicates

a decrease in s electron density about this nucleus. This decrease may result from two effects. Firstly, the 5s electrons can be effectively removed from the vicinity of the nucleus by increased participation in the Sb-X bonds. However, the resultant change in isomer shift to a more positive value occurs concurrently with an increasingly distorted antimony environment. This distortion, resulting from the presence of a lone pair, produces a quadrupole split spectrum. Secondly, the s electron density at the nucleus is reduced when shielded by p or d electrons. With an increase in strength of an Sb-X bond comprised of p and/or d orbitals, and a subsequent shortening of the bond, the s electrons become more shielded. If the Sb-X bonds about a particular antimony nucleus are unequal, a distorted electronic environment is generated, resulting in a quadrupole split spectrum. The quadrupole coupling constant resulting from this type of distortion is generally smaller than that resulting from the participation of the 5s electrons in the bonding. The magnitudes of both the isomer shift and quadrupole splitting parameters of all the compounds presented in Table 3.1 are consistent with a stereochemically active 5s electron pair.

The quadrupole coupling constants for all of the salts listed in Table 3.1 are large and positive. Since Q for ^{121}Sb is negative, the sign of V_{ZZ} must also be negative implying a concentration of charge along the symmetry axis. Since the lone pair provides a dominant negative contribution to the principle component of the electric field gradient tensor, the direction would be through the lone pair. This is clearly consistent with the proposed geometries of the various ions

shown in Figure 3.1. Only for the Sb_1 site in $K[Sb_2F_7]$ should eQV_{ZZ} be negative.

⇒ Some of the spectra listed in Table 3.1 were fitted to an eight line pattern using the Cranshaw transmission integral function,[91] modified to include η as a variable. If the axis of maximum electron density in these antimony(III) fluorides includes the stereochemically active lone pair, an η value greater than zero results from an asymmetry about this axis. That is, $(\frac{V_{XX} - V_{YY}}{V_{ZZ}})$ does not equal zero, where V represents the component of the electric field in the x, y or z direction.

Comparing the isomer shift for structurally related compounds, one notes a general increase to more positive values as the ratio of $SbF_3:F^-$ approaches 1:1. Hence, the s electron density at the antimony decreases as the negative charge per antimony atom approaches one. Presumably, this increase in negative charge per antimony brings about an expansion of the orbital wave function and results in the observed decrease in s electron density at the nucleus. As the negative charge per Sb increases, one also notes that one secondary Sb---F bond becomes quite long under the influence of the lone pair. At the same time, one of the secondary bond lengths decreases. At $[SbF_5^{2-}]$, the lone pair has expanded to such a degree that one fluorine is completely displaced. The 5s electrons are now shared almost equally between five fluorines, rather than six, and the $M_2[SbF_5]$ salts have the lowest s electron density at the antimony nucleus. A similar trend is observed in a Sn(II) fluoride study, although the $\frac{\Delta R}{R}$ term for ^{119}Sn is positive and a decrease in s electron density resulted in a decrease in isomer shift, i.e., to more negative values.

The stereochemistries about the antimony atom in $[Sb_4F_{13}^-]$ [6] and in SbF_3 [18] are very similar (Figure 3.1) except that in SbF_3 all the fluorines are involved in symmetric Sb-F-Sb' bridges, whereas in $[Sb_4F_{13}^-]$ there is one purely terminal Sb-F bond and another fluorine is tetrahedrally coordinated by four antimony atoms. The latter Sb-F bond length is 2.51 Å. Since there is little change in isomer shift between SbF_3 and $[Sb_4F_{13}^-]$, it seems reasonable to infer that the differences in bond length, i.e., one shorter secondary bond and one longer secondary bond, are self-compensating. The third secondary bond is essentially unchanged. One must conclude that the small changes observed for these secondary Sb---F bonds, that is, the fluorines supplying largely p-electrons, have no overall effect on the s electron density at the antimony nucleus. The lower 5s electron density for the caesium salt could be a result of the differing size of the cation. Similar changes in isomer shift have been noted previously for Sn(II) fluoride[107] systems, as a result of differing cation-anion interactions. The smaller quadrupole coupling constants noted for $[Sb_4F_{13}^-]$ compared to SbF_3, are possibly the result of a positive contribution by V_{ZZ}(lattice) resulting from the asymmetric distribution of cations about each antimony. V_{ZZ}(ion) is negative in each of these cases.

The crystal structure of $Na[Sb_3F_{10}]$ has been reported.[7] In the anion of this salt, the negative charge of one $[F^-]$ ion is shared by three SbF_3 units as compared to four SbF_3 units in the $[Sb_4F_{13}^-]$ anion, and hence a reduction in 5s electron density because of the increased negative charge per antimony seems plausible. However, the isomer shift

values of the ammonium and thallium salts are essentially unchanged from $K[Sb_4F_{13}]$. The sodium salt, on the other hand, has a more negative isomer shift, i.e., a higher s-electron density. An examination of Figure 3.1 reveals that the environment about each antimony in the ammonium salt resembles that in $K[Sb_4F_{13}]$. Infrared and Raman evidence[15] indicates that the antimony atoms in $Tl[Sb_3F_{10}]$ also have similar environments. It would appear that the expected increase in isomer shift due to the increased negative charge per antimony is nullified by changes in the bond lengths. The sodium salt, however, has one very long Sb-F bond which will contribute little to shielding the 5s electrons from the antimony nucleus. Since the other Sb-F secondary bonds in $Na[Sb_3F_{10}]$ are only slightly shorter than those in the $[Tl^+]$, or $[NH_4^+]$ salts, the resultant 5s electron density is increased and the isomer shift decreased. The quadrupole coupling constants in the $[Sb_3F_{10}^-]$ salts are slightly larger than the previously mentioned $[Sb_4F_{13}^-]$ salts, suggesting that the electronic environments about the antimony nuclei are more asymmetric.

Some data reported earlier by Donaldson et al.,[106] for a number of salts containing the $[Sb_2F_7^-]$ anion, are included in Table 3.1. The isomer-shift difference between $K[Sb_2F_7]$ and $[NH_4^+]$ and $[Tl^+]$ salts is greater than can be explained by interionic interactions.[107] To begin with, there are gross structural differences between the potassium and the caesium salts. In the latter, there is only one antimony site and its isomer shift and quadrupole coupling values are in the range expected for the geometry represented in Figure 3.1, that is, an anion with near AX_6E geometry with an increased negative charge per antimony compared to

the previously-discussed anions. In $K[Sb_2F_7]$, there are two Sb sites, one of which has the AX_6E geometry and the other the AX_4E geometry. The former site should have an isomer shift value similar to that in $Cs[Sb_2F_7]$. The latter site, however, should have a more positive isomer shift. A closer examination of Figure 3.1 indicates that eQV_{ZZ} for these two sites should be of opposite sign. Neither of the earlier workers[99,106] were able to resolve the two sites. These facts would probably result in the anomalous data reported for $K[Sb_2F_7]$. Infrared data[105] for the $[Sb_2F_7^-]$ salts suggests the presence of three structural types: $K[Sb_2F_7]$; $Cs[Sb_2F_7]$; and, $NH_4[Sb_2F_7]$, $Rb[Sb_2F_7]$, and $Tl[Sb_2F_7]$. The latter three salts appear to be structurally similar according to the infrared data, but slightly different from those of the caesium or potassium salts. Mascherpa et al.[105] suggest that in the case of the $[NH_4^+]$, $[Rb^+]$, and $[Tl^+]$ salts, the $[Sb_2F_7^-]$ anion has a less symmetric Sb-F-Sb bridge than in the case of $Cs[Sb_2F_7]$, but more symmetric than that in $K[Sb_2F_7]$. The Mössbauer isomer shift and quadrupole coupling constant data for $[NH_4][Sb_2F_7]$ included in Table 3.1 suggest that the geometry about the antimony is not a great deal different than that in $Cs[Sb_2F_7]$, but it is, however, substantially different from the geometry reported for the potassium salt.

The ^{121}Sb Mössbauer parameters reported for $[NH_4]_4[Sb_5F_{19}]$ are consistent with an AX_6E geometry about each antimony. The isomer shift value is more positive than that reported for SbF_3 and $K[Sb_4F_{13}]$. This is probably the result of the increased charge per antimony nucleus. As well, the quadrupole coupling constant is comparable to the other

fluoroanions which have been shown to contain a stereochemically active lone pair.

The isomer shift data reported in this work for $Na[SbF_4]$ disagree with the value reported earlier by Donaldson et al.[106] The reason for this is unclear and the data should be re-examined. However, despite the fact that the sodium and potassium salts have quite different structures (Figure 3.1), Donaldson et al.[106] reported identical Mössbauer parameters. It is not obvious from an examination of Figure 3.1 that the s electron density about the antimony nuclei of the sodium and potassium salts should be dfferent. However, the shorter secondary bonds of both sites of the potassium salt may result in more p and d electron density at the antimony nucleus and a subsequent decrease in s electron density. This difference is not expected to be large since the average secondary and primary bond lengths are nearly the same in the two cases. While Mascherpa et al.[104] concluded from an infrared and Raman investigation, that the structures of the ammonium and potassium salts are similar, but different to that of the caesium salt, the comparable isomer shift data reported in Table 3.1 suggests that these structural variations do not substantially alter the electrostatic environment about the antimony nucleus.

For the $[SbF_5^{2-}]$ salts there are large differences in Mössbauer parameters from the sodium to the hydrazinium salts and discrepancies between the current work and those reported by Donaldson et al.[106] All of these salts are isostructural except for the sodium salt,[5,10,11,12] but all have AX_5E geometry. The sodium salt has been reported by Mascherpa et al.[11] to be slightly distorted from a regular square pyramid.

This distortion was attributed to cation-anion interactions and presumably alters the s electron density at the antimony nucleus, producing a more negative isomer shift than recorded for the potassium, caesium, and ammonium salts. The current work gives similar values for the quadrupole coupling constants for $Na_2[SbF_5]$ and $K_2[SbF_5]$ in contrast to the previous workers,[106] who reported eQV_{ZZ} values that are of opposite sign for these two salts. The Mössbauer spectrum of $Na_2[SbF_5]$, reported here, is shown in Figure 3.3. If the quadrupole coupling constant were negative, as suggested by Donaldson et al.,[106] the distorted absorption band would tail off to positive velocities rather than to negative velocities as shown in Figure 3.3. A more negative isomer shift is observed for the hydrazinium salt and this suggests a higher s electron density at the antimony nucleus than found for the other salts. Presumably, this is the result of a reduction of the double negative charge on the anion by a strong hydrogen-bonded interaction with the hydrazinium dication.

The magnitudes of the quadrupole coupling constants for the compounds reported here are all approximately 18 mm/sec and the relatively small variations are probably due to the minor structural changes indicated in Figure 3.1, most of which have been discussed previously. Although χ^2 is good for the present computer fitting procedure, the misfit criterion[108] indicates that the spectra are not as good as they appear. A value for $M \leq 0.1$ indicates that the data from the fitted spectrum are extremely reliable. The parameter most affected by poor data is eQV_{ZZ} and, hence, a large error has been placed on the quadrupole

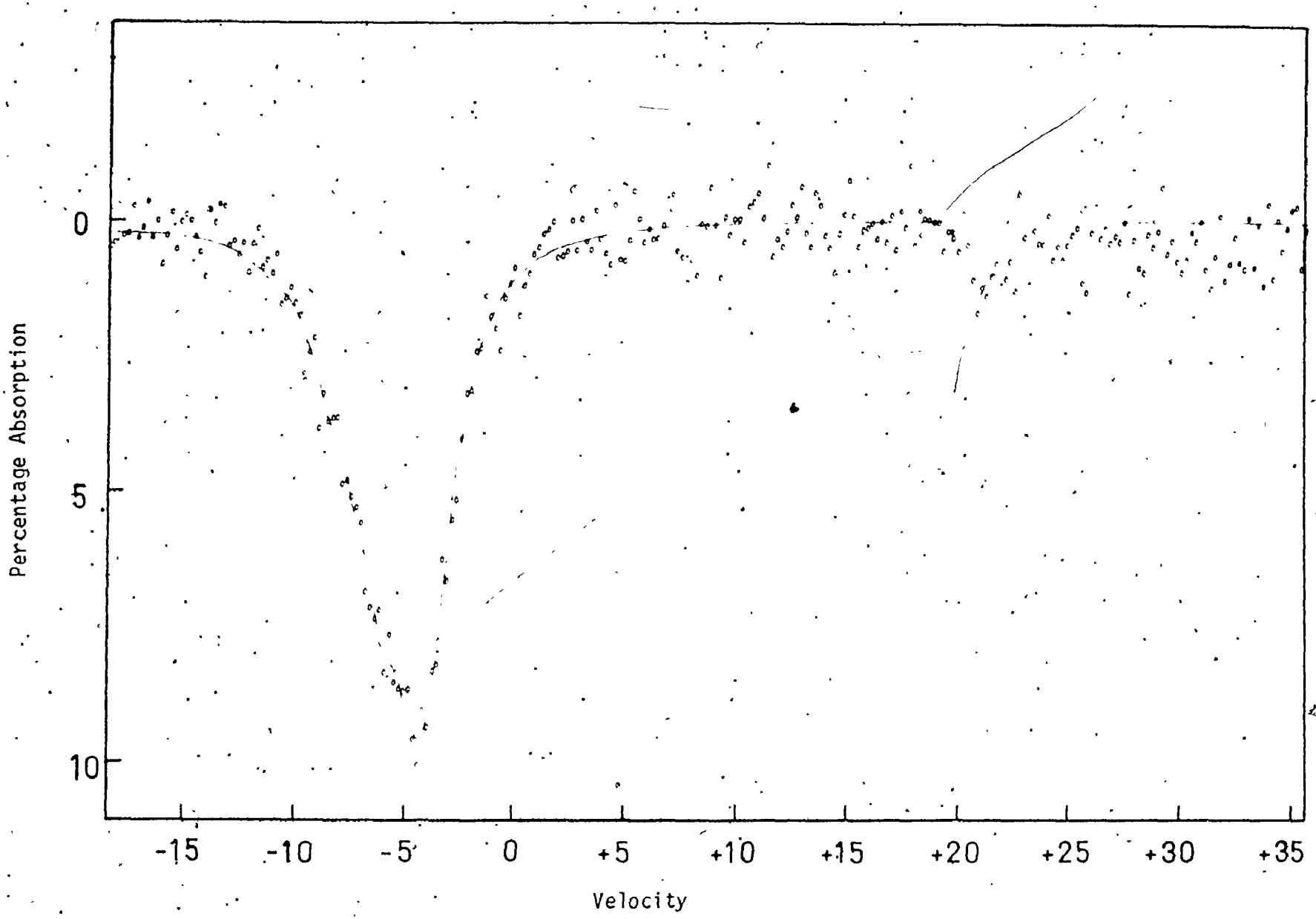

Figure 3.3: ^{121}Sb Mössbauer Spectrum of $Na_2[SbF_5]$ at 4°K.

coupling values.

Most of the spectra were fitted to an η value of zero. Of the data listed in Table 3.1, only that for the SbF_3 and $[NH_4][Sb_3F_{10}]$ salt did the goodness of fit criteria appear significantly better if η was greater than zero. The Mössbauer spectrum of SbF_3 fitted with an η value greater than zero is shown in Figure 3.4. This spectrum is fitted using the Cranshaw transmission integral[91] which allowed for the finite thickness of the sample. The parameters obtained from this analysis were not identical to those reported earlier by Ruby et al.[77] Presumably these differences arise from the different fitting routines employed. If, as mentioned earlier, the symmetry axis is through the lone pair orbital in SbF_3, a finite η value implies asymmetry about this axis. This asymmetry is not obvious from Figure 3.1 since the symmetry axis appears to be coincident with the C_3 axis of the anion. Although a finite η value was also fitted for $[NH_4][Sb_3F_{10}]$, it is difficult to relate this value to any asymmetry in the anion since all the angles and bond lengths of this complex are not known. The asymmetry parameters of $Na[Sb_3F_{10}]$ and $Tl[Sb_3F_{10}]$ are 0.16 and 0.14, respectively. These parameters also infer asymmetry about the principle axis. The η values for the remainder of the salts listed in Table 3.1 are zero except for $[NH_4][Sb_5F_{19}]$. Unfortunately, no structural data is available for this compound.

In each of the salts listed in Table 3.1, which have an anion with AX_6E geometry, the primary Sb-F bonds form a regular pyramidal arrangement with F-Sb-F' angles of approximately 86° and Sb-F bonds of 1.94 Å. These bonds together with a lone pair of electrons are usually

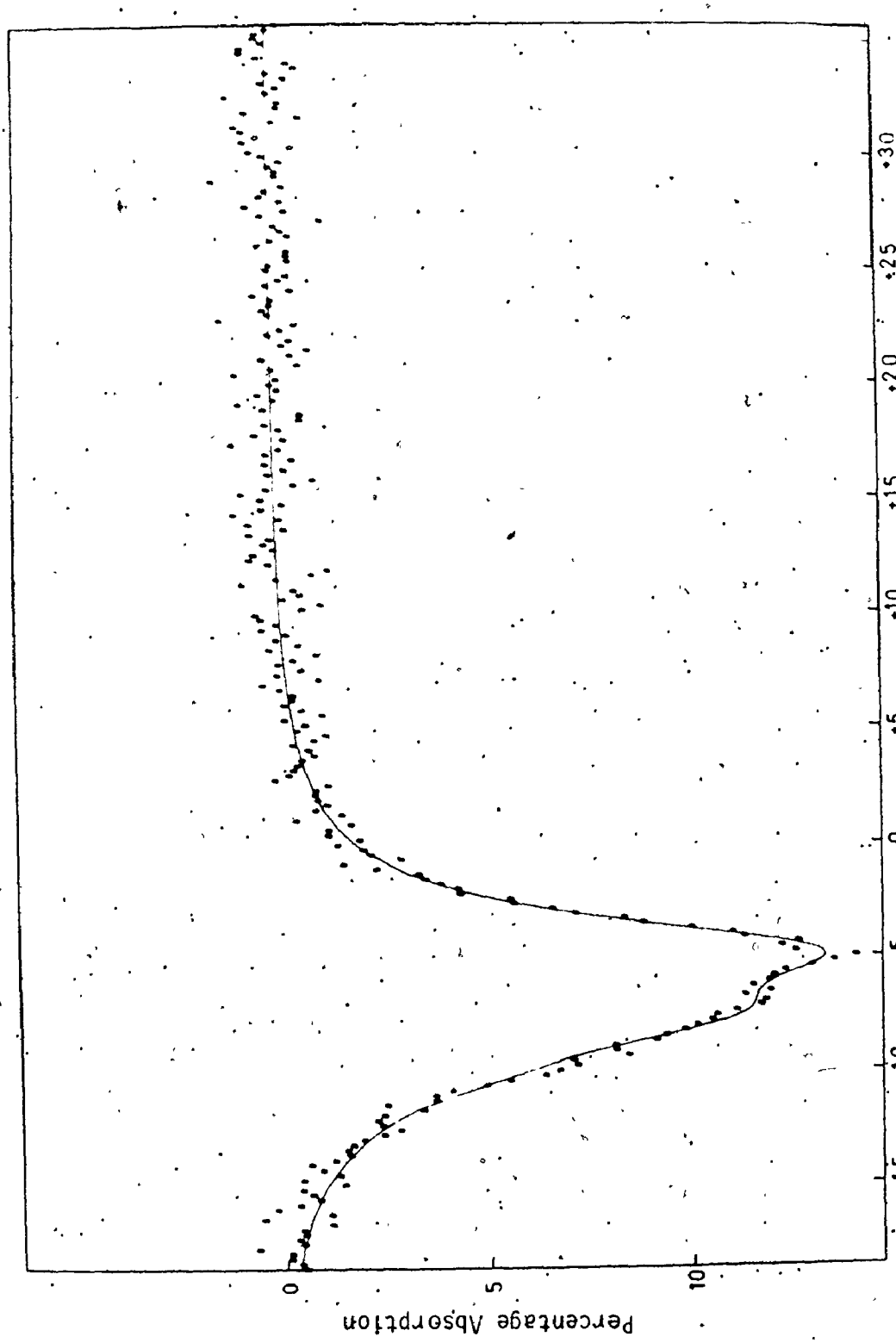

Figure 3.4. ^{121}Sb Mössbauer Spectrum of SbF_3 at 4°K Fitted with an Value Greater than Zero.

believed to form a regular tetrahedron. The secondary Sb---F bond lengths of a number of the anions represented in Figure 3.1 are, however, variable depending upon the particular anion. As well, the F---Sb---F' bond angles within an anion are not all the same and these differences vary from anion to anion. One would expect that the complexes with the least symmetry about the principle axis would have the higher η value. This, however, is not observed indicating that these distortions are not entirely responsible for the measurable asymmetry in the X,Y plane. For example, SbF_3, which appears to have the more regular AX_6E arrangement of secondary Sb---F bonds about the symmetry axis, has the largest η value of the antimony(III) fluoride system reported in Table 3.1.

Closer examination of Figure 3.1 reveals that the AX_6E geometry in SbF_3 is indeed distorted. The F---Sb---F' angles in SbF_3 are 126°, 126°, and 106°. The secondary Sb---F bonds form a distorted pyramid compressed along one side and tilted with respect to the C_3 axis of the primary bonds. This deformation allows sufficient space for the lone pair to be situated above the pyramid formed by the primary bonds, but displaced from the C_3 axis through this pyramid. This distortion from a regular tetrahedron is presumably the origin of the large asymmetry parameter. The large η value for $[NH_4][Sb_3F_{10}]$ indicates a similar distorted arrangement of Sb---F secondary bonds. $\eta = 0$ for $K[Sb_4F_{13}]$, indicating no asymmetry in the x,y plane. In $K[Sb_4F_{13}]$, the secondary bonds are of unequal lengths, although the angles between them average 116°. As well, the pyramid formed by these bonds is situated over that formed by the primary Sb-F bonds such that the C_3 axis for each are

coincident. The distortion observed for SbF_3 is not present in this case; there is sufficient space for the lone pair such that a regular tetrahedron of three primary bonds and a lone pair results, and, in effect, no asymmetry is present about the z axis. In the case of $Na[Sb_3F_{10}]$, the angles subtended by the secondary Sb---F bonds of 2.38 Å and 2.60 Å is 119° and the third Sb---F bond is much longer. This distortion presumably results in a distorted tetrahedron and accounts for the asymmetry parameter of 0.16. A similar effect probably occurs in $Tl[Sb_3F_{10}]$. For the remaining salts which have n = 0, the lone pair of electrons must be situated such that no asymmetry arises about the principle axis. This is more easily achieved in these salts because of one long Sb---F bond (Figure 3.1).

The salts containing an $[SbClF_3^-]$ anion were prepared by Mascherpa et al.[17] These workers determined the structures of two of these; $Na[SbClF_3]\cdot H_2O$,[10] and $K[SbF_3Cl]$,[17] to ascertain whether the anion consisted of a discrete $[SbClF_3^-]$ ion, or as $[SbClF_3^{-x}]_x$, a bridged polymer. The former anion would be expected to have AX_4E geometry, while the latter, by analogoy to the $[SbF_4^-]$ ion, would have the AX_6E geometry. The Mössbauer spectra were recorded for all of these salts. The discrete ion would have a lone pair in the equatorial position of the trigonal bipyramid and hence be expected to have a negative eQV_{ZZ}. The large positive quadrupole coupling constant found for each $[SbClF_3^-]$ salt clearly indicates that the discrete ion was not present. The isomer shift values reported for these salts were very similar to those reported for SbF_3 and $[Sb_4F_{13}^-]$, suggesting a similar antimony environment.

The large quadrupole coupling constants were indicative of an anion similar to that of $[Sb_4F_{13}^-]$ where the 5s electrons are substantially involved in the bonding. The isomer shift values for $K[SbClF_3]$ and $[NH_4][SbClF_3]$ are almost equal, while that of the hydrated sodium salt is more negative. This difference may be attributable to a hydrogen bonded interaction between the anion in $Na[SbClF_3]\cdot H_2O$ and the water molecule. This type of interaction may result in the chlorine or fluorine being less effective at withdrawing electron density and, as a result, leaving the antimony nucleus with a higher 5s electron density.

The structure of $K[SbClF_3]$ [17] was found to have three fluorines at 1.94 Å, 1.95 Å, and 1.96 Å, and three chlorines at 3.09 Å, 3.11 Å, and 3.16 Å. The F-Sb-F' angles were less than 90° (82.2°, 85.6°, 87.9°) while the Cl-Sb-Cl angles were 110.4°, 112.8°, and 110.5° with the lone pair presumably situated between the Sb-Cl bonds as shown in Figure 3.2. Crystallographic evidence[10] indicates that $Na[SbClF_3]\cdot H_2O$ is not isostructural with the other $[SbClF_3^-]$ salts. The complete crystal structure has not been reported in the literature. These structures are consistent with the Mössbauer data reported in Table 3.1.

TABLE 3.1

ANTIMONY-121 MÖSSBAUER DATA FOR SOME ANTIMONY(III) FLUORIDE COMPLEXES

Compound	δ/mm sec^{-1} ± 0.1	eQV_{ZZ} mm sec^{-1} ± 2.0		T_a [a]	χ^2/degree of freedom	M [b]	References
SbF_3	-6.26	18.9	0.38	0.75	1.21	0.17	
	-6.0	19.6					77
$K[Sb_4F_{13}]$	-6.32	17.7	0.0	0.30	0.97	0.19	
$Cs[Sb_4F_{13}]$	-5.83	16.3	0.02	0.28	1.10	0.36	
$Na[Sb_3F_{10}]$	-6.56	19.1	0.16	0.46	1.02	0.02	
$Tl[Sb_3F_{10}]$	-6.30	19.3	0.14	0.51	0.98	0.08	
$[H_4N][Sb_3F_{10}]$	-6.26	18.5	0.31	0.64	1.0	0.04	
$K[Sb_2F_7]$	-4.82	16.7					106
$Cs[Sb_2F_7]$	-5.50	18.6					106
$NH_4[Sb_2F_7]$	-5.33	17.7					106
$[NH_4]_4[Sb_5F_{19}]$	-5.93	18.5	0.24	0.62	1.11	0.09	

Continued.....

TABLE 3.1 (Continued)

Compound	δ/mm sec^{-1} ± 0.1	eQV_{ZZ} mm sec^{-1} ± 2.0	η	T_a[a]	χ^2/degree of freedom	M[b]	References
$NaSbF_4$	-5.73	18.3	0.0	0.20	0.97	0.31	
	-5.48	18.6					106
$KSbF_4$	-5.48	18.6					106
$CsSbF_4$	-5.61	18.6					106
NH_4SbF_4	-5.6	14.2					106
$Na_2[SbF_5]$	-5.30	15.4	0.0	0.48	0.87	0.47	
	-4.75	- 8.3					106
$K_2[SbF_5]$	-4.48	15.7	0.0	0.65	1.14	0.22	
	-4.09	14.3					106
$Cs_2[SbF_5]$	-4.42	14.8					106
$[NH_4]_2[SbF_5]$	-4.52	13.5					106
$[N_2H_6][SbF_5]$	-6.41	18.4	0.0	0.50	0.77	0.38	
$Na[SbClF_3]\cdot H_2O$	-6.29	16.5	0.0	0.80	1.17	0.07	
$K[SbClF_3]$	-5.78	19.2	0.01	1.05	1.90	0.38	
$[NH_4][SbClF_3]$	-5.89	20.1	0.0	0.30	0.95	0.34	
InSb	0.0[c]	--[d]			1.00	0.05	

Continued.....

[a] Absorber thickness (dimensionless)

[b] Misfit (Ref. 108)

[c] -8.50 mm/sec from $Ba^{121}Sn(Sb)O_3$

[d] Too small to calculate

CHAPTER FOUR

^{121}Sb MÖSSBAUER STUDIES OF CHLORO, BROMO, AND IODOANTIMONATES(III)

A. INTRODUCTION

The geometries about the central antimony atoms of the fluoroantimonates(III) discussed in Chapter Three are strongly influenced by the lone pair of electrons, as predicted by the V.S.E.P.R. theory of Gillespie.[28] Structural predictions, based upon this simple theory, are generally reliable for the antimony(III) fluoride complexes, but less so for the antimony(III) chloride, bromide, and iodide complexes. The structures of some of these compounds, for example, $[NH_4]_2[Sb_2Br_{12}]$ [80] and $[Co(NH_3)_6][SbCl_6]$ [28] have been reported in the literature. The 5s electrons in these cases do not appear to distort the octahedral geometry about the antimony atom, and in both of these examples the X-M-X' angles are $\approx$ 90°. There is, however, significant lengthening of the M-X bonds. All of the Sb-Cl bonds in $[Co(NH_3)_6][SbCl_6]$ [29] (2.643 Å) are significantly longer than those in $SbCl_3$ (2.36 Å).[109] This phenomenon is also observed in the $[TeBr_6^{2-}]$ and $[TeCl_6^{2-}]$ anions,[110] which have been shown to contain stereochemically inactive lone pairs, i.e., the anions have regular octahedral geometries. As mentioned in the previous chapter, when the 5s electrons are stereochemically inactive, they do not appear to participate directly in the bonding, but remain spherically distributed about the antimony nucleus. This has a marked effect on the chemical isomer shift of the antimony nucleus producing large negative values. On the

other hand, participation of the 5s electrons in the bonding scheme results in a distorted geometry about antimony, a quadrupole split spectrum, and an isomer shift in the opposite direction.

Donaldson et al.[76] have recently reported ^{121}Sb Mössbauer data for a number of antimony(III) salts. They concluded that the 6.8 mm/sec quadrupole coupling constant they observed for $[Co(NH_3)_6][SbCl_6]$ was the result of distortion from regular octahedral geometry, although earlier work[111] had concluded that the Sb(III) environment was regular. According to the X-ray crystallographic data of Schroeder and Jacobson,[29] the Sb(III) environment is indeed regular and hence the quadrupole coupling should be zero. Furthermore, the NaCl-like structure of this salt indicates that there should be no contribution to the quadrupole splitting parameter from the lattice. The results of Donaldson et al.[76] also indicated that the Sb(III) site in the corresponding bromide was distorted. Later discussions in this chapter will indicate that this conclusion, based on such a small value of the quadrupole coupling constant (4.5 mm/sec), is dubious. Donaldson et al.[106] have reported ^{121}Sb Mössbauer data also for some $[Sb_2X_9^{3-}]$ and $[SbX_4^-]$ salts, where X = Cl, Br or I. Some of these salts have been re-examined because of inconsistencies in the literature and also to ensure that any structural conclusions drawn, particularly from small values of quadrupole coupling constants, be based on well-established data. ^{121}Sb Mössbauer data for $Cs[Sb_2X_9]$ and $M[SbX_4]$ (X = Cl, Br, I) together with new data for a number of salts including $[Co(NH_3)_6][Sb_2F_9]$ and $[n\text{-}C_4H_9NH_3]_2[SbI_5]$ are presented in Table 4.1. Some of the data recorded by Donaldson et al.[76,106] are also included.

The results are discussed in terms of known and likely structures.

B. RESULTS AND DISCUSSIONS

In a large number of the complexes studied the estimated eQV_{ZZ} value is small. For situations where $eQV_{ZZ} \geq \sim 10$ mm/sec, the spectrum has a marked asymmetry (Figure 4.1). Such a spectrum can be fitted to a sum of Lorentzians and a reliable quadrupole coupling constant calculated. Where eQV_{ZZ} is $\sim$ 6 mm/sec or less, the asymmetry is not obvious (Figure 4.2.a) unless the isomer shift of the sample is approximately equal to that of the source material so that relatively slow sweep velocities can be employed. However, all of the Sb(III) spectra reported in this chapter have isomer shifts ranging from -15 to -19 mm/sec relative to the source. These spectra approximate more to a single Lorentzian, as can be seen from Figure 4.2, and make the abstraction of meaningful data very difficult. Clearly, the peak maximum cannot be taken as the isomer shift in cases where there is a finite quadrupole interaction.[76] The error incurred would be smaller if a single Lorentzian fit were used instead of the peak maximum, since the Lorentzian fit would be weighted to more positive or negative velocities, depending upon the sign of the eQV_{ZZ}. Where there is a large splitting, a single fit would be greatly inferior to one of eight lines. Table 4.1 contains data which have been fitted to a single Lorentzian as well as to a sum of eight Lorentzians.

Examination of Table 4.1 reveals the expected discrepancies between data fitted by these two procedures, particularly, where there is a large eQV_{ZZ} value. The spectrum of $[Co(NH_3)_6][Sb_2F_9]$ can only be

Figure 4.1. ^{121}Sb Mössbauer Spectra of $[Co(NH_3)_6][Sb_2F_9]$ using

(a) Eight-Line Quadrupole Split Pattern, and

(b) Single-Line Lorentzian Pattern.

(o, experimental counts; +, computed counts.)

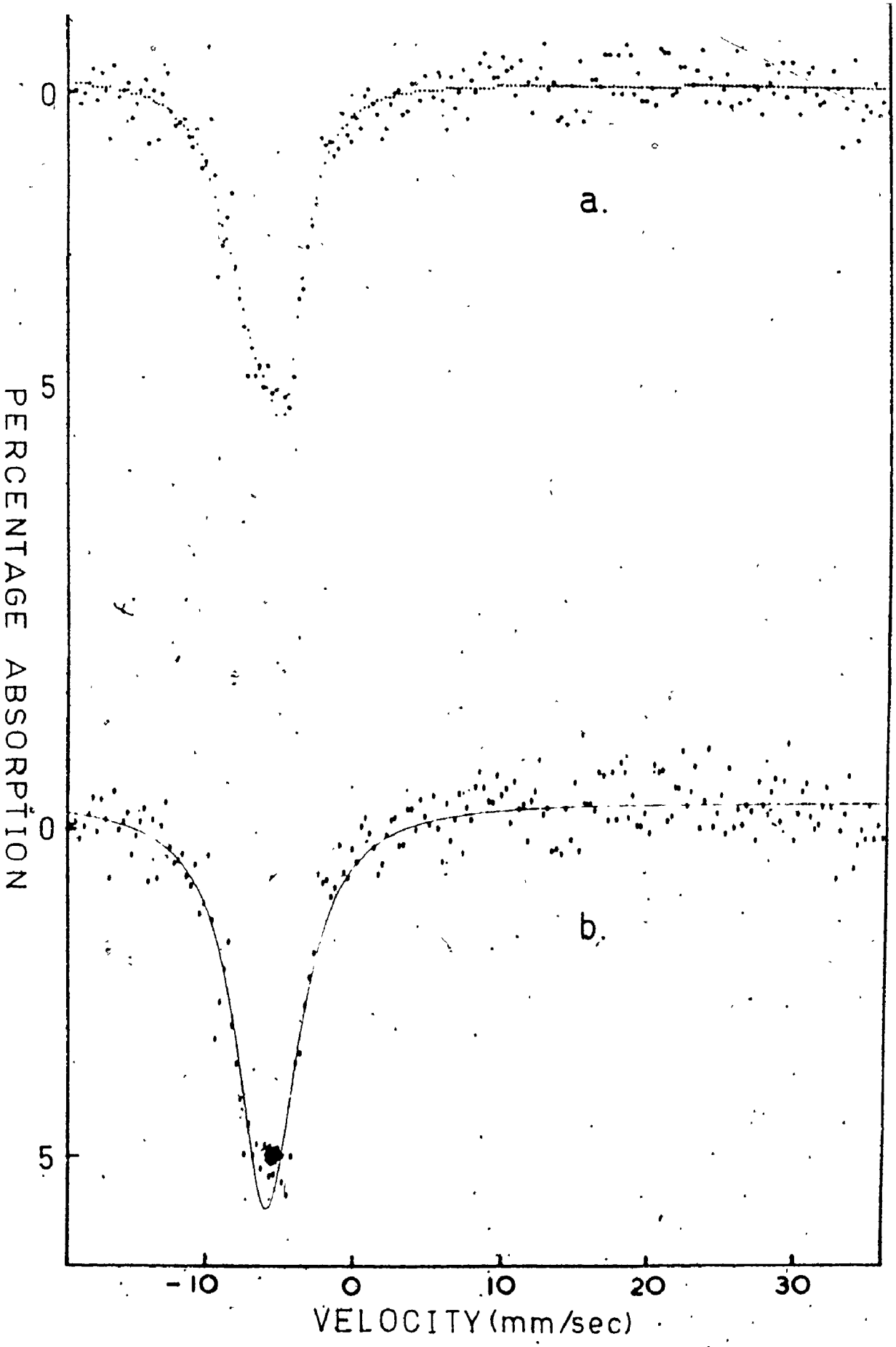
0
5
PERCENTAGE ABSORPTION
a.
0
5
b.
-10
0
10
20
30
VELOCITY (mm/sec)

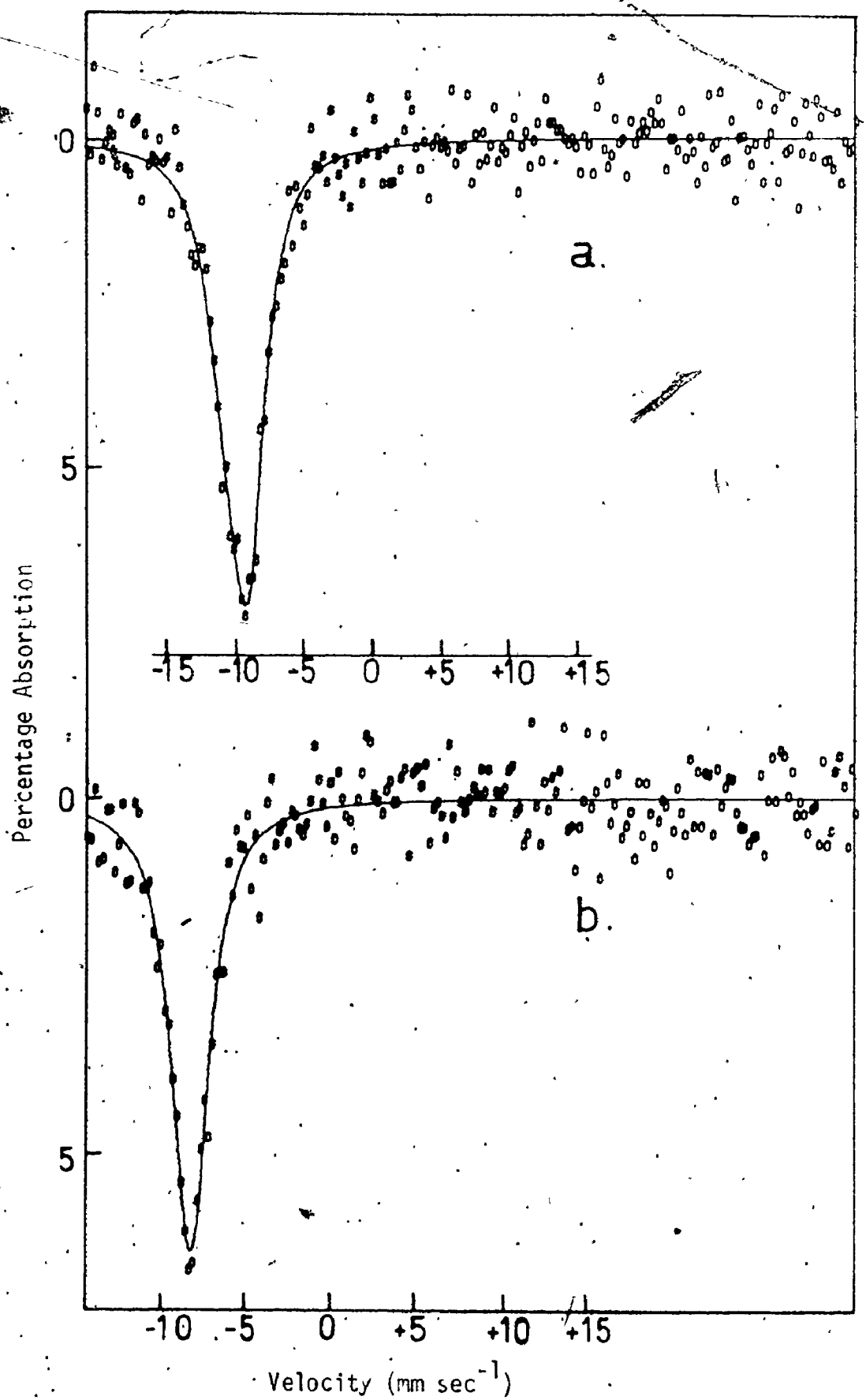

Figure 4.2. ^{121}Sb Mössbauer of (a) $[C_6H_5NH][SbCl_4]$ and (b) $[i\text{-}C_4H_9NH_3]_3[Sb_2I_9]$ at 4°K.

realistically fitted to the eight line pattern since the line width from the single Lorentzian fit (5.3 mm/sec) is more than double the natural line width (2.1 mm/sec), while the line width calculated from the eight line fit is a more realistic 2.9 mm/sec. A visual examination of the spectrum of $[Co(NH_3)_6][Sb_2F_9]$ (Figure 4.1) shows that it is clearly asymmetric. The spectrum of $[C_5H_5NH][SbCl_4]$ (Figure 4.2.a) is also asymmetric having an unacceptably high line width when a single line is employed, whereas the eight line fitted spectrum gives a fairly large quadrupole coupling constant. However, the isomer shifts calculated by the two fitting procedures are not appreciably different. A visual examination of Figure 4.2.a reveals a slightly asymmetric spectrum. For all the other compounds listed in Table 4.1, the isomer shifts computed by the two methods do not differ by more than ± 0.1 mm/sec, indicating that the presence of a small quadrupole coupling constant is not in practice reflected in the calculated isomer shift values, particularly at the high transducer velocities employed. There appears to be a correlation, however, between the difference in the line width computed by each method and the calculated quadrupole coupling constants. The greater the difference in line widths, the larger the coupling constant. A comparison of the data obtained by both fitting procedures was made in order to draw reliable structural conclusions. The large sweep velocities employed for recording ^{121}Sb spectra appear to cause large errors in the quadrupole splitting parameters, probably ~ ± 2 mm/sec.

The quadrupole coupling constants reported here are in reasonable agreement with those reported by Donaldson et al.,[76,106] but the isomer shift data are often much different (Table 4.1). The isomer shift re-

ported by Brill et al.[112] for $[CH_3NH_3]_3[Sb_2Br_9]$, -8.20 mm/sec, is very close to that of $[C_5H_5NH]_5[Sb_2Br_9]Br_2$ given in Table 4.1. This lends some support to the isomer shift data reported here. For the compounds $[(C_4H_9)_4N][SbI_4]$, $[(n\text{-}C_4H_9)_2NH_2][SbI_4]$, and $Cs_3[Sb_2Br_9]$, the computer program gave irreproducible results for the quadrupole coupling constants. Although the quadrupole coupling constants calculated in each of these cases were found to be small, the sign was not reproducible. Because of this, and taking into account the line width criterion discussed earlier, it was concluded that eQV_{ZZ} was negligible in these cases.

In each of the series, $[SbX_4^-]$ and $[Sb_2X_9^{3-}]$, where X = Cl, Br, or I, the isomer shift values become more positive from the chloride to the iodide (Table 4.1). If the Sb-X bond has some s character, then an increase in ligand electronegativity should result in an increase in isomer shift. On the other hand, if the halogen-antimony bonds have high p or d character, the converse is true since p and d electrons tend to shield the s electrons. When the 5s electrons participate in the Sb-X bonds, a stereochemically active lone pair results. This produces a distorted Sb environment which results in a significant quadrupole splitting. If the increase in the quadrupole coupling constants were attributable to increased stereochemical activity of the 5s electrons, then one would have expected an isomer shift trend to more positive values. Clearly, this is not the case, as the s electron density at the antimony increases on going from the iodide salts to those containing the more electronegative chloride. It follows, that the Sb-X bonds must be largely composed of p and/or d electrons, since removal of these

lowers the shielding of the s electrons remaining. Consequently, the isomer shift values are more negative. The increased eQV_{ZZ} values from I to Cl can be attributed to increasing lattice contributions with decreasing anionic size. One might expect these trends to be continued in the isostructural fluoride salts. However, the analogous fluorides have much more positive isomer shifts and larger quadrupole coupling constants. In these cases, the dominant factor affecting the s electron density at antimony appears to be the increased involvement of the 5s electrons in the bonding. As well, because of the increased "s character" in the Sb-X bonds, an increase in electronegativity of the halide results in a further decrease in s electron density at the nucleus. Taken together these facts account for the much more positive isomer shift of the fluoride anions.

In the $[SbX_4^-]$ series, where X = Cl, Br, or I, only the structure of pyridinium tetrachloroantimonate(III) has been determined.[113] In this salt, the anions are linked by halogen bridges to form an infinite chain. Two chlorine atoms of each $[SbCl_4^-]$ are bridged to neighbouring antimony atoms resulting in an octahedral arrangement of six chlorines about each antimony, two at 2.38 Å, two at 2.630 Å, and two at 3.126 Å. Donaldson et al.[106] considered that the two longest Sb-Cl distances were non-bonding and they discussed their Mössbauer data in terms of a trigonal bipyramidal (tbp) arrangement of four chlorines and a lone pair about the antimony atom. This would explain the rather large eQV_{ZZ} value they found for $[C_5H_5NH][SbCl_4]$. This explanation appears unrealistic since even the longest Sb-Cl distances are 0.9 Å less than

the sum of the van der Waals radii,[114] suggesting a significant bonding interaction. A tbp arrangement of four halogens and a lone pair would place excess electron density in the x y plane and result in a negative value for the eQV_{ZZ}. Positive values are found in all cases except one. The X-ray results[113] indicate that the Sb environment provides insufficient space to accomodate a localized lone pair of electrons in contrast to that found in the $[SbF_4^-]$ compounds discussed in the previous chapter. Therefore, it seems reasonable to infer that the 5s electron pair remains essentially in a spherical non-bonding orbital. However, the quadrupole coupling constants calculated for $[C_5H_5NH][SbCl_4]$ and $[(C_2H_5)_4N][SbCl_4]$ are significant. These quadrupole coupling constants may arise in two ways. Firstly, when the bond lengths are unequal, a distorted environment results producing a quadrupole coupling constant. Secondly, a quadrupole coupling constant may result from a contribution by V_{ZZ}(lattice) due to the cations. The Mössbauer data suggest that the structure of $[(C_2H_5)_4N][SbCl_4]$ is comparable to that determined by Jacobson et al.,[113] however, they imply a slightly more distorted environment about the antimony than that of the latter chloride salt.

The Mössbauer parameters of the remainder of the $[SbX_4^-]$ complexes can be explained using a similar structural model to that of the chloride, i.e., six halogens about the antimony with the Sb(III) having a stereochemically inactive pair of 5s electrons. This is contrary to the structures proposed by Ahlijah and Goldstein,[20] who concluded from infrared and Raman data that each of the complexes from the iodide through to the chloride contain a trigonal bipyramidal arrangement of electron pairs. Like Donaldson et al.,[106] they concluded that the two longest of the six

Sb-X distances about the antimony have little covalent character. The eQV_{ZZ} values for the bromide and iodide salts are also small. This is confirmed from the line width criterion developed at the beginning of this chapter. The small eQV_{ZZ} values are also consistent with the stereochemically inactive pair of 5s electrons.

The structures of two compounds containing the $[Sb_2Br_9^{3-}]$ anion have been reported.[25,26] The anion in each compound has approximately D_{3h} symmetry, i.e., composed of two distorted octahedra sharing a face. The distortion involves the lengthening of the three bridging antimony-bromine bonds in each octahedron. Since the Sb-Sb distance in these structures is less than the sum of the van der Waals radii, the localization of the lone pair in orbitals directed toward one another seems unreasonable. Consequently, it was concluded that the lone pair is not localized in any particular direction and remains in a spherical arrangement about the antimony atom. The average Sb-Br bond distances, 2.6 Å and 3.0 Å for the terminal and bridging bonds, respectively, are as a result longer than the Sb-Br bonds of $SbBr_3$ (2.51 Å).[115] $[NH_4]_4[Sb(III)Br_6]$-$[Sb(V)Br_6]$[30] and $[C_5H_5NH]_6[Sb(III)Br_6][Sb(V)Br_6]_3$[116] have been shown to contain a similar hexabromoantimonate(III) anion. This spherical arrangement of 5s electrons explains the large negative isomer shift data reported for $[(CH_3)_4N]_3[Sb_2Br_9]Br_2$ and $[C_5H_5NH]_5[Sb_2Br_9]Br_2$. The isomer shift of $Cs_3[Sb_2Br_9]$ is comparable to those of the above compounds, suggesting a similar structure.

The quadrupole coupling constant computed for $[C_5H_5NH]_5[Sb_2Br_9]Br_2$ is relatively small, but apparently significant from the line width criterion. Presumably, this is because there are three short and three long

bonds. The Mössbauer data for $[(CH_3)_4N]_3[Sb_2Br_9]Br_2$ suggest that the anion is less distorted than in the previously mentioned compound. Unfortunately, the standard deviation in the bond distances are such that no definite conclusions can be made from the crystallographic data in this regard. The quadrupole coupling constant calculated for $Cs_3[Sb_2Br_9]$ was essentially zero suggesting that the co-ordination about the antimony is regular. This interpretation is confirmed by the line width criterion. Although Donaldson et al.[106] reported a small quadrupole coupling constant for $Cs_3[Sb_2Br_9]$ and interpreted it in terms of distortions from regular octahedral geometry, they also concluded that the 5s electrons in this compound are not involved in the bonding.

The ^{121}Sb Mössbauer data of the compounds containing $[Sb_2I_9^{3-}]$ reported in Table 4.1 imply a regular structure for the anions similar to that reported for the analogous bromide. The spectrum of $[Sb_2I_9^{3-}]$, shown in Figure 4.2b, can be fitted to a single Lorentzian as indicated in Table 4.1 from the isomer shift and eQV_{ZZ} data.

Pflaum and Jacobson[27] reported that $Cs_3[Sb_2Cl_9]$ contains three bridging chlorines forming an anion similar to that reported for the corresponding $[Sb_2Br_9^{3-}]$ anions.[25,26] Both $Cs_3[Sb_2Cl_9]$ and $[nC_4H_9NH_3]_3[Sb_2Cl_9]$ have highly negative isomer shift values and small, but significant, quadrupole coupling constants. The negative isomer shifts indicate a high s electron density about the nucleus, which in turn suggest that as in the bromide and iodide salts, the 5s electrons are not involved to any great extent in the bonding. The quadrupole coupling constants computed for each compound are again relatively small and probably arise from either unequal Sb-Cl bond lengths or from lattice contributions. Un-

fortunately, this distortion cannot be confirmed since the complete crystal structure has never been reported.

The geometry about the antimony atoms in the nonafluoride is much different than the other $[Sb_2X_9^{3-}]$ anions, where X = Cl, Br or I. Jacobson and Schroeder[14] showed that the $[Sb_2F_9^{3-}]$ anion consisted of two octahedra sharing a corner, with each octanedron composed of four terminal fluorines, one bridging fluorine, and a lone pair of electrons (Figure 4.3). The fluorine bridge was reported to be asymmetric and hence the atoms have slightly different antimony environments which cannot be distinguished by Mössbauer spectroscopy. The parameters quoted in Table 4.1 for this compound were obtained by fitting the spectrum to one antimony site. This structure explains the much higher isomer shift reported for the fluoride and the much more distorted electron environment producing the large quadrupole coupling constant.

The structures of two compounds, $[NH_4]_2[SbCl_5]$ [32] and $K_2[SbCl_5]$,[32] which contain the $[SbCl_5^{2-}]$ anion have been reported in the literature. In each, the geometry about the Sb(III) was AX_5E, i.e., a lone pair occupying the sixth coordination site. The structure of $[NH_4]_2[SbCl_5]$ was determined by photographic techniques. In this structure, the four Sb-Cl bond distances on the base of the square pyramid were 2.6 Å and the axial Sb-Cl bond length was 2.3 Å. A later crystal structure of the potassium salt displayed a distorted square pyramidal configuration about antimony in which the axial Sb-Cl bond (2.385 Å) is shorter than the mean basal Sb-Cl bonds. Two of the basal Sb-Cl bonds are approximately the same length, at 2.622 Å and 2.625 Å, with the other two bond lengths, 2.799 Å and

Figure 4.3. Structural Representation of the $[Sb_2F_9^{3-}]$ Anion of $[Co(NH_3)_6][Sb_2F_9]$.

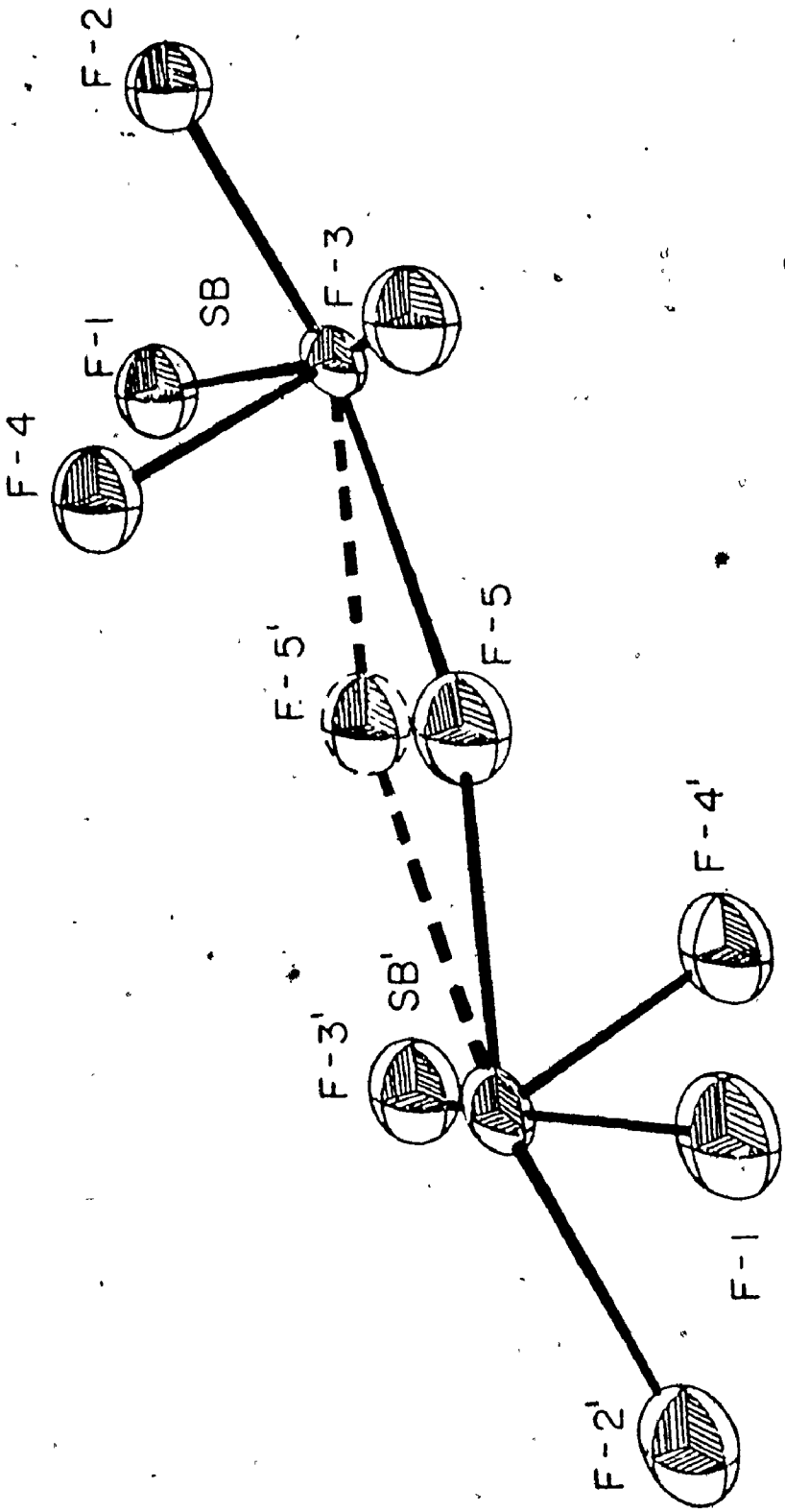
F-2
F-3
SB
F-1
F-4
F-5'
F-5
F-4'
SB'
F-3'
F-1
F-2'

2.509 Å. In both cases, there is sufficient room to accomodate a lone pair of electrons in the sixth coordination site of the octahedron. This involvement of the 5s electrons in the bonding would result in a much higher isomer shift than for the $[SbCl_4^-]$ anion and an asymmetric environment about the antimony nucleus. The ^{121}Sb Mössbauer of $[NH_4]_2[SbCl_5]$ was recorded earlier by Birchall et al.,[111] but the quadrupole coupling constant was never determined. However, the isomer shift (-6.7 mm/sec) was indeed higher than expected for a Sb(III) chloride complex and the line width calculated from a single Lorentzian fit was much broader than the natural line width, suggesting some quadrupole interaction. A similar isomer shift and quadrupole coupling constant would be expected for the K_2SbCl_5,[32] which also contains a stereochemically active lone pair.

The ^{121}Sb Mössbauer data of $[nC_4H_9NH_3]_3[SbI_5]$ is presented in Table 4.1. The isomer shift (-8.09 mm/sec) does not vary substantially from those of the $[Sb_2I_9^{3-}]$ and $[SbI_4^-]$ anions and the quadrupole coupling constant is very small. These Mössbauer parameters imply that the 5s electrons are not as stereochemically active as in the chloride complexes. In the series $[SbF_5]^{2-}$, $[SbCl_5^{2-}]$, and $[SbI_5^{2-}]$, the isomer shift decreases and the electric field becomes more symmetric. This decrease in isomer shift, i.e., to more negative values, represents an increase in s electron density at that nucleus. Assuming the geometry about the $[SbI_5^{2-}]$ anion is similar to that of the $[SbF_5^{2-}]$ and $[SbCl_5^{2-}]$ anions, i.e., assuming 5s electron involvement in the bonding, these trends are easily explicable in terms of the electronegativities of the halogens. As the electronegativity

of the halogen decreases, the electron density about the antimony nucleus increases and the isomer shift decreases. In addition, as the electronegativity of the halogens decrease, the electron density withdrawn from the x y plane compared with that along the z axis decreases. Conventionally, the lone pair of electrons are in the z direction. Hence, when this disparity is reduced, a small quadrupole coupling constant is expected.

It has been noted in Sb and Sn compounds that the chemical isomer shift of an ion is influenced by the counter ion.[107,111] Where there is interaction between a polarizing cation and a ligand attached to a Mössbauer nucleus, the effective electronegativity of the ligand is changed resulting in a different isomer shift. The isomer shift of the $[Sb_2X_9^{3-}]$ ions having a cation with an active hydrogen, i.e., $[R_3N\text{-}H]$, are more positive than those that do not have this feature. It is suggested that this is indicative of hydrogen bonding between the N-H and the halogen of the anion, which results in a smaller withdrawal of p- or d-electron density from the antimony nucleus, an increase in shielding, and hence a reduction in s electron density. This effect is not as noticeable in the $[SbX_4^-]$ salts.

TABLE 4.1

ANTIMONY-121 MÖSSBAUER DATA FOR SOME ANTIMONY(III) CHLORIDE, BROMIDE AND IODIDE COMPLEXES

Compound	EIGHT LORENTZIANS δ/mm sec^{-1} ± 0.1	eQV_{ZZ}/ mm sec^{-1} ± 2.0	Γ_{exp} mm sec^{-1}	χ^2/degrees of freedom	ONE LORENTZIAN δ/mm sec^{-1} ± 0.1	Γ_{exp} mm sec^{-1}	References
$[(C_2H_5)_4N][SbCl_4]$	- 8.17	+ 8.9	2.6	1.01	-8.09	3.8	
	- 7.47	+10.6	3.3				106
$[(n\text{-}C_4H_9)_4N][SbBr_4]$	- 8.15	+ 4.6	3.7	1.00	-8.18	3.9	
$[(n\text{-}C_4H_9)_4N][SbI_4]$	- 7.37	---[a]	2.7	0.91	-7.28	3.3	
	- 6.88	- 3.3	3.4				106
$[C_5H_5NH][SbCl_4]$	- 8.10	+11.4	3.6	1.0	-7.95	4.9	
	- 7.98	+ 9.1	2.2				106
$[(n\text{-}C_4H_9)_2NH_2][SbI_4]$	- 7.38	---[a]	2.7	0.90	-7.37	3.8	
$[NH_4]_2[SbCl_5]$[b]	---	---	---	---	-6.7	4.4	111
$[n\text{-}C_4H_9NH_3]_2[SbI_5]$	- 8.09	+ 1.8	2.7	1.00	-8.14	3.5	
$[Co(NH_3)_6][Sb_2F_9]$	- 6.30	+15.9	2.9	0.99	-5.86	5.3	
$Cs_3[Sb_2Cl_9]$	- 9.67	+ 7.7	2.8	1.16	-9.50	3.7	
	-10.9	+ 6.8	3.0				76

Continued.....

TABLE 4.1 (Continued)

EIGHT LORENTZIANS

Compound	δ/mm sec^{-1} ± 0.1	eQV_{ZZ}/ mm sec^{-1} ± 2.0	Γ_{exp} mm sec^{-1}	χ^2/degrees of freedom	δ/mm sec^{-1} ± 0.1	Γ_{exp} mm sec^{-1}	References
$Cs_3[Sb_2Br_9]$	- 8.97	---[a]	3.3	0.98	-8.97	3.4	
	-10.3	+ 6.4	2.9				76
$Cs_3[Sb_2I_9]$	- 8.35	+ 2.9	2.5	1.01	-8.36	2.7	
	- 9.7	+ 5.0	3.2				76
$[n\text{-}C_4H_9NH_3]_3[Sb_2Cl_9]$	- 9.16	+ 8.2	2.9	0.95	-9.14	3.9	
$[(CH_3)_4N]_3[Sb_2Br_9]Br_2$	- 8.50	+ 3.8	2.8	0.96	-8.50	3.0	
$[C_5H_5NH]_5[Sb_2Br_9]Br_2$	- 8.22	+ 7.2	2.8	0.99	-8.16	3.6	
$[i\text{-}C_4H_9NH_3]_3[Sb_2I_9]$	- 8.05	+ 7.5	2.0	0.82	-7.95	2.9	

[a] Reliable eQV_{ZZ} not found since the value is probably very small.

[b] Recorded at 77°K, reference to InSb at the same temperature.

CHAPTER FIVE

THE ANTIMONY(V) CHLORIDE FLUORIDES; THEIR PREPARATION AND CHARACTERIZATION

(A) INTRODUCTION

Antimony(V) chloride fluorides have been of considerable interest as Lewis acids ever since the early work of Swartz.[34] The synthesis of the first antimony(V) chloride fluoride, reported by Swartz in 1895, involved the reaction of SbF_3 and $SbCl_5$ with an excess of chlorine gas, producing a compound which was identified by the elemental analysis as $SbCl_3F_2$. Other antimony(V) chloride fluorides were prepared by Ruff et al.[35] in 1909. They reacted appropriate mixtures of SbF_5 and $SbCl_5$ to give a series of crystalline compounds — $(SbF_5)_3(SbCl_5)$, $(SbF_5)_2(SbCl_5)_2$, ---- $(SbF_5)(SbCl_5)_3$ — which were identified by elemental analysis.

The synthesis of $SbCl_4F$ was first reported by Kolditz[37] in 1957, who prepared it from a reaction of $SbCl_5$ and AsF_3 as outlined in equation 5.1. In 1965, Dehnicke and Weidlein[40] claimed, on the basis of Raman data,

$$3SbCl_5 + AsF_3 \rightarrow 3SbCl_4F + AsCl_3 \qquad (5.1)$$

that $SbCl_4F$ contained a tetrahedral $[SbCl_4^+]$ cation in the solid state. A later X-ray crystallographic analysis carried out by Preiss,[41] however, demonstrated that $SbCl_4F$ was a cis-fluorine bridged tetramer. The Raman data published by Beattie et al.[97] in 1969 were interpreted in terms of this structure.

The preparation of $SbCl_2F_3$ was first reported by Henne et al.[36]

in 1947. This compound, allegedly prepared from reaction 5.2, was never

$$SbF_3 + Cl_2 \xrightarrow{> 100°C} SbCl_2F_3 \qquad (5.2)$$

isolated, but the mixture was used as a fluorinating agent. In 1961, Kolditz and Leith[38] repeated this preparation and isolated a material melting at 68°C, which they identified by the elemental analysis as $SbCl_2F_3$. They also concluded from conductivity measurements that this compound had an ionic formulation, i.e., $[SbCl_4^+][SbF_6^-]$. In a later Raman and infrared study by Dehnicke and Weidlein,[39] it was concluded that $SbCl_2F_3$ had a trigonal bipyramidal geometry. However, in an ensuing paper, Muetterties et al.[43] suggested, from the ^{19}F n.m.r. spectrum of a supercooled mixture of $SbCl_2F_3$ and chlorine, and by comparison with the chemical properties of SbF_5, that $SbCl_2F_3$ did not consist of $[SbCl_4^+]$ and $[SbF_6^-]$ ions, or have bipyramidal geometry, but was present primarily as an associated species with a six-coordinate antimony atom having bridged chlorine or fluorine atoms.

In 1966, the compound presumed to be $SbClF_4$ was reported by Davies.[117] It was prepared from a mixture of SbF_5 and $SbCl_5$ in the appropriate proportions. Unfortunately, the product was neither isolated nor characterized.

More recently, since the beginning of this work, Dove and Ali[118] investigated a number of antimony(V) chloride fluorides and claimed to have prepared $SbCl_4F$, $SbCl_3F_2$, and $SbCl_2F_3$ by the solvolysis of $SbCl_5$ in anhydrous HF. The melting points were reported to be 83°, 68°, and 54°C, respectively. The existence of substantiating analytical, Raman, and infrared data was inferred, but never published. In 1972, Preiss[44]

carried out the X-ray crystallographic analysis of $SbCl_2F_3$, prepared by Kolditz and Leith's[38] method. He concluded that $SbCl_2F_3$ was ionic having $[SbCl_4^+]$ cations and $[Sb_2Cl_2F_9^-]$ anions. It is difficult to confirm whether this compound is identical to that published earlier,[36,38] since neither the melting point nor any spectroscopic data were reported. Although Raman data were presented in Preiss' paper,[44] they were simply a reassignment of that presented earlier by Dehnicke and Weidlein.[39] In the same year, Miller et al.[45] reported the preparation of a compound identified as $[SbCl_4^+][Sb_2F_{11}^-]$, from a preliminary X-ray structural analysis. This compound was prepared from a 3:7 mole ratio of $SbCl_5$ and SbF_5. However, the melting point range of 12°C, reported for the bulk material, suggests that the product was impure. A fully refined structure has never been published. Very recently, further results on the solvolysis of $SbCl_5$ in anhydrous HF were published by Dove and Ali.[119] In this paper, the preparations of the compounds $SbCl_4F$, $SbCl_3F_2$, and $SbCl_2F_3$ were again reported, but they were only identified by their elemental analyses.

In the light of these inconsistencies in the literature, an investigation was undertaken to prepare and characterize a number of antimony(V) chloride fluorides. Characterization was achieved using Mössbauer and Raman spectroscopies, X-ray crystallography, and mass spectrometry. The results of these investigations are reported and discussed in this chapter together with the analytical data. In addition, this chapter includes a study of some complex compounds formed from the reaction of $SbCl_4F$ with the following fluoride-ion acceptors; AsF_5, SbF_5, and NbF_5. Kolditz et al.[51] prepared the complex $[AsCl_4^+][SbF_6^-]$ in 1962 by

reacting "$SbCl_2F_3$" with AsF_3. An alternative preparative method for this complex is presented here. In addition, an alternate preparative method is presented for $[SbCl_4^+][Sb_2Cl_2F_9^-]$. Evidence for a new adduct, $SbCl_4F\cdot(NbF_5)_x$ (where x = 1 or 2) is also reported.

(B) RESULTS AND DISCUSSION

(i) Preparation and Chemical Properties

a. $SbCl_4F$

$SbCl_4F$ is a pale yellow solid at room temperature. The reaction conditions used in this work were the same as those used earlier by Kolditz and Leith.[38] That is, the reaction was carried out at 70°C for one hour. In some instances, however, where the mole ratio of $SbCl_5$:AsF_3 was greater than 1:1, and when the temperature was greater than 70°C, further fluorination occurred and a mixture of $SbCl_4F$ and an antimony(V) chloride fluoride with a higher F:Cl ratio were produced. Because of the difficulties encountered when analysing this hygroscopic material, the purity of the $SbCl_4F$ was best monitored using the Raman and the melting point data.

SbF_3 can also be used as a fluorinating agent for $SbCl_5$. A pale yellow product was produced from this reaction and identified as a mixture of $SbCl_3$ and $SbCl_4F$ by Raman spectroscopy. Unfortunately, since the sublimination temperatures of these products were almost identical, they were not easily separated.

The $SbCl_4F$ produced by the first procedure was usually an oil which crystallized in liquid SO_2. Isolation and subsequent sublimation gave pure $SbCl_4F$ (m.p. 79-81°C), remarkably akin to that reported in 1909

by Ruff[35] for the product $(SbF_5)(SbCl_5)_3$, m.p. 81°C. Kolditz and Leith[38] had earlier reported the melting point of $SbCl_4F$ as 83°C.

b. $Sb_3Cl_{10.75}F_{4.25}$

A compound produced from a mixture of $SbCl_5$ and SbF_5 in the ratio of slightly greater than 3:2 in liquid SO_2 was shown from crystallographic studies (see later) to have the formulation $Sb_3Cl_{10.75}F_{4.25}$. This white crystalline product melts at 64-69°C and sublimes at 20°C under vacuum. The elemental analysis of the bulk material, reported in Chapter II, indicates that the product has a Sb:Cl:F mole ratio of 1:3.3:2.6. Since the crystal used in the structure determination consisted of a 3:1 mixture of $Sb_3Cl_{11}F_4$ and $Sb_3Cl_{10}F_5$, it is reasonable to suppose that these two compounds are present in the bulk material, but not necessarily in this ratio. This type of mixture is comparable with the melting point data. In this case, a great deal of emphasis cannot be attributed to the analytical data since the errors involved in analysing this extremely hygroscopic material are large. However, the analysis does indicate the ratios of Sb:Cl:F in the bulk material.

c. $SbCl_3F_2$

The product $SbCl_3F_2$, prepared from the reaction of $SbCl_4F$ and SbF_5 in liquid SO_2, sublimes at 40°C under vacuum and the resultant white crystalline solid melts at 62-63°C. This material was formulated as $SbCl_3F_2$ from the spectroscopy discussed later in this chapter. The melting point of this compound is identical to that reported for $(SbF_5)_2(SbCl_5)_3$ by Ruff,[35] 62°C. Dove and Ali have claimed a melting point of

68°C,[118] but later reported a value of 55-60°C [119] for this material.

d. $SbCl_2F_3$

$SbCl_2F_3$ is a pale yellow crystalline material prepared by the method of Kolditz[37] outlined in equation 5.1. The unit cell parameters obtained from crystals of this compound are identical to those reported by Preiss[44] (section 5.B2), who formulated the compound as $[SbCl_4^+][Sb_2Cl_2F_9^-]$. A pure sample could only be obtained if pure SbF_3 and Cl_2 gas were used, as described in Chapter Two. The product prepared in this work melts at 49-53°C. Initial preparations, carried out using these reactants before extensive purification, resulted in a material which appeared, from Raman and Mössbauer Data, to be an antimony(V) chloride fluoride whose melting point was 68°C. Earlier workers[38,39] had reported that the melting point of $SbCl_2F_3$ was 68°C, but the current work suggests that this product was not the same material as that prepared here. A later preparation by Ali and Dove[118] yielded a material melting at 54°C which agrees more favourably with our data. When $[SbCl_4^+][Sb_2Cl_2F_9^-]$ is melted in a sealed capillary, it forms a highly viscous liquid which, on cooling very slowly, recrystallizes. This suggests the presence of a polymeric species in the liquid form. In some instances, the sample never recrystallized, suggesting that some decomposition at its melting point had occurred. Either of these factors could contribute to the large melting point range observed for this compound. At slightly higher temperatures (65-70°C), the sample decomposes. This decomposition was discovered when attempting to grow single crystals in a sealed tube in a temperature gradient. The resultant crystal was tetragonal with unit cell dimensions a = 12.87 Å,

C = 7.84 Å, and γ = 90°, which are identical to that of $SbCl_4F$ reported earlier by Preiss.[41] This decomposition reaction also produced a clear viscous liquid whose principle Raman bands at 665 cm^{-1} and 720 cm^{-1} resembled those of SbF_5,[97] suggesting that the decomposition can be represented by equation 5.3.

$$SbCl_2F_3 \rightleftharpoons SbF_5 + SbCl_4F \qquad (5.3)$$

A similar reaction was noted by Kolditz and Leith.[38] The reverse of equation 5.3 appears to be a probable alternate method of preparation for $SbCl_2F_3$ and is discussed in a later section.

e. $[SbCl_4^+][Sb_2F_{11}^-]$

The material identified as $[SbCl_4^+][Sb_2F_{11}^-]$ and prepared from the reaction of a 4:1 mixture of SbF_5:$SbCl_5$ is a white solid at room temperature. An alternate preparative method is illustrated in equation 5.4.

$$SbCl_4F + 2SbF_5 \xrightarrow[20°C]{SO_2} [SbCl_4^+][Sb_2F_{11}^-] \qquad (5.4)$$

In both cases, a product melting at 80-82°C is isolated. This material seems to correspond to $(SbF_5)_3(SbCl_5)$ (m.p. 81°C) reported by Ruff.[35] In addition, when the ratio of SbF_5:$SbCl_4F$ in equation 5.4 is increased, the products are $[SbCl_4^+][Sb_2F_{11}^-]$ and $SbF_5 \cdot SO_2$. The product $[SbCl_4^+][Sb_2F_{11}^-]$ is, therefore, not further fluorinated and the excess SbF_5 reacts with SO_2 to produce the $SbF_5 \cdot SO_2$ adduct. This adduct was identified as an impurity in $[SbCl_4^+][Sb_2F_{11}^-]$ by the presence of its characteristic Raman bands. $SbF_5 \cdot SO_2$ is discussed in more detail in Chapter Seven.

f. $[AsCl_4^+][SbF_6^-]$

$[AsCl_4^+][SbF_6^-]$, prepared from the reaction of $SbCl_4F$ and AsF_5, is a solid at room temperature but appears to decompose at its melting point. The Raman spectrum of this compound contains bands that can be attributed to the $[AsCl_4^+]$ cation[120] (section 5.B4). In an attempt to prepare the $[SbCl_4^+]$ analogue, using the reverse of the reaction described by equation 5.3, a sample of $[SbCl_4^+][Sb_2Cl_2F_9^-]$ was obtained. This material was identified by Raman spectroscopy and melting point data. Similar reactions involving increased quantities of SbF_5, with respect to the quantity of $SbCl_4F$, were discussed earlier in this section. Unlike AsF_5 and SbF_5, which undergo halogen exchange with $SbCl_4F$ to produce the $[MCl_4^+]$ (M = As, or Sb) cation, NbF_5 reacts with $SbCl_4F$ to form a molecular adduct (m.p. 55°C). This adduct has not been completely characterized, but appears, from the Raman and Mössbauer data, to be a molecular adduct of the form $SbCl_4F\cdot(NbF_5)_x$, where x = 1, or 2.

(ii) X-Ray Crystallography

a. $Sb_3Cl_{10.75}F_{4.25}$

The collection of the preliminary data, the solution and the refinement of the structure were carried out by Dr. D. R. Slim of this department. $Sb_3Cl_{10.75}F_{4.25}$ is monoclinic with $\underline{a}$ = 12.359(6) Å, $\underline{b}$ = 16.480(10) Å, $\underline{c}$ = 9.387(3) Å; β = 103.96(5)°; V = 1856 Å^3, Z = 4, D_c = 2.96 g cm^{-3}, and F.W. = 827.5. The structure was refined in space group $P2_1/n$ to a final agreement index R_2 of 0.113 for 2415 independent reflections. One Sb-Cl bond appeared shorter than the remainder, hence the occupational parameters of this site were varied and the refinement

terminated when the site contained approximately 75% Cl and 25% F.

Figure 5.1 shows the configuration of $Sb_3Cl_{10.75}F_{4.25}$, while Table 5.1 lists the interatomic distances and angles. The projection of the structure down the c axis is shown in Figure 5.2. Information on the X-ray intensity measurements and information on the solution and refinement of the structure are published elsewhere.[121]

As can be seen from Figure 5.1, each antimony atom has a distorted octahedral configuration of chlorine and fluorine atoms. Sb(1) has two cis-fluorines bridging to the other two antimony atoms of the trimer, plus four terminal chlorine atoms. Sb(2) has a similar arrangement except that one of the chlorine sites consists of 75% chlorine and 25% fluorine, while Sb(3) has one terminal fluorine atom and two bridging fluorine atoms in cis-positions and three mutually cis-terminal chlorines.

Examination of Table 5.1 indicates that the mean Sb-Cl distance is $\sim$ 2.26 Å, which is comparable to the corresponding distances found in $SbCl_4F$.,[41] $Sb_3Cl_9F_4O$,[122] and $[SbCl_4^+][Sb_2F_{11}^-]$,[45] of 2.29 Å, 2.26 Å, and 2.23 Å, respectively. However, this comparison is less meaningful for the latter compound since it has not been refined to a satisfactory level. The mean bond lengths are longer than the corresponding mean found in $[SbCl_4^+][Sb_2Cl_2F_9^-]$,[44] 2.18 Å. In this compound, one might have expected to find two Sb-Cl distances, one for the cation and another for the anion, somewhat larger. This was not observed. The cis Cl-Sb-Cl' angles in $Sb_3Cl_{10.75}F_{4.25}$, which vary from 94.2° to 102.4°, are intermediate between the 90° angle expected for octahedral coordination and the tetrahedral angle achieved in the $[SbCl_4^+]$ cation.[44] This suggests that there

Figure 5.1. View of the $Sb_3Cl_{10.75}F_{4.25}$ Structure.

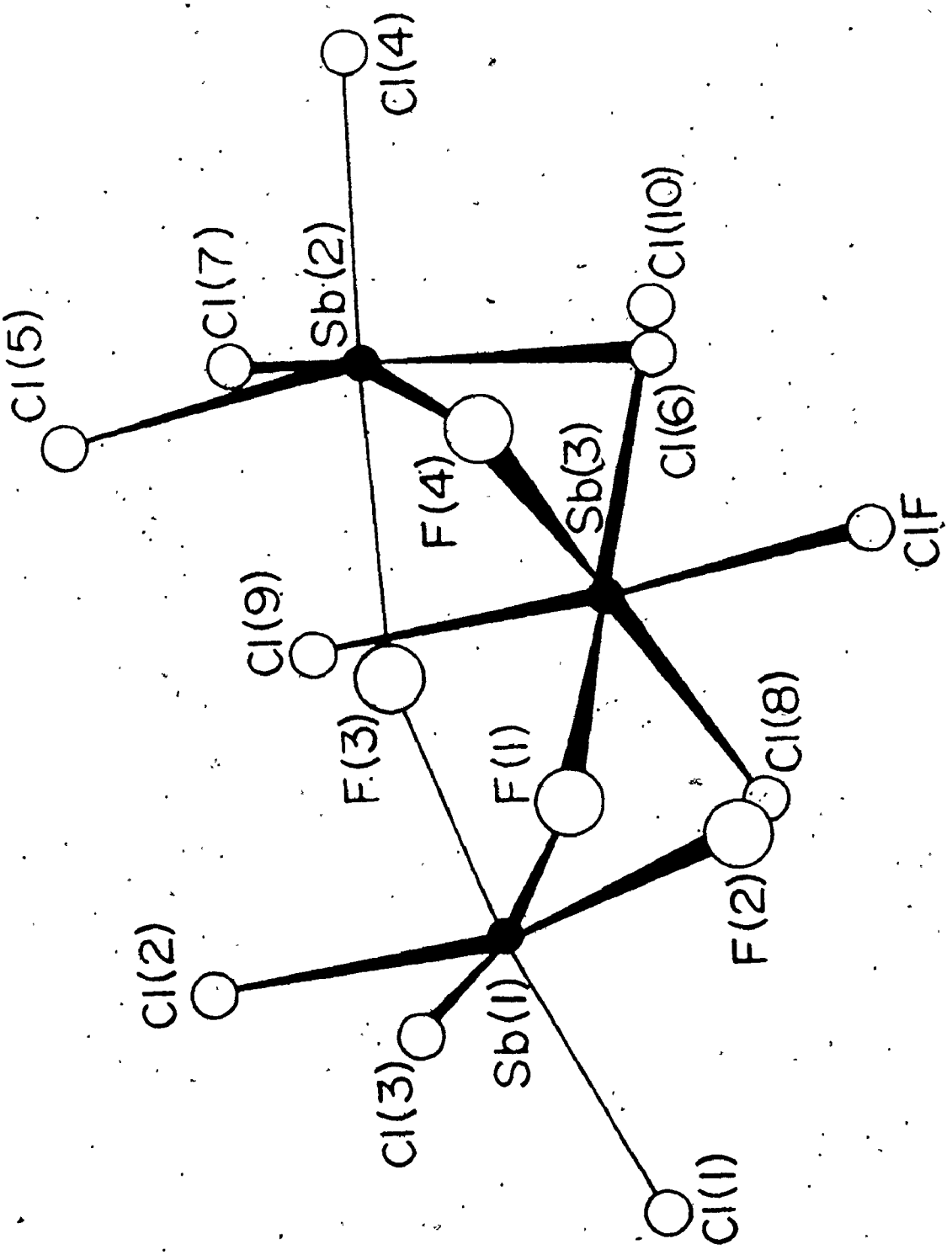
Cl(4)
Cl(7)
Sb(2)
Cl(5)
Cl(10)
Cl(6)
F(4)
Sb(3)
ClF
Cl(9)
F(3)
F(1)
Cl(8)
F(2)
Cl(2)
Cl(3)
Sb(1)
Cl(1)

Table 5.1. Interatomic Distances and Angles for $Sb_3Cl_{10.75}F_{4.25}$.[a]

(a) Bond Lengths

Bonds	Length (Å)	Bonds	Length (Å)	Bonds	Length (Å)
Sb(1)-Cl(1)	2.28(1)	Sb(2)-Cl(4)	2.28(1)	Sb(3)-Cl(8)	2.27(1)
-Cl(2)	2.28(1)	-Cl(5)	2.24(1)	-Cl(9)	2.25(1)
-Cl(3)	2.26(1)	-Cl(6)	2.20(1)	-Cl(10)	2.27(1)
-F(1)	2.04(2)	-Cl(7)	2.28(1)	-ClF[b]	2.12(1)
-F(2)	1.87(2)	-F(3)	2.11(2)	-F(1)	2.12(2)
-F(3)	2.06(2)	-F(4)	2.10(2)	-F(4)	2.08(2)

(b) Bond Angles

Bonds	Angle (deg)	Bonds	Angle (deg)	Bonds	Angle (deg)
Cl(1)-Sb(1)-Cl(2)	98.9(3)	Cl(4)-Sb(2)-Cl(5)	95.6(4)	Cl(8)-Sb(3)-Cl(9)	95.6(4)
-Cl(3)	100.4(4)	-Cl(6)	94.2(5)	-Cl(10)	101.1(5)
-F(1)	90.2(6)	-Cl(7)	102.4(5)	-ClF[b]	94.9(5)
-F(2)	92.6(7)	-F(3)	168.5(6)	-F(1)	89.0(6)
-F(3)	169.3(6)	-F(4)	90.0(6)	-F(4)	168.5(6)
Cl(2)-Sb(1)-Cl(3)	97.6(6)	Cl(5)-Sb(2)-Cl(6)	164.7(5)	Cl(9)-Sb(3)-Cl(10)	97.5(4)
-F(1)	84.4(5)	-Cl(7)	95.1(4)	-ClF	161.7(5)
-F(3)	162.4(7)	-F(3)	82.2(5)	-F(1)	83.4(5)
-F(3)	84.2(5)	-F(4)	84.1(6)	-F(4)	84.5(5)

Continued.....

Table 5.1 (Continued)

Bonds	Angle (deg)	Bonds	Angle (deg)	Bonds	Angle (deg)
Cl(3)-Sb(1)-F(1)	168.8(6)	Cl(6)-Sb(2)-Cl(7)	94.2(5)	Cl(10)-Sb(3)-ClF	95.2(5)
-F(2)	93.4(8)	-F(3)	85.9(6)	-F(1)	169.7(6)
-F(3)	89.3(6)	-F(4)	84.2(6)	-F(4)	90.3(6)
F(1)-Sb(1)-F(2)	82.3(8)	Cl(7)-Sb(2)-F(3)	89.1(6)	ClF[b]-Sb(3)-F(1)	81.8(6)
-F(3)	79.9(7)	-F(4)	167.6(6)	-F(4)	82.3(6)
F(2)-Sb(1)-F(3)	82.2(8)	F(3)-Sb(2)-F(4)	78.6(7)	F(1)-Sb(3)-F(4)	79.6(7)
Sb(1)-F(1)-Sb(3)	159.1(9)	Sb(1)-F(3)-Sb(2)	158.4(1.0)	Sb(2)-F(4)-Sb(3)	160.4(9)

[a] Standard errors are given in parentheses.

[b] Represents 0.75 occupation of Cl, 0.25 occupation of F.

Figure 5.2. Projection of the Unit Cell of $Sb_3Cl_{10.75}F_{4.25}$ Down the c Axis (Circles of Increasing Size Represent Sb, Cl, and F, respectively.)

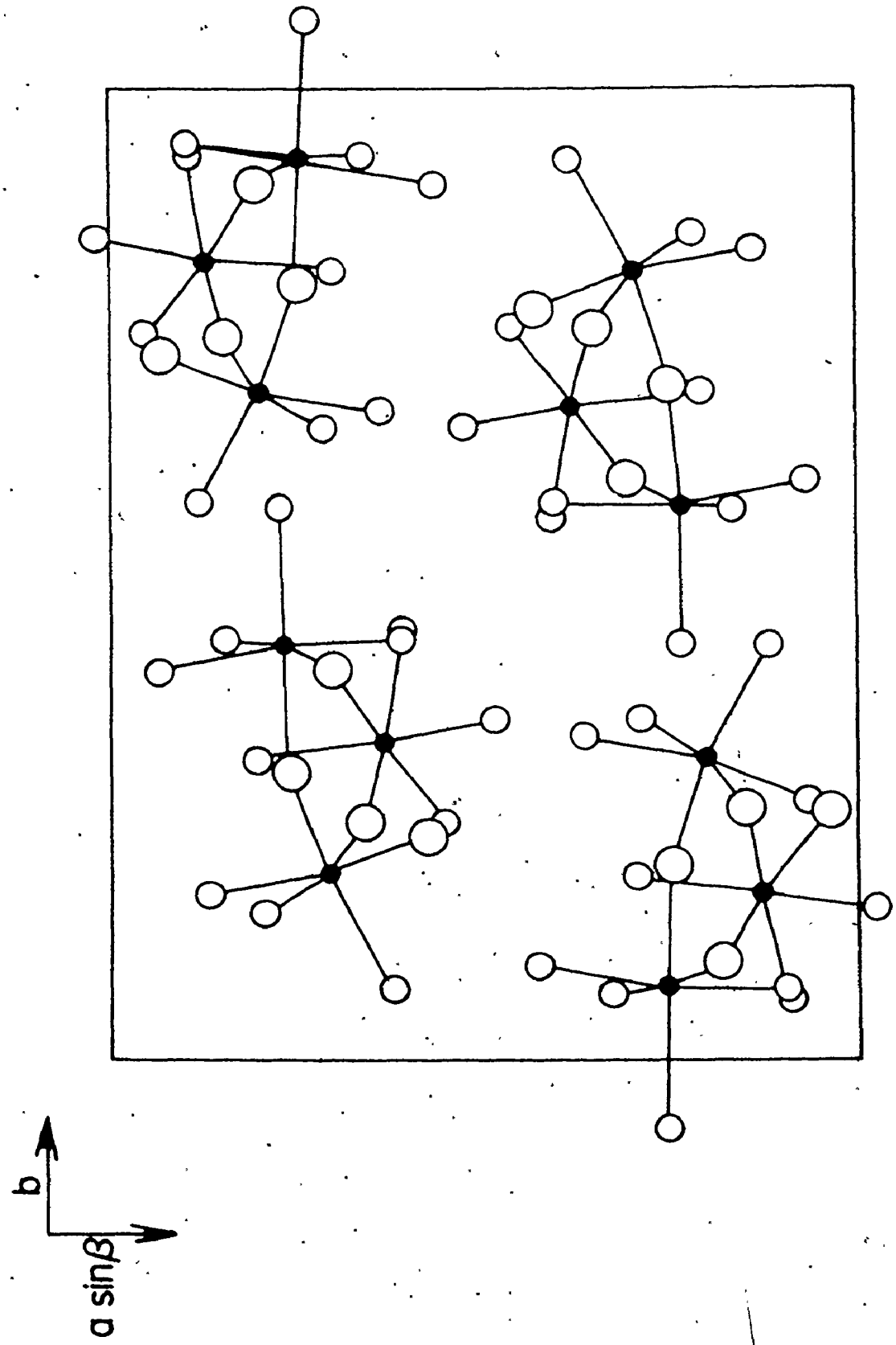
b
a sinβ

is some contribution to the structure from the $[SbCl_4^+]$ cationic species.

The Sb-F terminal bond length, 1.87 Å, is somewhat shorter than those found in $Sb_3Cl_9F_4O$ [122] and $SbCl_3F_2$ (discussed later in this section), 1.94 Å and 1.92 Å, respectively. The Sb-F terminal bond lengths in the $[Sb_2Cl_2F_9^-]$ anion vary over a wide range, 1.83-1.99 Å.

The bridge between Sb(2) and Sb(3) is symmetric (mean Sb-F = 2.08 Å), whereas those between Sb(1) and Sb(2), and Sb(1) and Sb(3) are asymmetric (mean 2.08 Å). These bridging fluorines complete the distorted octahedral coordination about each antimony atom. The mean bridge distance is comparable to the corresponding means in $Sb_3Cl_9F_4O$ [122] and $SbCl_4F$,[41] at 2.07 Å and 2.12 Å, respectively, all of which are longer than that in the $[Sb_2Cl_2F_9^-]$ anion (2.00 Å).[44]

The Sb(ClF) bond length has approximately the value expected for a site consisting of 75% chlorine and 25% fluorine. This analysis means that the crystal can be considered to be a mixture of $Sb_3Cl_{11}F_4$ and $Sb_3Cl_{10}F_5$. One site has four chlorines and two cis-bridging fluorines as in $SbCl_4F$ [41] and the other sites have three chlorines, one terminal fluorine and two cis-bridging fluorines as in $SbCl_3F_2$ (see later). Two of the former and one of the latter units constitute the trimer $Sb_3Cl_{11}F_4$ and the converse is true for $Sb_3Cl_{10}F_5$. The relative orientation of the terminal fluorines in $Sb_3Cl_{10}F_5$ is the same as those in $SbCl_3F_2$.

The Sb_3F_3 trimer is considerably distorted with a mean F-Sb-F' angle of 79.4° and a mean Sb-F-Sb' angle of 158.2°. These are in sharp contrast to the corresponding O-Sb-O' and Sb-O-Sb' angles of the trimeric anion $[Sb_3O_3F_{12}^{3-}]$ [123] of 101° and 130°, respectively. $Sb_3Cl_{10.75}F_{4.25}$

presumably forms a less efficiently packed entity and the large chlorine atoms would tend to reduce the F-Sb-F' angles and hence increase the Sb-F-Sb' angles. It is interesting to compare these angles with the corresponding angles in $SbCl_4F$ [41] and $SbCl_3F_2$, i.e., 82.7° and 173°, and 78° and 164°, respectively. Packing considerations are probably dominant since in these compounds there is an attempt to form an approximate cubic close packed array. Also, the constraints in going from a trimer to a tetramer must be considered.

b. $SbCl_3F_2$

The crystallographic work on this compound was performed by Dr. D. R. Slim of this department. $SbCl_3F_2$ is tetragonal with $\underline{a}$ = 12.81(1) Å, $\underline{c}$ = 7.28(1) Å, U = 1194.6 Å^3, Z = 8, D_c = 2.96 g cm^{-3}, and FW = 266.1, space group I4 (No 79 C_4^5).[124] The structure was refined to a final agreement index R_2 = 0.073 for 265 independent reflections. The structure consists of cis-fluorine bridged tetramers with each antimony having a distorted octahedral arrangement of three fluorines and three chlorines. The geometry about each antimony is given in Figure 5.3. Figure 5.4 contains a projection of the structure of $SbCl_3F_2$ down the c axis of the unit cell and the interatomic distances and angles are lised in Table 5.2. The details of the solution and the refinement of the structure are published elsewhere.[125]

The terminal fluorine is cis to the two bridging fluorines and hence the three chlorine atoms are each trans to a fluorine atom, as shown in Figure 5.3. All of the terminal fluorines are situated on the same side of the plane formed by the antimony and bridging fluorine atoms.

Figure 5.3. The Octahedral Coordination of Light Atoms about Antimony with Bond Lengths and Selected Bond Angles.

(● Sb, ○ Cl, ○ F.)

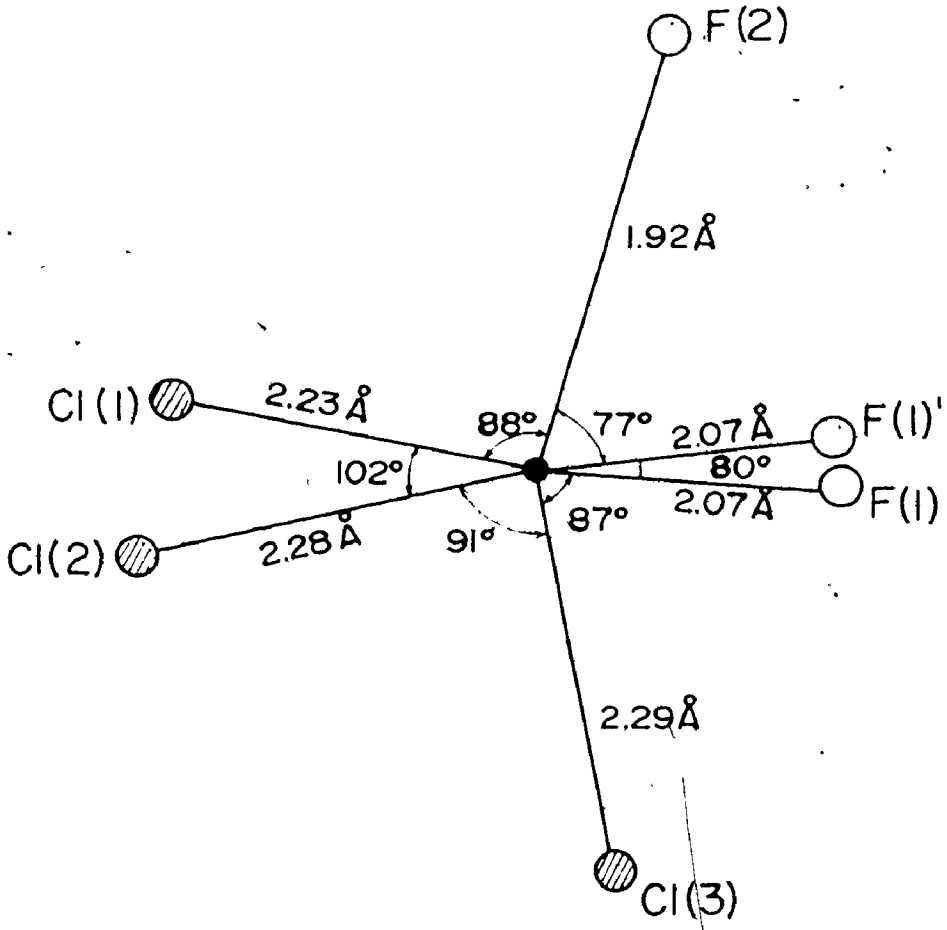
F(2)
1.92Å
Cl(1)
2.23Å
88°
77°
2.07Å
F(1)'
102°
80°
2.07Å
F(1)
87°
Cl(2)
2.28Å
91°
2.29Å
Cl(3)

Figure 5.4. Projection of the Structure of $SbCl_3F_2$ along the c Axis. (● Sb, ○ Cl, ○ F).

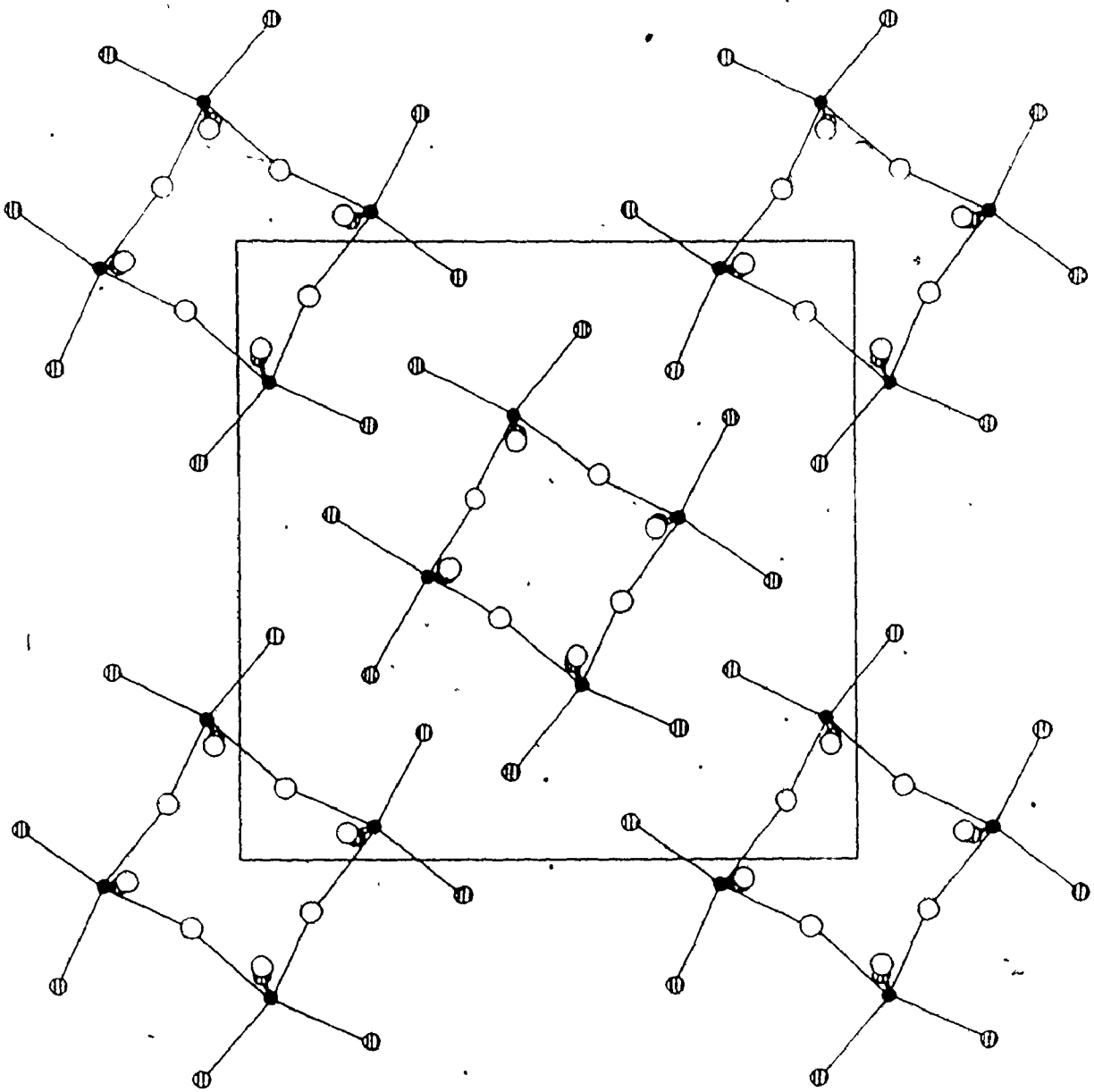

Table 5.2. Interatomic Distances and Angles for $SbCl_3F_2$.[a]

(a) Bond Lengths

Bond	Length (Å)	Bond	Length (Å)
Sb-Cl(1)	2.23(1)	Sb-F(1)	2.07(2)
Sb-Cl(2)	2.28(2)	Sb-F(1)'	2.07(2)
Sb-Cl(3)	2.29(2)	Sb-F(2)	1.92(3)

(b) Bond Angles

Bonds	Angle (deg)	Bonds	Angle (deg)
Cl(1)-Sb-Cl(2)	101.6(5)	Cl(3)-Sb-F(1)	87(1)
-Cl(3)	104.1(9)	-F(1)'	87(1)
-F(1)	163(1)	-F(2)	160(1)
-F(1)'	87.2(7)		
-F(2)	88(1)	F(1)-Sb-F(1)'	80.2(9)
		-F(2)	77(1)
Cl(2)-Sb-Cl(3)	91.2(9)		
-F(1)	91.1(7)	F(1)'-Sb-F(2)	78(1)
-F(1)'	171.7(7)		
-F(2)	100.9(9)	Sb-F(1)-Sb'	164(2)

[a] Standard errors are given in parentheses.

The mean Sb-Cl bond length, 2.27 Å, is comparable to the corresponding mean 2.26 Å in both $Sb_3Cl_{10.75}F_{4.25}$ and $Sb_3Cl_9F_4O$.[122] These bond lengths were discussed earlier in this section.

The Sb-F terminal bond length, 1.92 Å, is similar to that found in $Sb_3Cl_9F_4O$, 1.94 Å,[122] and the mean Sb-F terminal bond of the $[Sb_2Cl_2F_9^-]$ anion, 1.94 Å, of $[SbCl_4^+][Sb_2Cl_2F_9^-]$,[44] however, it is longer than that in the $[Sb_2F_{11}^-]$ anion of $[SbCl_4^+][Sb_2F_{11}^-]$,[45] 1.87 Å. It must be noted that the errors in the bond lengths in $[SbCl_4^+][Sb_2Cl_2F_9^-]$ [44] and $[SbCl_4^+][Sb_2F_{11}^-]$ [45] are large. All of these Sb-F bond lengths for the compounds which contain chlorine atoms are longer than those found for the $[Sb_2F_{11}^-]$ ion in $[ClO_2^+][Sb_2F_{11}^-]$,[126] mean 1.82 Å, and for the $[SbF_6^-]$ ion of $[ClF_2^+][SbF_6^-]$,[127] mean 1.86 Å. These observed increases in length may be attributed to the presence of the relatively bulky chlorine atoms, allowing a shift in electrons toward the more electronegative fluorine atoms.

The Sb-F bridging bond length, 2.07 Å, is also longer than that found in $[ClO_2^+][Sb_2F_{11}^-]$,[126] 2.01 Å, but is similar to the mean value found in $Sb_3Cl_{10.75}F_{4.25}$ and $Sb_3Cl_9F_4O$ [122] of 2.07 and 2.08 Å, respectively. In the $SbCl_4F$ tetramer[41] a similar lengthening of the bridge bonds is observed but here the fluorine bridge is asymmetric with Sb-F distances of 2.05 Å and 2.18 Å. It should be noted, however, that the errors reported for $SbCl_4F$ are large.

The $SbCl_3F_3$ octahedra show considerable angular distortion as illustrated in Figure 5.3. Two of the Cl-Sb-Cl' angles are opened up from the 90° angle expected for an octahedral arrangement to approximately 102°, whereas, the third angle, Cl(2)-Sb-Cl(3), is 91°. In addition,

all of the Cl-Sb-F angles are 90° except for Cl(2)-Sb-F(2), which is 101°. The average F-Sb-F' angles are 79°. This distortion is thought to be due to the presence of the large chlorines which tend to close down the F-Sb-F' angles. As a result, the Cl-Sb-Cl' angles are opened up, i.e., the average Cl-Sb-Cl' angle is 98°.

In the Sb_4F_4 tetramer, the reduction of the F(1)-Sb-F(1)' angle has a considerable influence on the Sb-F(1)-Sb' angle. In $SbCl_3F_2$, the former angle is 79° compared to 82.7° in $SbCl_4F$, while the corresponding angles at the bridging fluorine are 164° and 173°, respectively, for these two compounds. This tetramer also resembles that of SbF_5,[128] where two different Sb-F-Sb' angles are found, namely 170° and 141°. In the latter compound, it was suggested that these different angles were a consequence of the structure consisting of a mixture of cubic and hexagonal close-packed arrays of fluorine atoms.[128] If this analogy can be continued to the chloride fluoride structures, it suggests that both $SbCl_3F_2$ and $SbCl_4F$ consist of approximate cubic close-packed arrays of halogen atoms. One would expect distortions from the ideal close-packed arrangements in these cases since all the halogens are not the same size. $SbCl_4F$ contains a higher percentage of close-packed atoms of the same size than does $SbCl_3F_2$, hence, one would anticipate that the latter structure should deviate more from the cubic close-packed arrangement than $SbCl_4F$. This deviation is reflected in the smaller Sb-F-Sb' angles in $SbCl_3F_2$ than in $SbCl_4F$.

Comparisons with the $NbCl_4F$ and $TaCl_4F$ structures[129,130] bear out these generalizations. For example, the F-Nb-F' angle is 81°, i.e.,

between that of $SbCl_3F_2$ and $SbCl_4F$, and the Nb-F-Nb' angle is 171° again between the values for the two antimony chloride fluorides, whereas, the F-Ta-F' angle is close to 90° and the bridging angle has opened up to 180°. Therefore, both of these molecules, $NbCl_4F$ and $TaCl_4F$, can be considered to have a cubic close-packed array.

c. $[SbCl_4^+][Sb_2Cl_2F_9^-]$

The cell dimensions of a crystal of this compound were measured by Dr. D. R. Slim of this department. They were identical to those found by Preiss,[44] who had concluded that $SbCl_2F_3$ is ionic, consisting of a tetrahedral $[SbCl_4^+]$ cation and a $[Sb_2Cl_2F_9^-]$ anion. The bond lengths and bond angles of this compound have been recalculated using Preiss' atomic coordinates.[44] In this subsequent analysis, four additional interactions between the antimony atom of the cation and fluorine atoms of neighbouring anions were observed. These had previously been ignored by Preiss. Admittedly, these interactions are weak, but should be considered when discussing the chemistry of this material.

The interatomic bond lengths and bond angles of the $[SbCl_4^+]$ cations are listed in Table 5.3. This Table includes the longer Sb-F interactions mentioned above. The geometry of the cation is depicted in Figure 5.5 and the packing diagram in Figure 5.6.

The specific bond lengths and bond angles have been discussed by Preiss and the Sb-Cl bond lengths were compared earlier in this chapter with those of $Sb_3Cl_{10.75}F_{4.25}$ and $SbCl_3F_2$. In each of these cases, the Sb-Cl bond lengths were longer than the mean Sb-Cl bond length of the

Figure 5.5. A View of the Antimony Environment in the Cation of $[SbCl_4^+][Sb_2Cl_2F_9^-]$. (The F Numbering Refers to the Anion.)

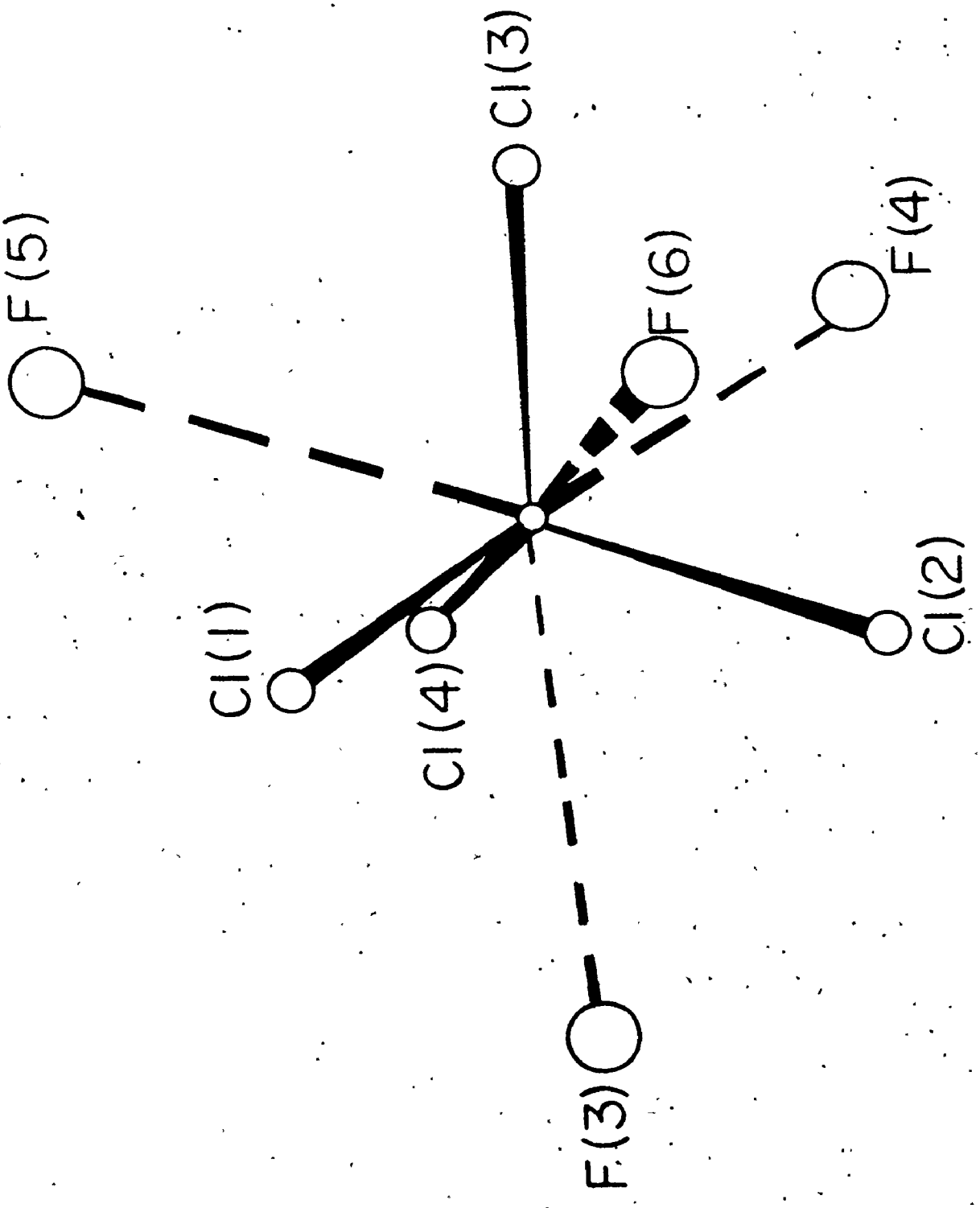
F(5)
Cl(3)
F(6)
F(4)
Cl(1)
Cl(4)
Cl(2)
F(3)

Figure 5.6. Projection of the Unit Cell of $[SbCl_4^+][Sb_2Cl_2F_9^-]$ down the c Axis (Circles of Increasing Size Represent Sb, Cl, and F, respectively.)

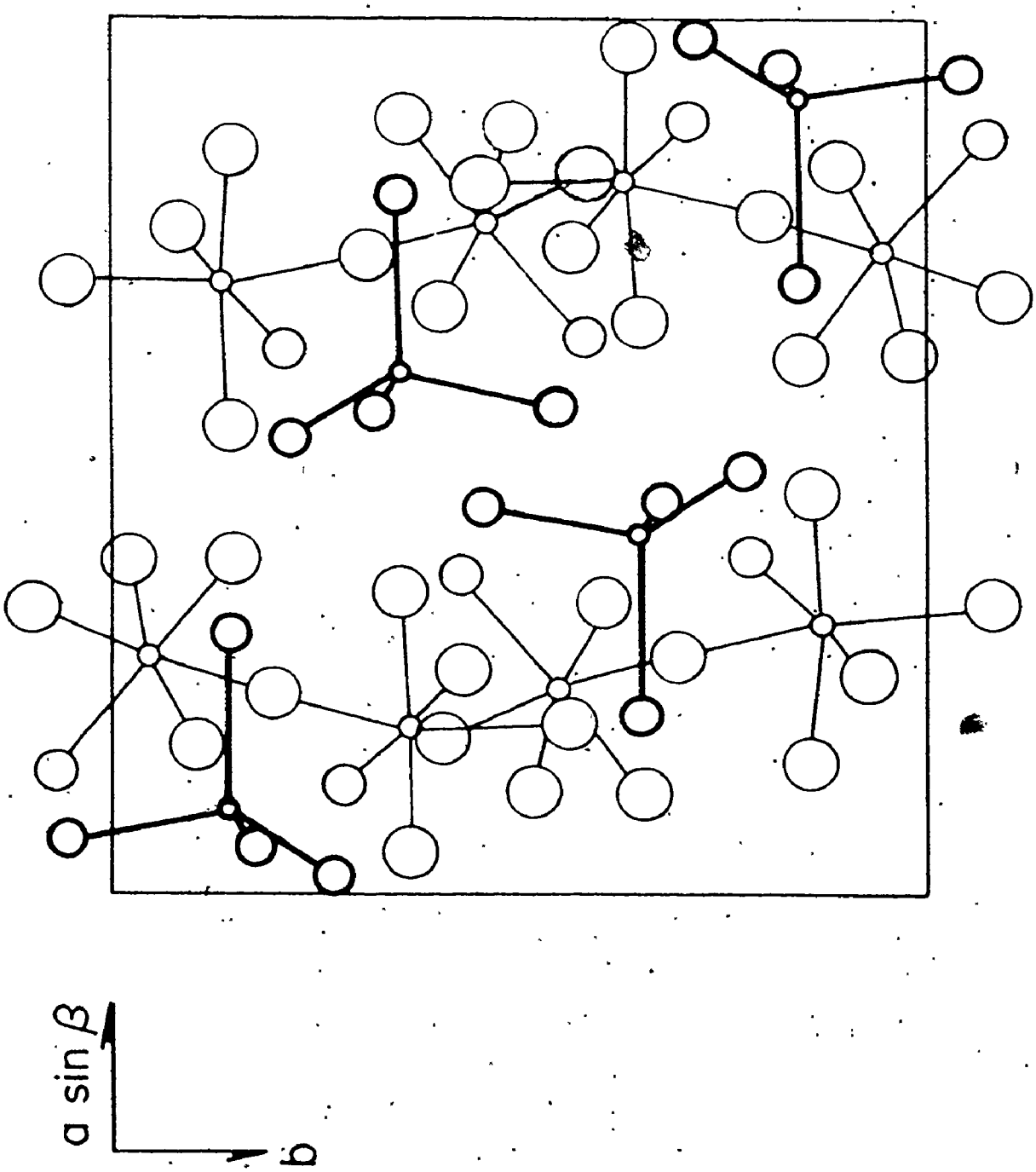
a sin β
b

Table 5.3. Interatomic Distances and Angles for the $[SbCl_4^+]$ Cation of $[SbCl_4^+][Sb_2Cl_2F_9^-]$.[a]

(a) Bond Lengths

Bond	Length (Å)	Bond	Length (Å)
Sb-Cl(1)	2.16	Sb-F(2)	3.16
-Cl(2)	2.21	-F(4)	3.26
-Cl(3)	2.15	-F(5)	2.90
-Cl(4)	2.19	-F(6)	2.93

(b) Bond Angles

Bonds	Angle (deg)	Bonds	Angle (deg)	Bonds	Angle (deg)
Cl(1)-Sb-Cl(2)	107.9	Cl(2)-Sb-Cl(3)	108.6	Cl(3)-Sb-Cl(4)	109.9
-Cl(3)	116.8	-Cl(4)	107.3	-F(3)	172.5
-Cl(4)	107.9	-F(3)	64.0	-F(4)	67.3
-F(3)	67.6	-F(4)	71.9	-F(5)	73.2
-F(4)	175.6	-F(5)	178.3	-F(6)	72.9
-F(6)	71.2				
				Cl(4)-Sb-F(3)	74.2
		F(3)-Sb-F(4)	108.6	-F(4)	68.9
F(4)-Sb-F(5)	109.9	-F(5)	114.3	-F(5)	71.9
-F(6)	112.9	-F(6)	104.2	-F(6)	178.9
F(5)-Sb-F(6)	108.0				

[a] Recalculation of the bond lengths from the structure reported by Preiss.[13]

[b] Standard errors not determined.

$[SbCl_4^+]$ cation discussed here. Presumably, this is the result of the tetrahedral coordination in the latter case, as opposed to the octahedral coordination in the two former chloride fluorides. That is, as a result of fewer halogens about the antimony, the Sb-Cl bond length is shorter. The average Sb-Cl bond length of $[SbCl_4^+][Sb_2F_{11}^-]$, 2.22 Å,[45] is essentially the same as that of $[SbCl_4^+][Sb_2Cl_2F_9^-]$, 2.18 Å.[44] This is to be expected since the structures are comparable, although the errors in each case are relatively large.

The mean Sb---F bond length of the cation, 3.06 Å, is considerably longer than any Sb-F bonds in $SbCl_4F$,[41] $Sb_3Cl_{10.75}F_{4.25}$, or $SbCl_3F_2$, 1.94 Å, 1.87 Å, and 1.92 Å, suggesting a weak although significant interaction between the cation and the neighbouring anions, since the sum of the van der Waal radii is 3.55 Å.[131] As indicated in Figure 5.6, the $[SbCl_4^+]$ cation is situated in the unit cell such that fluorine atoms from adjacent $[Sb_2Cl_2F_9^-]$ anions form a tetrahedron of fluorine atoms perpendicular to the faces of the $[SbCl_4^+]$ tetrahedron giving an overall eight coordination about the antimony. This cation is situated such that two antimony atoms of the anion and the antimony atom of the cation form a trimeric arrangement similar to that found for $Sb_3Cl_{10.75}F_{4.25}$.

It appears that in the trimeric species, the $SbCl_4$ unit is the dominant structural component. In both of the compounds discussed earlier, $Sb_3Cl_{11}F_4$ and $Sb_3Cl_{10}F_5$, the $SbCl_4$ unit was cis-fluorine bridged to two more highly fluorinated antimony atoms to form a trimer. In the case of $[SbCl_4^+][Sb_2Cl_2F_9^-]$ the $SbCl_4$ unit is also cis-fluorine bridged to a $Sb_2Cl_2F_9$ unit forming a trimer. In the latter case, the number of fluorines

involved in the trimer was substantially greater, thus increasing the basicity of the $Sb_2Cl_2F_9$ fragment, resulting in a more ionic structure. However, an ionized form of the $[SbCl_4^+]$ cation is not present in the $Sb_3Cl_{11}F_4$ or $Sb_3Cl_{10}F_5$ species, because of the lower basicity of the $Sb_2Cl_7F_4$ and $Sb_2Cl_6F_5$ fragments, respectively. This hypothesis might be further substantiated if the intermediate compound $Sb_3Cl_8F_7$ could be prepared and characterized. That is, this compound would likely be partially ionized because of the increased basicity of the $Sb_2Cl_4F_7$ unit compared to those of $Sb_2Cl_7F_4$ and $Sb_2Cl_6F_5$. However, this compound could not be prepared although several attempts were made. The preliminary structure reported for $[SbCl_4^+][Sb_2F_{11}^-]$ [45] indicates that this compound is ionized as in $[SbCl_4^+][Sb_2Cl_2F_9^-]$.[44] The shortest $SbCl_4$---F bond length in $[SbCl_4^+][Sb_2F_{11}^-]$ is 3.0 Å and the increased number of fluorines in this compound are bonded such that the $SbCl_4$ unit is preserved. As mentioned in section 5.B(i), a still more highly fluorinated species could not be prepared inspite of several attempts to fluorinate $SbCl_4F$ with greater than 2:1 mole ratios of SbF_5 to $SbCl_4F$. Hence, the $SbCl_4$ unit is again preserved.

The structure found for $[SbCl_4^+][Sb_2Cl_2F_9^-]$ is consistent with its chemical nature. For example, $[SbCl_4^+][Sb_2Cl_2F_9^-]$ is low melting and as a liquid, resembles the highly viscous SbF_5. Perhaps this implies a more polymeric nature for the molten state. The fact that an interaction is found between the cation and the anion in the solid state is, therefore, not surprising.

(iii) Mössbauer Spectroscopy

The results obtained from an analysis of the ^{121}Sb Mössbauer spectra of the $SbCl_{5-x}F_x$ compounds are listed in Table 5.4. This Table also includes the ^{121}Sb Mössbauer data for $[AsCl_4^+][SbF_6^-]$ and the $SbCl_4F\cdot(NbF_5)_x$ (x = 1,2) adduct.

The isomer shift values for all of these compounds are positive, ranging from +4.4 mm/sec for the $[SbCl_4^+]$ site of $[SbCl_4^+][Sb_2Cl_2F_9^-]$ and $[SbCl_4^+][Sb_2F_{11}^-]$ to +10.96 mm/sec for the $[SbF_6^-]$ anion of $[AsCl_4^+][SbF_6^-]$. In each of these compounds, the Sb(V) electronic configuration can be considered to be $5s^0$. The isomer shift, which represents the s electron density at the antimony nucleus, is dependent upon this configuration modified by the covalent interactions with the chlorine and fluorine ligands.

The quadrupole coupling constants in these compounds are all positive, except for $SbCl_5$. A finite quadrupole coupling indicates a finite electric field gradient about the antimony nucleus arising either from the presence of non-equivalent ligands about this nucleus or an asymmetric distribution of electron density. The absolute value of this quadrupole interaction (eQV_{zz}) decreases as these ligands become more equivalent, i.e., the covalent interaction between the ligands and the antimony nucleus become more alike. A positive quadrupole coupling constant is expected when the electron population in the z direction of the antimony atom is higher than that in the x or y directions. When the reverse is true, the electric field gradient tensor is positive, and, since Q is negative, the quadrupole coupling constant is negative.

The most common coordination geometry about the antimony in the

Table 5.4. ^{121}Sb Mössbauer Parameters at 4°K for $SbCl_{5-x}F_x$ Compounds and Related Adducts

Compound	δ/mm sec^{-1} ± 0.1	eQV_{ZZ} mm sec^{-1} ± 2.0	Γ^a/ mm/sec^{-1}	η	T_a	m	$(CHI)^2$/ deg of freedom
$SbCl_5$	5.28	-5.7	2.3	--	--	0.35	0.94
$SbCl_4F$	6.34	11.8	3.6	0.71	0.60	0.17	1.28
$Sb_3Cl_{10.75}F_{4.25}$	7.69 5.30	2.7 8.9	3.9 2.6	-- --	-- --	0.10	0.87
$SbCl_3F_2$	6.84	9.8	3.3	0.88	0.53	0.01	1.01
$[SbCl_4^+][Sb_2Cl_2F_9^-]$	8.66 4.38	13.1 3.2	4.0 2.0	-- --	-- --	0.37	1.99
$[SbCl_4^+][Sb_2F_{11}^-]$	10.11 4.43	14.3 0.0	3.4 3.1	-- --	-- --	0.02	1.06
SbF_5	10.26	8.7	2.2	--	--	0.72	1.05
$SbCl_4F \cdot AsF_5$	10.96	--- [b]	3.1	--	--	0.16	1.14
$SbCl_4F \cdot NbF_5$	6.16	8.0	3.4	--	--	0.49	1.18

[a] Line width (mm/sec)

[b] Too small to properly evaluate.

antimony(V) chloride fluorides is a distorted octahedron. Exceptions to this are $SbCl_5$, which has been shown by Ohlberg[46] to have a trigonal bipyramidal structure at 243°K, and the $[SbCl_4^+]$ cation of $[SbCl_4^+][Sb_2Cl_2F_9^-]$[44] and $[SbCl_4^+][Sb_2F_{11}^-]$,[45] which has tetrahedral geometry. However, doubt has been cast in the literature over the structure of $SbCl_5$ at lower temperatures, i.e., an ionic form, $[SbCl_4^+][SbCl_6^-]$, has been suggested.[132,133] The Mössbauer data for $SbCl_5$ at 4°K, presented here, indicates a single antimony site and the negative quadrupole coupling constant is consistent with the structure proposed by Ohlberg.[46] This rules out $[SbCl_4^+][SbCl_6^-]$ at the low temperature phase since the experimental spectrum cannot be fitted to the two antimony sites expected for this formulation, especially since the isomer shift of an $[SbCl_4^+]$ cation is now known (Table 5.4).

The ^{121}Sb Mössbauer spectrum of $SbCl_4F$, shown in Figure 5.7, was fitted to a single antimony site. The spectrum was best fitted using the transmission integral function[91,134] and a variable asymmetry parameter. $SbCl_4F$ is a tetramer with cis-fluorine bridges completing an octahedral arrangement about each antimony.[41] Presumably, the quadrupole coupling constant results from the presence of two ligands of differing electronegativity situated about each antimony in such a way as to produce an electric field gradient. Since Q is negative, a positive quadrupole coupling constant results from a negative electric field gradient and the concentration of charge along the symmetry axis. An η value of 0.71 indicates an asymmetry about this axis. This is not a surprising result in view of the crystallographic evidence,[41] although the η value does seem rather large.

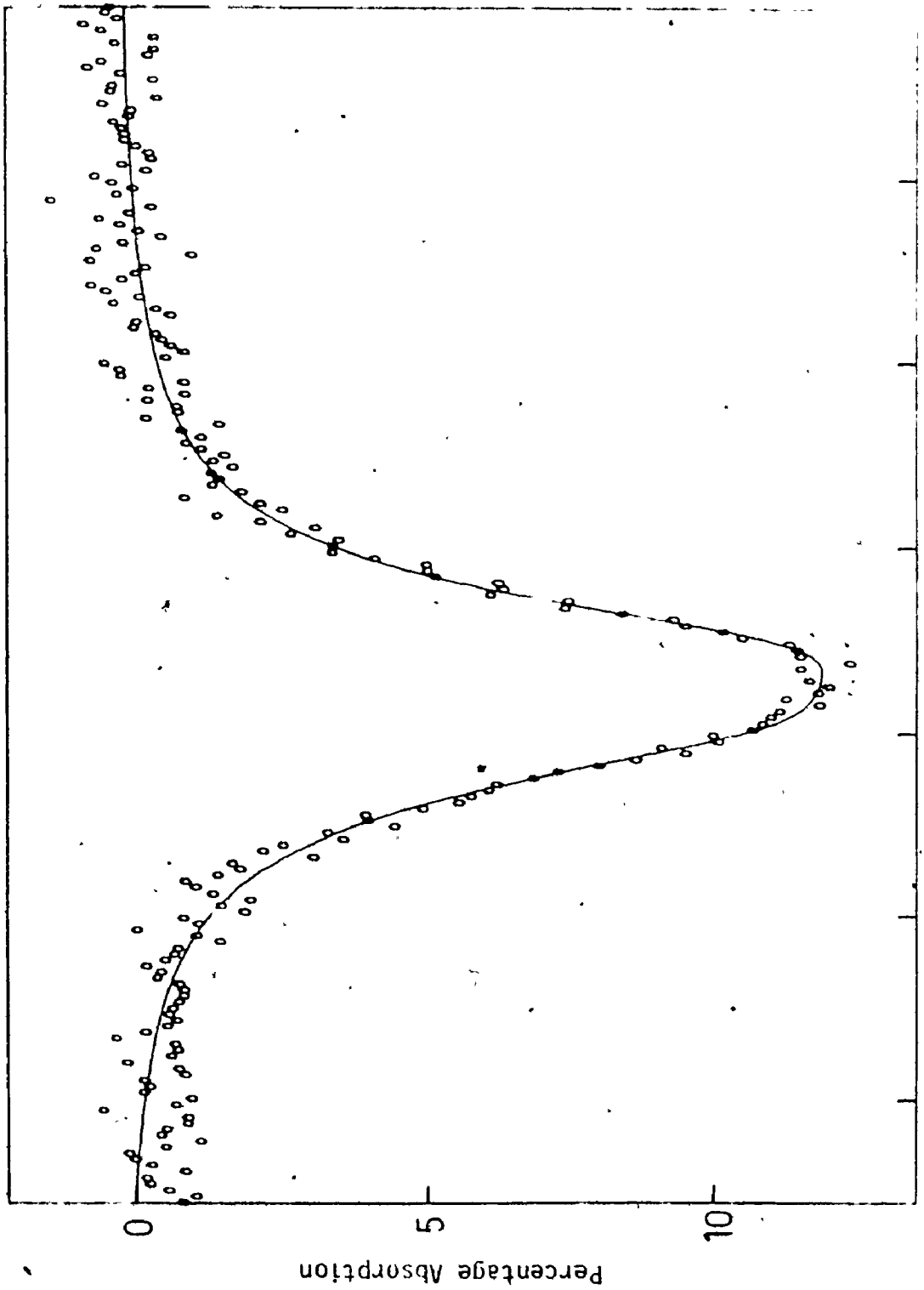

Figure 5.7. ^{121}Sb Mössbauer of $SbCl_4F$ at 4°K with an Asymmetry Parameter ?.

The ^{121}Sb Mössbauer spectrum of $SbCl_3F_2$ contains one antimony site. From the data presented in Table 5.4, it appears that this site has a less distorted environment than that found in the previously mentioned case. $SbCl_3F_2$ has been shown earlier to have a tetrameric structure similar to that of $SbCl_4F$ with three chlorines, a terminal fluorine and two cis-bridging fluorines about each antimony. The positive quadrupole coupling constant and large η value indicate that the environment about each antimony in this compound is very distorted. This distortion is to be expected from the arrangement of halogen atoms about the antimony, Figure 5.3.

The ^{121}Sb Mössbauer spectrum for $Sb_3Cl_{10.75}F_{4.25}$ could not be fitted to a single site and a good fit was obtained only when two antimony sites were considered. The subsequent crystallographic work indicated that there were indeed two antimony sites in this compound. The ^{121}Sb Mössbauer parameters of one of these sites should resemble that of $SbCl_4F$, while those of the other site should be similar to the parameters reported in Table 5.4 for $SbCl_3F_2$. However, from an examination of Table 5.4, it is evident that the isomer shift of the ($SbCl_4F$---F) site of this trimer is less positive than that of the corresponding site in $SbCl_4F$. This indicates that the s electron density about the antimony site of the trimer is greater than that of the tetramer. The isomer shift for the ($SbCl_3F_2$---F) site is greater than that of the corresponding site of the $SbCl_3F_2$ tetramer, signifying a lower s electron density about the antimony of the former compound. Clearly, this compound does not contain an $[SbCl_4^+]$ cation as is the case in the other trimeric chloride fluorides.

However, the isomer shift of the ($SbCl_4F$---F) site, although more positive than that of $[SbCl_4^+]$, is lower than that of the analogous site in $SbCl_4F$. This perhaps implies some contribution from the ionized forms, for example, $[SbCl_4^+][Sb_2Cl_7F_4^-]$ and $[SbCl_4^+][Sb_2Cl_6F_5^-]$. Such contributions are not immediately obvious from the crystallographic data discussed earlier. However, it should be noted that the F-Sb-F' angle of the bridging fluorines is smaller (78.6°) than that of $SbCl_4F$ (86.7°).[41] In addition, the antimony fluorine ($Sb(2)Cl_4$---F_2) bridging bonds of the trimer are equal in length, whereas those of $SbCl_4F$ are asymmetric. The Sb-Cl bonds perpendicular to the plane of the trimer are short, 2.20 Å and 2.24 Å, compared to those of the $SbCl_4F$, 2.32 Å. Presumably, these small variations contribute to the lower isomer shift value found for one of the sites of the trimer compared to an analogous site in the tetramer. The ($SbCl_3F_2$---F) site of the trimer is not significantly different crystallographically from that of $SbCl_3F_2$. The quadrupole coupling constants found for $Sb_3Cl_{10.75}F_{4.25}$ are consistent with the proposed structure. The quadrupole coupling constant of the ($SbCl_4F$---F) site is larger than that of the ($SbCl_3F_2$---F) site. This indicates that the former site has the more asymmetric environment. The eQV_{zz} values of both sites of the trimer are smaller than those of the corresponding tetramers indicating a more regular environment. It should be pointed out, however, that it is very difficult to analyze two complex overlapping spectra and extract accurate Mössbauer parameters.

Two of the compounds listed in Table 5.4, $[SbCl_4^+][Sb_2Cl_2F_9^-]$ and $[SbCl_4^+][Sb_2F_{11}^-]$, give Mössbauer spectra which clearly show the presence

of two different antimony sites. These spectra are shown in Figure 5.8. Both have a narrow resonance at low velocity, 4.4 mm/sec, and a broad more intense resonance at higher velocity. One of these sites has a very symmetrical environment, while the other has an asymmetric environment. Clearly, the narrow Mössbauer resonance at 4.4 mm/sec is assignable to the $[SbCl_4^+]$ cation in each of the compounds. The $[Sb_2F_{11}^-]$ anion of $[SbCl_4^+][Sb_2F_{11}^-]$ [45] has an isomer shift value in much the same region of the spectrum as SbF_5 (Table 5.4). This is not surprising since in both compounds the antimony is surrounded by six fluorine atoms. The isomer shift value of the $[Sb_2F_{11}^-]$ anion, however, is lower than that of $Cs[Sb_2F_{11}]$.[99] By replacing a terminal fluorine in $[Sb_2F_{11}^-]$ by a chlorine to give $[Sb_2Cl_2F_9^-]$ there is a reduction in the isomer shift. Since chlorine is less electronegative than fluorine, the withdrawal of electron density from the antimony would be reduced, s electron density would increase, and the isomer shift value should be less positive. The quadrupole coupling constants of the anions, $[Sb_2Cl_2F_9^-]$ and $[Sb_2F_{11}^-]$, are large, implying considerable asymmetry about the antimony nuclei. As discussed earlier, there is some bridging interaction between the anion and the cation of $[SbCl_4^+][Sb_2Cl_2F_9^-]$.[44] This interaction, together with the fact that each antimony of the anion is surrounded by nonequivalent ligands, results in a large quadrupole coupling constant. A completely ionic formulation for $[SbCl_4^+][Sb_2F_{11}^-]$ [45] is inconsistent with the large quadrupole coupling constant reported here for the anion. For example, the quadrupole coupling constant of $Cs[Sb_2F_{11}]$ is +5.2 mm/sec, considerably smaller than that reported for the anion of $[SbCl_4^+][Sb_2F_{11}^-]$, 14.31 mm/sec. Perhaps,

Figure 5.8. ^{121}Sb Mössbauer at 4°K of

(a) $[SbCl_4^+][Sb_2Cl_2F_9^-]$ and of

(b) $[SbCl_4^+][Sb_2F_{11}^-]$ each with Two Antimony Sites.

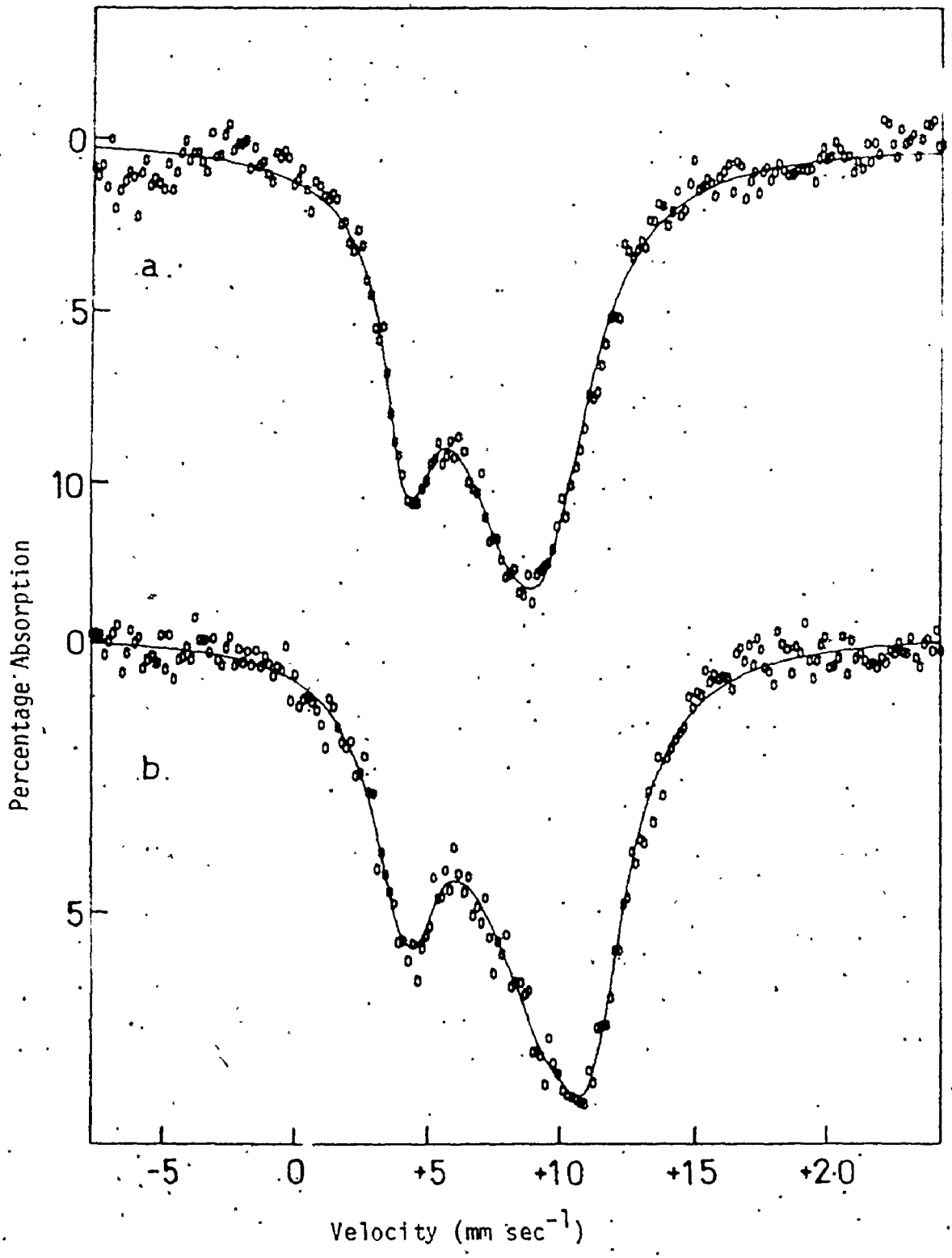
0
5
10
0
5
a.
b.
Percentage Absorption
-5
0
+5
+10
+15
+20
Velocity (mm sec^{-1})

Sb-F-Sb' interactions are present between the cation and anion of $[SbCl_4^+][Sb_2F_{11}^-]$ similar to those found for the analogous $[Sb_2Cl_2F_9^-]$ analogues resulting in a large quadrupole coupling constant. However, this type of interaction cannot be substantiated from the crystallographic data since the positional parameters were not reported by Miller et al.[45]

The $[SbCl_4^+]$ cation of $[SbCl_4^+][Sb_2Cl_2F_9^-]$ has a fluorine at each face of the tetrahedron formed by the chlorines, giving an overall eight coordination about the antimony as depicted in Figure 5.5. In spite of these Sb--F interactions, the quadrupole coupling constant is very small indicating that the coordination about the antimony of the cations is almost tetrahedral.

The ^{121}Sb Mössbauer spectrum of SbF_5 at 4°K is similar to that reported earlier at liquid-nitrogen temperatures.[57] X-ray crystallography has shown that SbF_5 is a tetramer in the solid state[128] with each antimony surrounded by four terminal and two bridging fluorines in a distorted octahedral arrangement. A large positive isomer shift results from the electronegative fluorines withdrawing electron density from the antimony. Presumably, the quadrupole coupling arises from the fact that all fluorines about each antimony are not equivalent, nor are the F-Sb-F' angles 90°,[128] and an asymmetric electronic charge distribution results. It should be pointed out, however, that the spectrum fitted almost as well to a single Lorentzian line.

In all of the antimony(V) chloride fluorides, where the immediate coordination about the antimony is six, the isomer shift of the nucleus is consistent with the relative number of coordinated chlorine or fluorine

atoms. This relationship is graphically depicted in Figure 5.9. Antimony pentafluoride, with each antimony atom having six fluorine neighbours, has the most positive isomer shift, i.e., the lowest s electron density at the antimony nucleus, while $SbCl_4F$ with four chlorines and two fluorines per antimony has the lowest isomer shift. Figure 5.9 shows that such a correlation, i.e., isomer shift versus ΔF, could be used to predict the coordination about the antimony sites in analogous compounds and subsequently be of some use in structure determination.

The deviation of the Sb sites of $Sb_3Cl_{10.75}F_{4.25}$ from this smooth curve have been explained as being due to contributions from ionic structures, for example $[SbCl_4^+][Sb_2Cl_7F_4^-]$ and $[SbCl_4^+][Sb_2Cl_6F_7^-]$ as described earlier. The smooth curve was not drawn through the $[SbCl_6^-]$ anion since the isomer shift of this alkali metal hexachloroantimonate(V) might be expected to be somewhat higher than the highly bridged antimony(V) chloride fluoride, as a result of the charge on the anion.

The isomer shift of the antimony in $[AsCl_4^+][SbF_6^-]$ is similar to that of the six coordinate antimony(V) fluoride salts (Chapter Six). This rules out any possibility that the structure contains the more complex anion found in $[SbCl_4^+][Sb_2Cl_2F_9^-]$.[44] There appears to be a considerable contribution to the structure from the ionic formulation $[AsCl_4^+][SbF_6^-]$. This is suggested both by the large positive isomer shift value, which is similar to that of the $[SbF_6^-]$ alkali metal salts,[103] and by the relatively small quadrupole coupling constant, which signifies a near regular octahedral geometry. All attempts to prepare the analogous $[SbCl_4^+]$ species failed in favour of the now well-characterized $[SbCl_4^+][Sb_2Cl_2F_9^-]$.

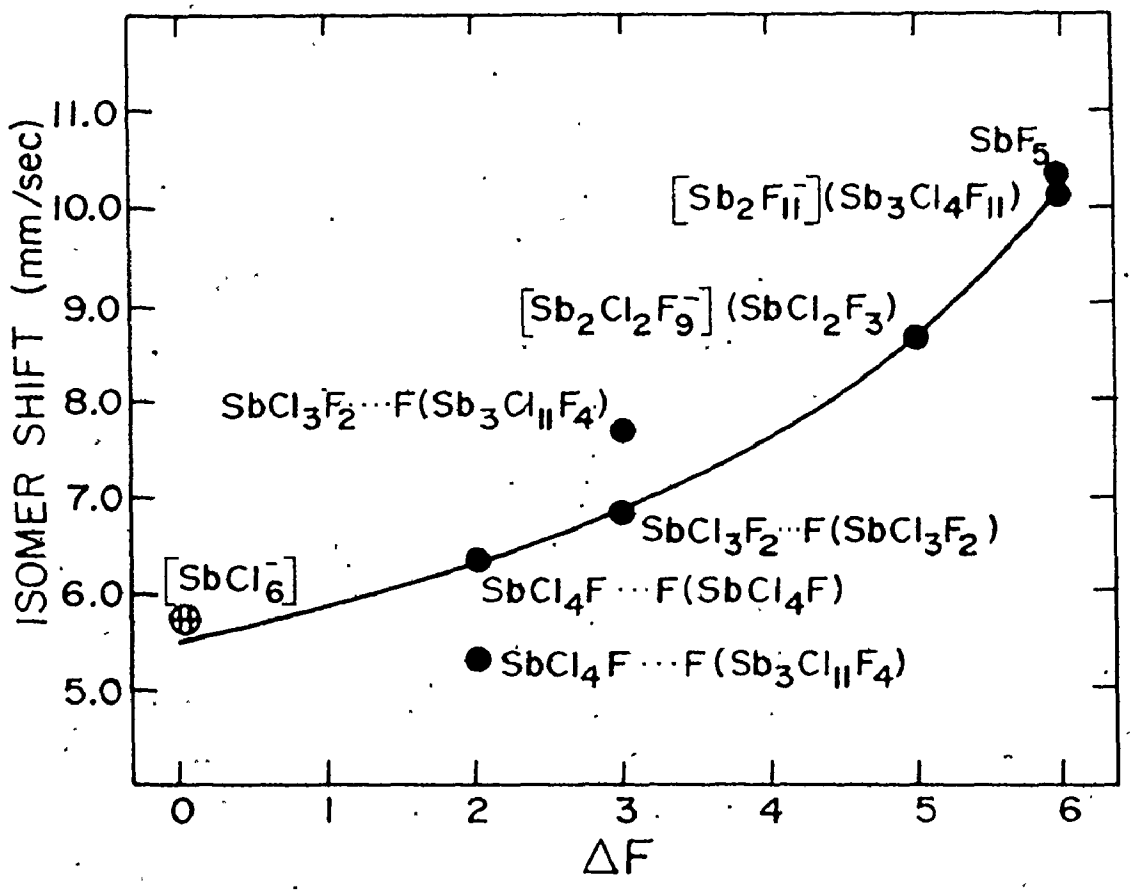

Figure 5.9. Graphical Representation of the Change in Isomer Shift of an Antimony Site Surrounded by Six Halogens as the Chlorines are Replaced by Fluorines. ($Sb_3Cl_{11}F_4$ represents one of the Trimers making up $Sb_3Cl_{10.75}F_{4.25}$, and ΔF represents the Change in the Number of Fluorines about the Antimony Site.)

The isomer shift of the adduct formed from NbF_5 and $SbCl_4F$ is included in Table 5.4. According to the correlations developed in Figure 5.9 between the antimony(V) sites and the isomer shift values, the antimony(V) site of this adduct has a coordination number of six, i.e., four near chlorines and possibly two bridging fluorines. It is evident that halogen exchange between the NbF_5 and $SbCl_4F$ does not occur in this case, as was observed in the AsF_5-$SbCl_4F$ reaction, since there is no formation of the $[SbF_6^-]$ anion. Both NbF_5 and SbF_5 are good fluoride ion acceptors as is evident from the numerous adducts that have been isolated.[135,136] SbF_5 forms an adduct with NbF_5, which has been described as having some contribution from the ionic form, $[NbF_4^+][SbF_6^-]$,[137] suggesting that SbF_5 is the stronger fluoride ion acceptor. In light of the Mössbauer isomer shift value of the NbF_5-$SbCl_4F$ adduct, it seems reasonable to assume that NbF_5 is a stronger fluoride ion accepter than $SbCl_4F$. This follows from the fact that the isomer shift of the antimony of this adduct is slightly lower than that found for $SbCl_4F$, suggesting a small contribution from the $[SbCl_4^+][(NbF_5)_x^-]$ species (x = 1 or 2). Since both NbF_5 [138] and $SbCl_4F$ [41] form cis-bridged tetramers in the solid state and since the NbF_5-SbF_5 adduct is a cis-bridged zig-zag endless chain, it seems reasonable to assume that this adduct contains similar fluorine bridges. However, the exact structure cannot be predicted. From the data presented in this thesis, the adduct corresponding to one $SbCl_4F$ to two NbF_5 molecules cannot be ruled out.

(iv). Raman Spectroscopy

The Raman spectra of solid $Sb_3Cl_{10.75}F_{4.25}$ and $SbCl_3F_2$ are shown

in Figure 5.10 and the corresponding Raman frequencies are listed in Table 5.5, together with the tentative assignments. Due to the complexity of these systems, assignments are difficult, especially in the case of $Sb_3Cl_{10.75}F_{4.25}$, where the bulk material may be any combination of $Sb_3Cl_{10}F_5$ and $Sb_3Cl_{11}F_4$. However, tentative assignments are useful in that they indicate certain characteristic bands which are common to both compounds and to $SbCl_4F$ which was previously studied by Beattie et al.[97] The Raman bands presented in Table 5.5 for $SbCl_4F$ prepared here, are identical to those reported earlier.[97]

The assignments shown for $SbCl_3F_2$ are made on the basis of a monomeric unit, $SbCl_3F_3$, of which four such units compose a tetramer. These simple units, if weakly coupled, can be considered to have C_{3v} symmetry. However, since these monomeric units are relatively strongly coupled, the symmetry is lowered from C_{3v} to Cs. Such a unit should have a total of 15 fundamental vibrations, 9A' and 6A", all of which are active, both in the Raman and infrared. The bulk solid and single crystal spectra contain 12 and 15 bands, respectively. This difference may be the result of the very weak bands being masked in the base line noise of the bulk material. The band at 648 cm^{-1} and 621 cm^{-1} can be tentatively assigned to antimony fluorine stretching frequencies by analogy to the symmetric axial antimony fluorine stretching frequency of SbF_5, which occurs at 670 cm^{-1}.[97] The bands at 380 cm^{-1} can be attributed to the symmetric equatorial Sb-Cl stretch, while that at 346 cm^{-1} can be assigned to the symmetrical axial Sb-Cl stretch by analogy to the corresponding bands in $SbCl_4F$, which occur at 390 and 348 cm^{-1}, respectively. Beattie et al.[97] attributed the weak band at 365 cm^{-1} in $SbCl_4F$ (Table 5.5) to the asymmetric

Figure 5.10. Raman Spectra (20°C) of

(A) Solid $Sb_3Cl_{10.75}F_{4.25}$ and of

(B) Solid $SbCl_3F_2$;

The Spectra were recorded in Glass Melting Point Tubes.

(* represents a Base Line Adjustment.)

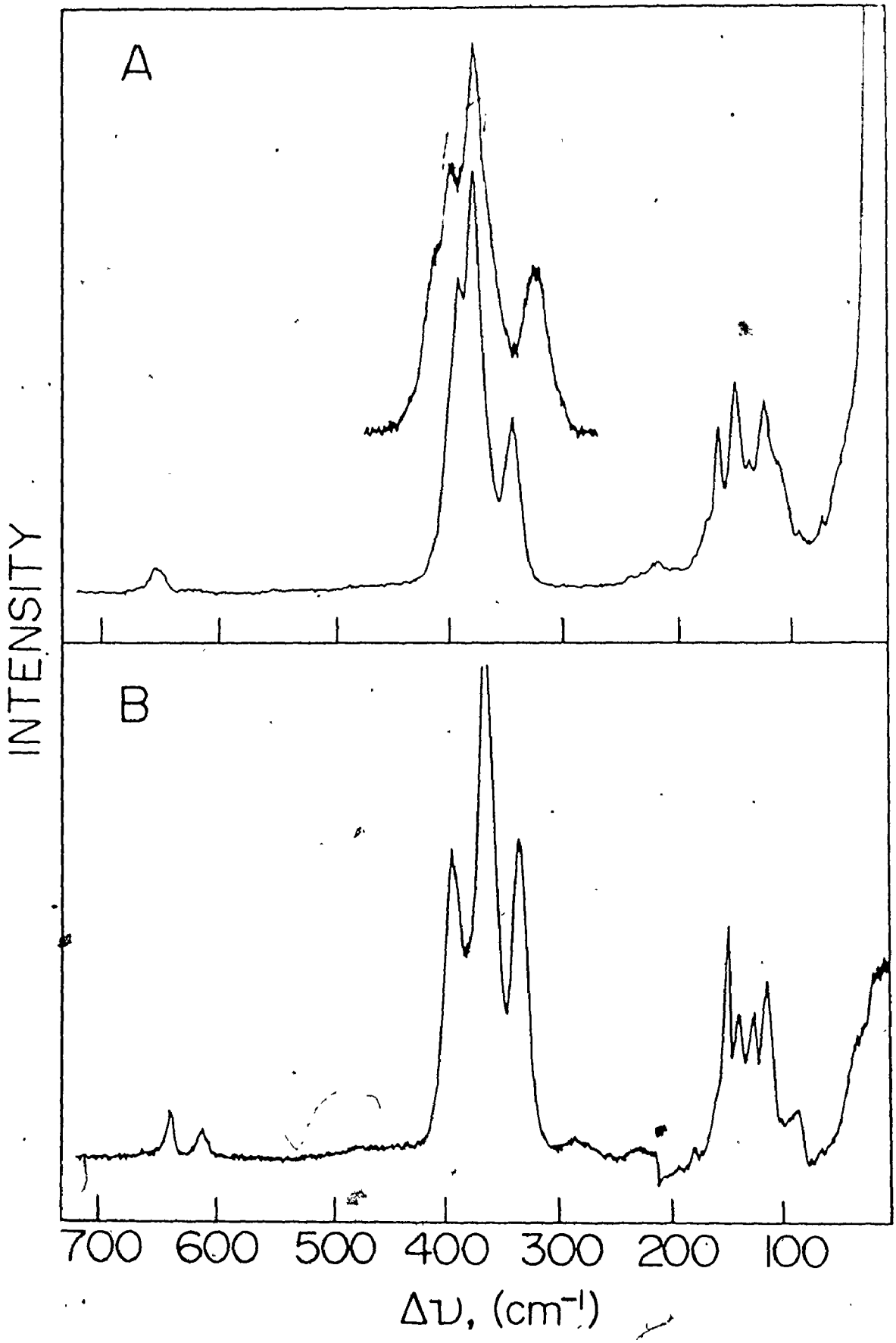
A
B
INTENSITY
700
600
500
400
300
200
100
Δυ, (cm⁻¹)

Table 5.5. Vibrational Frequencies for $Sb_3Cl_{10.75}F_{4.25}$ in the Solid and Liquid, and $SbCl_3F_2$ in the Solid

$SbCl_4F$[a]	$Sb_3Cl_{10.75}F_{4.25}$			$SbCl_3F_2$		Assignments
Solid[d]	Solid[d]	Melt[c]	Depolarization Ratio[e]	Solid[d]	Single Crystal[f]	
	654(5)br	659(4)p[b](?)	.07	649(11) 621(8)	648(11) 621(6)	(Sb-F) str.
490(1) 447(1)	413(5)sh	431(6)p	.54	488(2)br		(Sb-F-Sb)str.
398(39) 390(36)sh	401(48)sh 393(69)sh 380(100)	380(100)p	.08	406(73)sh 380(100)	406(71) 376(100)	equit (Sb-Cl)str.
365(9)sh 348(100)	346(42)	351(51)p	.07	349(73)	346(76)	axial (Sb-Cl)str.
274(2)		301(2)p[b](?)	.20		296(3)	Deformation
219(1)	237(3)br 221(5)br			240(4)	239(3) 215(2)	and bending
202(2)					204(4)	modes.
179(4)[g]sh	175(11)	176(8)dp[b](?)			172(8)	Deformation
161(22)	162(34)	162(17)dp	.81	161(50)	161(62)	and
151(29)	148(42)	149(19)dp	.80	152(36)sh	150(36)	bending
135(16)	137(21)sh			139(37)sh	137(37)	modes.
124(11)br	121(39)	122(13)dp	.67	125(48)	125(48)	
113(10)sh	110(22)sh 104(13)sh					
96(7)		97(11)p[b](?)	.13	93(24)	95(12)	(Continued ...

Table 5.5 (Continued)

a. Spectrum recorded in this work and found to be the same as reported in Reference 97.

b Depolarization ratio uncertain because of intensity.

c Melt at +70°C; p: polarized; dp: depolarized; sh: shoulder; br: broad.

d Solid at 20°C.

e Depolarization ratios for these bands were obtained from the melt.

f Raman data collected on the same crystal as used for X-ray analysis.

g Intensity relative to strongest band given in brackets.

axial Sb-Cl stretch. A similar band is not present for $SbCl_3F_2$, but the band at 406 cm^{-1} can probably be assigned to this Sb-Cl asymmetric stretch. No attempt was made to assign the ring deformation and bending modes as insufficient information is available on which to base such an analysis. However, the bands representing these modes compare favourably with the analogous bands in $SbCl_4F$.[97] The weak bands at 447 cm^{-1} and 490 cm^{-1} were assigned to the Sb-F-Sb' bridging modes. A very weak band at 488 cm^{-1} was also observed in $SbCl_3F_2$ (Figure 5.10B) and is tentatively assigned to the Sb-F-Sb' bridge mode. The vibrational frequencies of the single crystal are almost identical to those of the solid except for the relative intensities (Table 5.5). Because of this close agreement, it has been concluded that the crystal which was used for X-ray crystallographic analysis (section 5B(ii)) is representative of the bulk sample.

It is more difficult to assign the Raman spectra of the trimer $Sb_3Cl_{10.75}F_{4.25}$ on the basis of the monomeric unit, as in the previous case, since the trimer contains two different sites. For this reason, the tentative assignments are made by drawing an analogy to the spectra of $SbCl_4F$ [97] and $SbCl_3F_2$. These assignments are supported by the polarization data of the melt, which are included in Table 5.5. The Raman spectra of the solid and the melt are essentially identical except that a number of the bands coalesce on melting. However, it is concluded that $Sb_3Cl_{10.75}F_{4.25}$ has the same cyclic fluorine bridged trimeric structure in the solid and the liquid although a certain amount of halogen exchange may take place. Two bands at 351 cm^{-1} and 380 cm^{-1} are strongly polarized and hence represent totally symmetric stretches. The band at 351 cm^{-1} is assigned

to the symmetric axial Sb-Cl stretching frequency. This band is very similar to the analogous band in $SbCl_3F_2$ (349 cm^{-1}) and the band in $SbCl_4F$ (348 cm^{-1}) assigned by Beattie et al.[97] to the axial Sb-Cl stretch. The band at 380 cm^{-1} is attributed to the symmetric equatorial Sb-Cl stretch by analogy to the 394 cm^{-1} band in $SbCl_4F$. The band at 659 cm^{-1} probably represents an antimony fluorine axial stretching mode similar to that assigned in $SbCl_3F_2$. The only band in the region expected for the Sb-F-Sb bridge stretching mode is that at 431 cm^{-1}, which is lower than the corresponding band in $SbCl_3F_2$ (488 cm^{-1}) and $SbCl_4F$ (446 and 490 cm^{-1}).[97] The Sb-F-Sb angle is 158.2° in $Sb_3Cl_{10.75}F_{4.25}$ compared with 164° and 173° for $SbCl_3F_2$ and $SbCl_4F$, respectively. This may result in a lower frequency for this vibration. The bands designated as bending and deformation modes are very similar to those found in $SbCl_4F$ and $SbCl_3F_2$ but these assignments cannot be definite.

The Raman spectra of $[AsCl_4^+][SbF_6^-]$, $[SbCl_4^+][Sb_2Cl_2F_9^-]$, and $[SbCl_4^+][Sb_2F_{11}^-]$ are shown in Figure 5.11. The corresponding frequencies of these compounds are listed in Table 5.6 along with those of other related compounds, i.e., $[PCl_4^+][PCl_6^-]$,[140] $[PCl_4^+][SbCl_6^-]$,[139] and $[AsCl_4^+][AsF_6^-]$,[141] together with assignments.

The assignments of the normal modes of $[AsCl_4^+][SbF_6^-]$ are made on the basis of a tetrahedral $[AsCl_4^+]$ cation and a slightly distorted octahedral $[SbF_6^-]$ anion. The cation has Td symmetry and a total of four fundamentals are expected with symmetry designation a_1, e, and $2t_2$, all of which are Raman active. The band at 415 cm^{-1} agrees favourably with the band at 422 cm^{-1} of $[AsCl_4^+][AsF_6^-]$ assigned by Weidlein and Dehnicke.[141]

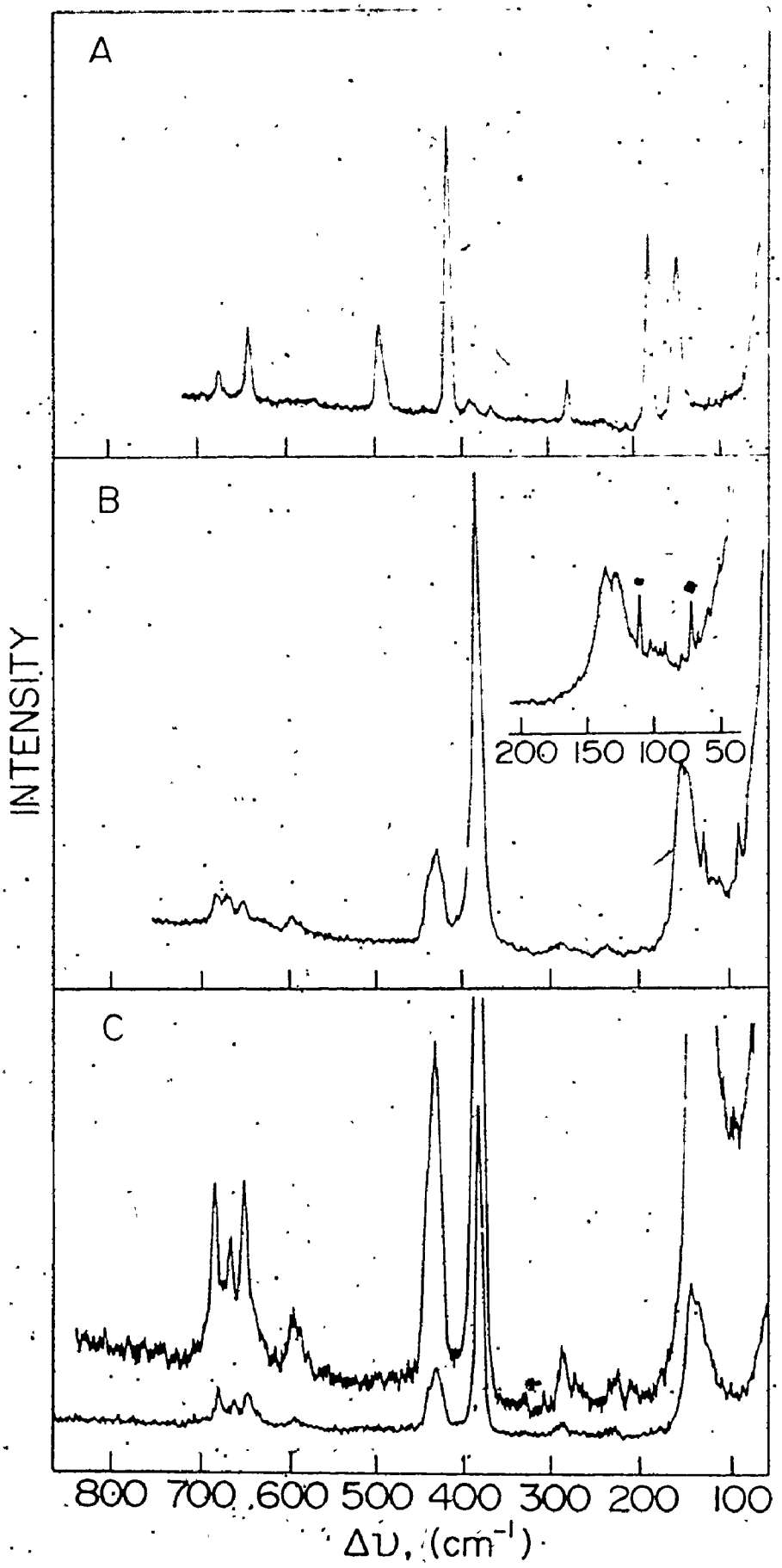
A
B
C
INTENSITY
200 150 100 50
800 700 600 500 400 300 200 100
Δυ, (cm⁻¹)

Table 5.6 Vibrational Frequencies for Group Five Chloride Fluoride Compounds Containing an $[MCl_4^+]$ Cation

$[PCl_4^+][PCl_6^-]$[a] Solid	$[PCl_4^+][SbCl_6^-]$[b] Solid	$[AsCl_4^+][AsF_6^-]$[c] Solid	$[AsCl_4^+][SbF_6^-]$ Solid[d]	$[SbCl_4^+][Sb_2Cl_2F_9^-]$ Solid[d]	melt[e]	dp ratio	$[SbCl_4^+][Sb_2F_{11}^-]$ Solid[d]	melt[e]	dp ratio	T_d	Description of Motion
658(10)dp	--	500(50)	496(30) 488(13)	441(33) 430(19)	436(1)	.68	438(13) 433(20)	437(11)	.69	$\nu_3(t_2)$	$\nu_{as}(M\text{-}Cl)_4$ degenerate stretch
458(30)p	459(30)	422(100)	415(100)	385(100)	388(100)	.06	388(100)	386(100)	.03	$\nu_1(a_1)$	$\nu_{sym}{}^{M\text{-}Cl}{}_4$
251(40)dp	248(10)	187(60)	184(66)	137(40)	144(16)	.68	139(44)	140(22)	.78	$\nu_4(t_2)$	$\nu_{as}{}^{M\text{-}Cl}{}_4$ degenerate bend
171(30)dp	143(20)	156(70)	149(56)	128(36)	126(12)	.68	130(38) 124(24)	123(16)	.75	$\nu_2(e)$	$\nu_{sym}(MCl_4)$
										O_h	
				675(5) 663(6) 646(6) 591(5)	674(9)		682(12) 663(8) 649(10)	678(8) 651(10)			
360(100)	334(100)	682(40)	645(25)	392(27)sh[g]	604(4)	$Sb_2F_9Cl_2^-$	591(3)	599(2)	$Sb_2F_{11}^-$	$\nu_1(a_{1g})$	$\nu_{sym}(M\text{-}X)_6$
281(40)	290(10) 281(10)	583(10)	574(2)	287(3) 276(2) 241(3)			327(1) 288(4)			$\nu_2(e_g)$	$\nu_{sym}{}^{M\text{-}X}{}_4$
--	--	--	678(1)				271(1)sh 225(2) 210(1)	294(3)		$\nu_3(t_{1u})$	degenerate stretch
			390(5)[f] 368(4)								
--	--	--	241(2) 218(1)							$\nu_4(t_{1u})$	degenerate bend
150(20)	168 30	372(30)	278(15)							$\nu_5(t_{2g})$	M-X angle deformation
			120(1) 80(1)								lattice modes

continued

Ref. 140

Ref. 139

Ref. 141

Solid at 20°C

e Melt at 70°C; p: polarized; dp: depolarized; sh: shoulder

Sb-Cl impurity

Sb-Cl band of $[Sb_2Cl_2F_9^-]$ (see Fig. 5.10)

The bands at 496 cm^{-1} and 488 cm^{-1} are assigned to the asymmetric degenerate stretch $\nu_3(t_2)$ which corresponds to the band at 500 cm^{-1} in $[AsCl_4^+][AsF_6^-]$ [141] (Table 5.6). This band in $[AsCl_4^+][SbF_6^-]$ is probably split as a result of some cation-anion interaction which would lower the symmetry. The bands at 184 and 149 cm^{-1} of $[AsCl_4^+][SbF_6^-]$ are attributed to the $\nu_4(t_2)$ asymmetric stretch and the $\nu_2(e)$ bend, respectively. These assignments parallel those made earlier[141] for $[AsCl_4^+][AsF_6^-]$.

The spectrum of the $[SbF_6^-]$ anion in $[AsCl_4^+][SbF_6^-]$ was assigned on the basis of a slightly distorted octahedron and the assignments given in Table 5.6 agree favourably with the similarly distorted octahedral $[SbF_6^-]$ anion in $[Xe_2F_3^+][SbF_6^-]$.[142] Two additional bands at 390 and 368 cm^{-1} in the antimony chlorine stretching region are probably due to an antimony(V) chloride fluoride impurity. If the $[SbF_6^-]$ anion were to have O_h symmetry, only three bands, $\nu_1(a_{1g})$, $\nu_2(e_g)$ and $\nu_5(t_{2g})$, would be Raman active. However, since more than three bands are observed, there must be a lowering of symmetry due to cation-anion interactions. However, such an association is not evident from the Mössbauer data (see earlier). The Raman spectra of the anions in $[PCl_4^+][PCl_6^-]$,[140] $[PCl_4^+][SbCl_6^-]$,[139] and $[AsCl_4^+][AsF_6^-]$ [141] indicate regular octahedra in each case, suggesting little cation-anion interaction. This is also consistent with regular tetrahedral cations in each case as evidenced by the Raman data.

The Raman spectra of the cations of $[SbCl_4^+][Sb_2Cl_2F_9^-]$ and $[SbCl_4^+][Sb_2F_{11}^-]$ are assigned by comparison to that of the $[AsCl_4^+]$ cations. This similarity is obvious from Figure 5.11. The depolarization ratios of the bands belonging to the $[SbCl_4^+]$ cations are also reported in Table 5.6.

Preiss[44] had reinterpreted the Raman data of Dehnicke and Weidlein[39] after determining the structure of $[SbCl_4^+][Sb_2Cl_2F_9^-]$ in 1972. Preiss attributed a band at 393 cm^{-1} to both the symmetric Sb-Cl stretch of the tetrahedral cation and the Sb-Cl stretch expected for the anion $[Sb_2Cl_2F_9^-]$. He assigned the bands at 145 cm^{-1} and 445 cm^{-1} to asymmetric Sb-Cl t_2 bands. He was unable to observe the band designated $\nu_2(e)$ in Table 5.6 and he made no attempt to assign the Sb-F bands of the $[Sb_2Cl_2F_9^-]$ anion. The Raman spectra shown in Figure 5.11 and the frequencies of the bands listed in Table 5.6 are similar to the spectrum reported earlier for $[SbCl_4^+][Sb_2Cl_2F_9^-]$.[39] The highly polarized bands at 388 and 386 cm^{-1} of the spectra reported in Table 5.6 are assigned to the $\nu_1(a_1)$ symmetric stretch. The bands at 436 and 437 cm^{-1} of the melts of $[SbCl_4^+][Sb_2Cl_2F_9^-]$ and $[SbCl_4^+][Sb_2F_{11}^-]$, respectively, are assigned to the $\nu_3(t_2)$ asymmetric degenerate stretch. In the solid state, this band is split into two components in both compounds, suggesting cation-anion interactions which would lower the symmetry of the cations. This reduction is also suggested by the X-ray crystallographic analysis and the Mössbauer data. A similar splitting is observed for the band designated $\nu_2(e)$ in $[SbCl_4^+][Sb_2F_{11}^-]$, 124 and 130 cm^{-1}, which is also consistent with the cation-anion interaction predicted earlier for this compound. However, the corresponding band in the $[Sb_2Cl_2F_9^-]$ ion does not show resolvable splitting, but this band is broad. The bands at 144 and 140 cm^{-1} for $[SbCl_4^+][Sb_2Cl_2F_9^-]$ and $[SbCl_4^+][Sb_2F_{11}^-]$, respectively, are assigned to $\nu_4(t_2)$, which are analogous to the bands at 187 and 184 cm^{-1} for the $[AsCl_4^+]$ cation in the $[AsF_6^-]$ and $[SbF_6^-]$ compounds. This band in $[PCl_4^+]$ [140] was depolarized, as are

those for the analogous $[SbCl_4^+]$ spectra.

As observed in Table 5.6, there is a general reduction in frequency down the series from $[PCl_4^+]$ to $[SbCl_4^+]$, as expected for the increase in mass. The polarization ratios of the $[PCl_4^+]$ bands of $[PCl_4^+][PCl_6^-]$ [140] are equal to those observed for $[SbCl_4^+]$. The bands of the $[PCl_4^+]$ cations are not split contrary to that found for the $[AsCl_4^+]$ and $[SbCl_4^+]$ cations. No distortion from tetrahedral geometry occurs for $[PCl_4^+]$ and $[AsCl_4^+]$ and as a result, only the expected bands are observed in the spectra of the associated anions.

The anion bands of $[SbCl_4^+][Sb_2F_{11}^-]$ and $[SbCl_4^+][Sb_2Cl_2F_9^-]$ are not assigned although they are generally representative of an $[M_2F_{11}^-]$ anion as found in $[XeF^+][Sb_2F_{11}^-]$.[143] At first sight, there appears to be very little difference between the Raman spectra for $[SbCl_4^+][Sb_2F_{11}^-]$ and $[SbCl_4^+][Sb_2Cl_2F_9^-]$. however, upon a closer examination of the spectrum of the latter, a side band is visible at 392 cm^{-1}. The band is assigned to the Sb-Cl stretch of the anion. This side band is more visible on a magnified portion of the spectrum, Figure 5.12. A similar band was not observed when the spectrum of $[SbCl_4^+][Sb_2F_{11}^-]$ was treated in a similar fashion. The depolarization ratios were not recorded for the bands of the anion because of their low intensity.

The Raman data of $SbCl_4F(NbF_5)_x$ are listed in Table 5.7 along with the data for $SbCl_4F$ and NbF_5. A careful examination of this table reveals a certain similarity between the spectrum of $SbCl_4F(NbF_5)_x$ and both of the parent compounds. Crude tentative assignments are made on the basis of the parent compounds and are included in Table 5.7. The

Figure 5.12. Enlarged Section of the Raman Spectrum of Solid $[SbCl_4^+][Sb_2Cl_2F_9^-]$ at 20°C.

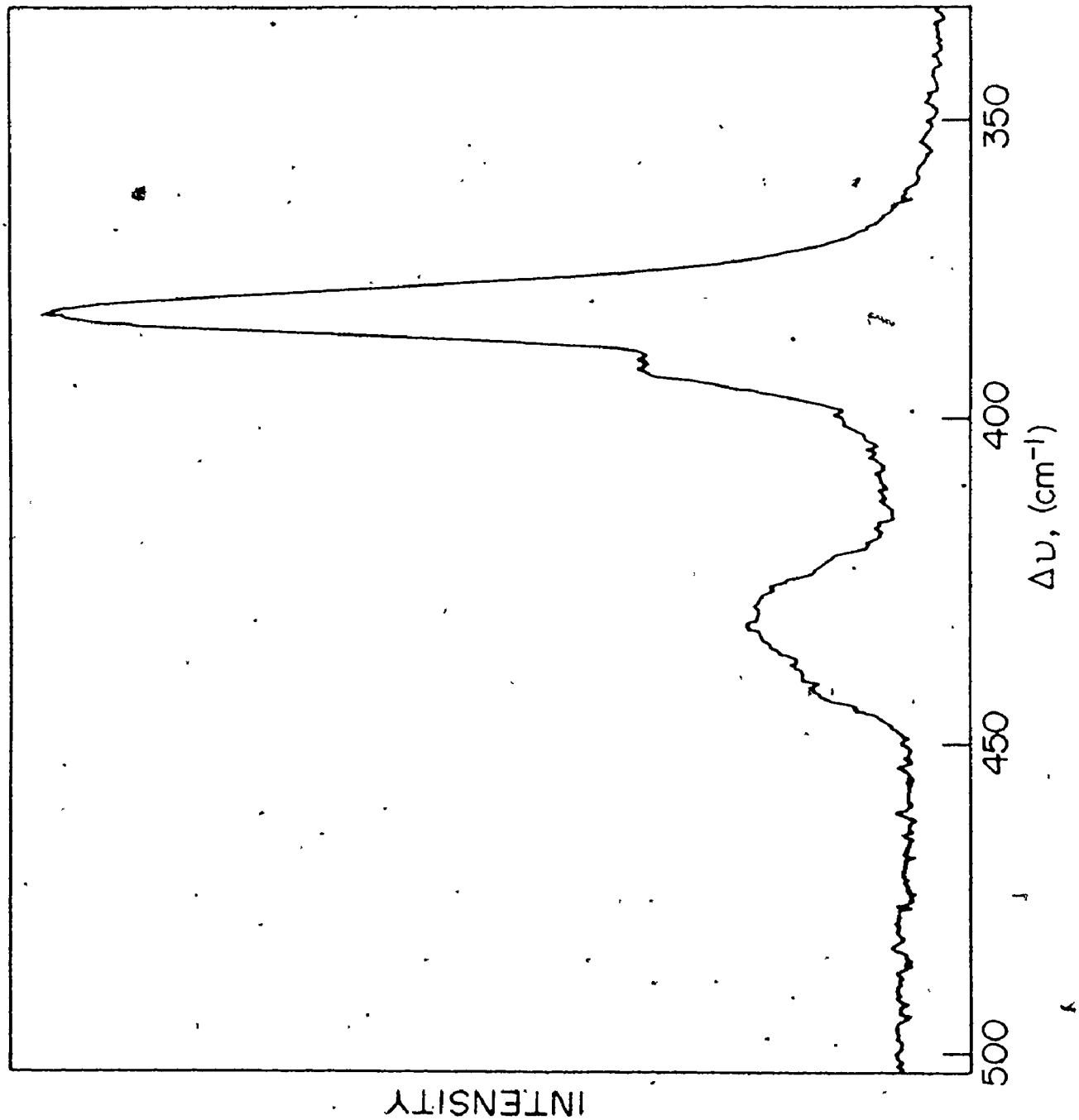
INTENSITY
350
400
450
500
Δυ, (cm⁻¹)

Table 5.7. Vibrational Frequencies for $SbCl_4F(NbF_5)_x$, where x = 1 or 2

$SbCl_4F$[a]	$SbCl_4F(NbF_5)_x$[b]	NbF_5[a]	Assignments
96(7)	98(12)		Lattice Modes
113(10)	110(24) 117(24)		Deformation Modes
124(11)			
135(16)	139( )sh		
151(29)	147(22)		
161(22)	161(36)		
179(4)			
202(2)			
219(1)		218(w)	
	232(3)	232(w)	
	260(3)	245(vw)	
274(2)		264(m)	
348(100)	343(100)		νSbCl
365(9)sh	370(20)sh		
	382(55)		
390(36)sh			
398(39)			
	403(12)sh		
447(1)			
490(1)			
	651(1)	648(m)	
		664(w)	
		675(vw)	
	705sh		νNb-F
	711(6)	713(s)	
	740(9)		
	748sh	748(w)	
	761(11)	766(vs)	
	784(4)		

[a] Reference 97.

[b] Solid at 50°C.

Raman data shows clearly that the compound does not contain either an $[SbCl_4^+]$ cation as was the case for the $SbCl_4F \cdot SbF_5$ adducts or an $[SbF_6^-]$ anion. This suggests that NbF_5 is a stronger Lewis acid than AsF_5, which formed $[AsCl_4^+][SbF_6^-]$. A great deal more work is necessary to completely characterize this compound, however, from the data presented here it seems likely that an adduct similar to that suggested in section 5.B(iii) is present in the solid state, i.e., a fluorine bridged adduct.

(v) Mass Spectrometry

The relative abundance of ions with varying numbers of central nuclei are presented in Table 5.8. A graphic representation of the monomeric ions in the mass spectra of the antimony(V) chloride fluorides is given in Figure 5.13. The intensities of the dimers are not graphically represented, but as indicated in Table 5.8, are much less intense than those of the monomers. For simplicity, the ion clusters observed in Figure 5.13 are represented as a single peak in Table 5.8. The intensity of each ion listed in Table 5.8 represents the intensity of the largest isotopic peak. The intensity of these peaks, however, cannot be readily compared since the largest peak in an isotopic cluster is not always representative of the relative abundance. For example, the comparison of $[SbF_4^+]$ vs. $[SbCl_4^+]$ would be distorted by a factor of ν 1.5, the biggest peak of $[SbF_4^+]$ being 57% of the total and that of $[SbCl_4^+]$ being 38% of the latter. These percentages are determined by calculating the peak intensities of each cluster and are normalized such that they add to 100.0.[144]

The experiments reported here show that electron impact on the

Figure 5.13. Mass Spectra of

(A) $SbCl_4F$,

(B) $Sb_3Cl_4F_{11}$,

(C) $[SbCl_4^+][Sb_2Cl_2F_9^-]$, and

(D) $[SbCl_4^+][Sb_2F_{11}^-]$.

(* Unidentified Impurity.)

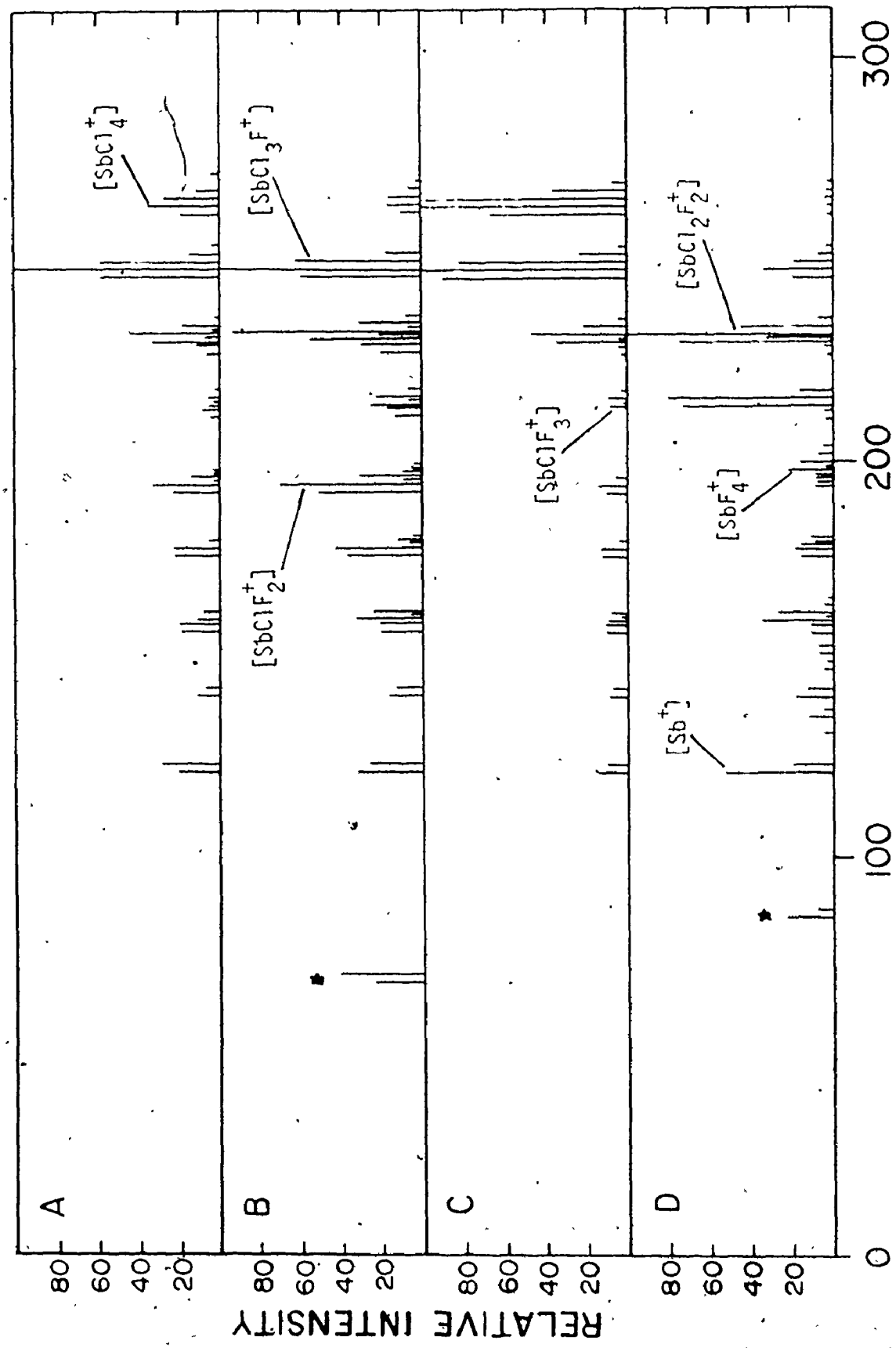
A
B
C
D
[SbCl4+]
[SbCl3F+]
[SbClF2+]
[SbClF3+]
[SbCl2F2+]
[SbF4+]
[Sb+]
RELATIVE INTENSITY
80
60
40
20
0
100
200
300
m/e

Table 5.8. Mass Spectra of Antimony(V) Chloride Fluorides

Ions	Relative Intensities[c]			
Compound[a]	$SbCl_4F$	$Sb_3Cl_{11}F_4$	$SbCl_2F_3$	$Sb_3Cl_4F_{11}$[d]
$[Sb^+]$	0.29	0.29	0.15	0.53
$[SbF^+]$	0.12	0.13	0.09	0.18
$[SbCl^+]$	0.21	0.21	0.12	0.11
$[SbF_2^+]$	0.11	0.33	0.10	0.35
$[SbClF^+]$	0.23	0.42	0.13	0.18
$[SbF_3^+]$	ND[b]	0.06	ND	0.16
$[SbCl_2^+]$	0.34	0.70	0.14	0.10
$[SbF_2Cl^+]$	0.03	0.09	0.01	0.08
$[SbF_4^+]$	ND	ND	ND	0.22
$[SbCl_2F^+]$	0.08	0.17	0.03	0.04
$[SbF_3Cl^+]$	0.06	0.23	0.10	0.80
$[SbCl_3^+]$	0.13	0.31	0.04	0.04
$[SbF_2Cl_2^+]$	0.46	0.93	0.48	1.00
$[SbCl_3F^+]$	1.00	1.00	1.00	0.32
$[SbCl_4^+]$	0.36	0.17	1.00	0.04

Continued.....

Table 5.8 (Continued)

Ions	Relative Intensities			
Compound[a]	$SbCl_4F$	$Sb_3Cl_{11}F_4$	$SbCl_2F_3$	$Sb_3Cl_4F_{11}$[d]
$[Sb_2Cl^+]$	ND	ND	ND	0.05
$[Sb_2ClF_2^+]$	ND	ND	ND	0.20
$[Sb_2Cl_2F^+]$	ND	ND	0.02	0.04
$[Sb_2ClF_3^+]$	ND	ND	0.04	ND
$[Sb_2Cl_2F_2^+]$	0.07	ND	0.06	ND
$[Sb_2Cl_3F^+]$	0.07	ND	0.05	ND
$[Sb_2Cl_3^+]$	0.10	ND	0.03	ND
$[Sb_2ClF_4^+]$	ND	ND	0.04	ND
$[Sb_2Cl_2F_3^+]$	ND	ND	0.09	ND
$[Sb_2Cl_3F_2^+]$	0.12	0.11	0.20	ND
$[Sb_2Cl_4F^+]$	0.18	0.18	0.12	ND
$[Sb_2Cl_2F_5^+]$	ND	ND	ND	0.02
$[Sb_2Cl_3F_4^+]$	ND	ND	0.03	0.04
$[Sb_2F_9^+]$	ND	ND	ND	0.02
$[Sb_2Cl_4F_3^+]$	ND	ND	0.08	0.06
$[Sb_2Cl_5^+]$	0.20	0.20	0.05	ND

Continued.....

Table 5.8 (Continued)

Ions	Relative Intensities			
Compound[a]	$SbCl_4F$	$Sb_3Cl_{11}F_4$	$SbCl_2F_3$	$Sb_3Cl_4F_{11}$[d]
$[Sb_2Cl_5F_2^+]$	0.07	0.15	0.19	0.03
$[Sb_2Cl_2F_7^+]$	ND	ND	ND	0.01
$[Sb_2Cl_6F^+]$	ND	0.12	0.17	0.01
$[Sb_2Cl_7^+]$	ND	ND	0.05	ND
$[Sb_2Cl_3F_6^+]$	0.07	ND	ND	ND

[a] Sample temperature 50-60°C, minor impurity of N_2, HCl, HF.

[b] ND: not detectable.

[c] Peak intensity based on isotope with maximum intensity.

[d] Presence of SbO, SbO_2, relative intensity, 0.04, 0.05, respectively.

neutral species sampled from the vapour, lead to an abundant concentration of monomer and dimer ions, whereas ions with three or more antimony atoms are undetected or absent. The parent molecule ions are not observed in any of the mass spectra recorded here. Vasile and Falconer[145] reported that the highest agglomerate found from the mass spectrometric studies of the SbF_5 and BiF_5 were $[Sb_3F_{14}^+]$ and $[Bi_3F_{14}^+]$, respectively. They were unable to detect the parent molecule ion. The most intense peaks reported for the SbF_5 and BiF_5 were those corresponding to the $[MF_4^+]$ ion. The most intense peaks observed for the antimony(V) chloride fluoride reported here were those representing the $[SbCl_xF_{4-x}^+]$ ions. In fact, volalitization of the antimony(V) chloride fluorides yielded most of the $[SbCl_xF_{4-x}^+]$ ions from $[SbCl_4^+]$ through $[SbCl_3F^+]$ and $[SbCl_2F_2^+]$ to $[SbClF_3^+]$. One exception to this general pattern is $[SbF_4^+]$, which was not detected in any of the antimony(V) chloride fluorides except for $[SbCl_4^+][Sb_2F_{11}^-]$. It may be worth noting, however, that this compound is the only one studied here which contains an antimony nucleus surrounded by six fluorines. In addition, J. M. Miller[144] mentioned that in many systems, the $[MX_n^+]$ species are more abundant for heavier halogens, where M is heavy, and for fluorine when M is a lighter element in a group.

The spectra depicted in Figure 5.13 also contain peaks which represent the ions $[SbCl_3^+]$ through $[SbClF_2^+]$, $[SbCl_2^+]$ through $[SbF_3^+]$ and $[SbCl^+]$ plus $[SbF_2^+]$. It should be pointed out that peaks representing $[SbF_3^+]$ were not found in all of the spectra as indicated in Table 5.8. In addition, a number of peaks were observed corresponding to $[Sb_2X_9^+]$, $[Sb_2X_7^+]$, and $[Sb_2X_5^+]$ with some peaks down to $[Sb_2X^+]$, where X = chlorine or

fluorine. Vasile and Falconer[145] were able to detect all of these ions with the addition of $[Bi_2F_4^+]$ from BiF_5, but only the $[Sb_2F_9^+]$ ion from SbF_5. However, Lawless[146] in a slightly different experiment, observed all of the ions from $[Sb_2F_9^+]$ to $[Sb^+]$, but was unable to detect any ions with an m/e greater than the dimer ions (m = mass, e = charge).

There were not any metastable ions in the spectra. The absence of these ions prevents detailed assignment of the fragmentation pathways.

As shown in Figure 5.3, the most intense peaks in the spectrum of $SbCl_4F$ and $Sb_3Cl_{10.75}F_{4.25}$ correspond to the $[SbCl_3F^+]$ and $[Sb_2F_2^+]$ ions. The most intense peaks observed for $[SbCl_4^+][Sb_2Cl_2F_9^-]$ correspond to the $[SbCl_4^+]$ and $[SbCl_3F^+]$ ions, while those observed for $[SbCl_4^+][Sb_2F_{11}^-]$ correspond to the $[SbCl_3F^+]$ and $[Sb_2F_2^+]$ ion. The strongest peaks can reflect: the ratio of chlorine to fluorine atoms in the sample, assuming completely free halogen exchange between fragments at the walls of the ionization chamber; direct fracturing of the complex tetramer or trimer with little exchange; or, the mode of volatilization from the solid. As mentioned earlier, the strongest peaks found in the spectrum of $[SbCl_4^+]$-$[Sb_2Cl_2F_9^-]$ are those corresponding to the $[SbCl_4^+]$ and $[SbCl_3F^+]$ ions, whereas the strongest peak in the $SbCl_4F$ spectrum was $[SbCl_3F^+]$ inspite of the increased ratio of chlorines to fluorines in this compound. This crude evaluation suggests that the intensity of the ions of the former compound is related to the fragmentation to some extent. However, it is worth noting that $[SbCl_4^+][Sb_2F_{11}^-]$, which also contains an $[SbCl_4^+]$ cation, does not have an intense peaks in the spectrum which corresponds to this cation. This anomaly may be the result of exchange of gaseous ions and

molecules or as a result of decomposition before volatilization.

The occurrence of dimeric ions is not easily rationalized in view of the many possible fragmentation patterns, exchange processes and modes of volatilization from the solid. The small intensities of the peaks corresponding to these ions and the absence of trimer and tetramer ions suggest that the trimeric and tetrameric bridged ring structures known for the crystalline compounds do not persist in the vapour phase.

CHAPTER SIX

ANTIMONY(V) CHLORIDE FLUORIDE ANIONS: THEIR PREPARATION AND CHARACTERIZATION

(A) INTRODUCTION

Antimony(V) pentafluoride and pentachloride are both potent acceptors forming $[SbX_6^-]$ anions, where X = chlorine, or fluorine. A few of the alkali metal hexafluoroantimonates(V) have been characterized using Mössbauer,[99,103] Raman and infrared spectroscopy.[147] In each of these, the Sb(V) atom is surrounded by six fluorine atoms in an octahedral configuration. The alkali metal hexachloroantimonates(V) are very similar, with chlorine atoms replacing the fluorines. Burgard et al.[148] assigned the vibrational spectrum of the anion of $K[SbCl_6]$ on the basis of an octahedral hexachloroantimonate(V). This anion has been identified in a number of systems.[148,149,48] The only Mössbauer spectrum reported for these alkali metal hexachloroantimonate(V) salts is that for the rubidium salt.[111]

In addition to the $[SbF_6^-]$ and $[SbCl_6^-]$ anions, a number of mixed chloride fluoride anions have been reported in the literature. In 1962, Kolditz, Weisz, and Calov[51] reported that the reaction between SbF_5 and NaCl in liquid SO_2 yielded a soluble mixed chloride fluoride salt, $Na[SbCl_2F_4]$, and the difficultly soluble $Na[SbF_6]$ (equation 6.1). These materials were identified by elemental analysis. In 1968, Müller et al.[50]

$$2SbF_5 + 2NaCl \xrightarrow[SO_2]{-50°C} Na[SbCl_2F_4] + Na[SbF_6] \qquad (6.1)$$

reported that the same reaction, carried out at a slightly higher temperature, yielded a mixture of $Na[SbCl_4F_2]$ and $Na[SbF_6]$ as shown by equation 6.2. The former salt was soluble in liquid SO_2 at room temperature.

$$4SbF_5 + 4NaCl \xrightarrow[SO_2]{-15°C} Na[SbCl_4F_2] + 3Na[SbF_6] \qquad (6.2)$$

They identified $Na[SbCl_4F_2]$ by elemental analysis and inferred from its infrared spectrum that this salt contained only cis-$[SbCl_4F_2^-]$ ions. This reaction has been repeated in this work and the resultant products examined by Mössbauer and Raman spectroscopy.

In 1970, the salt $Na[SbCl_5F]$, prepared from a reaction of NaF with an excess of $SbCl_5$, was reported.[150] This salt, previously employed as a catalyst for fluorination reactions,[151] was identified by chemical analysis. No attempts were made to further characterize this compound and spectroscopic data were not reported.

In the present work, attempts were made to prepare and isolate each of the mixed chloride fluoride antimony(V) salts from $[SbCl_6^-]$ to $[SbF_6^-]$. In this chapter, we present further Mössbauer and Raman data of the alkali metal hexafluoro- and hexachloroantimonates(V). In addition, we report the preparation and spectroscopic characterization of two of the mixed chloride fluoride antimonate(V) anions.

(B) RESULTS AND DISCUSSION

(i) Mössbauer Spectroscopy

The Mössbauer isomer shift values listed in Table 6.1 for the alkali metal hexahaloantimonate(V) anions are all large and positive. This is to be expected since antimony in the higher oxidation state has

no non-bonding electrons. In addition, the antimony sites are surrounded by highly electronegative chlorine or fluorine atoms, which remove s electron density from the antimony. The data in Table 6.1 have been arranged in order of decreasing isomer shift or increasing s electron density, with the antimony surrounded by six chlorines having the lowest isomer shift. This trend is depicted in Figure 6.1, showing that with an increase in the number of fluorines, the isomer shift increases along a smooth curve. This relationship can be of some use in predicting the ratio of chlorine to fluorine in unknown hexacoordinate antimony(V) anions.

In the antimony(V) anions, a finite quadrupole coupling constant is indicative of an electric field gradient about the antimony nucleus. As described earlier, the electric field gradient usually results from the unequal distribution of electron density about the antimony atom as a result of either the different electronegativities of the ligands surrounding the antimony, or slight distortions of the anion from octahedral geometry.

Of the anions studied, the best characterized is the hexafluoroantimonate(V). Each of the $[SbF_6^-]$ anions reported in Table 6.1 have large positive isomer shift values as a result of the six fluorines removing s electron density from the vicinity of the antimony nucleus. As observed in Table 6.1, the isomer shift data reported for the sodium and caesium salts agree favourably with those reported recently by Devort and Friedt.[103] As expected, the isomer shift values of all the alkali metal hexafluoroantimonates(V) are similar.

Devort and Friedt[103] computer fitted all the spectra of the alkali metal hexafluoroantimonates(V) to single lines of Lorentzian

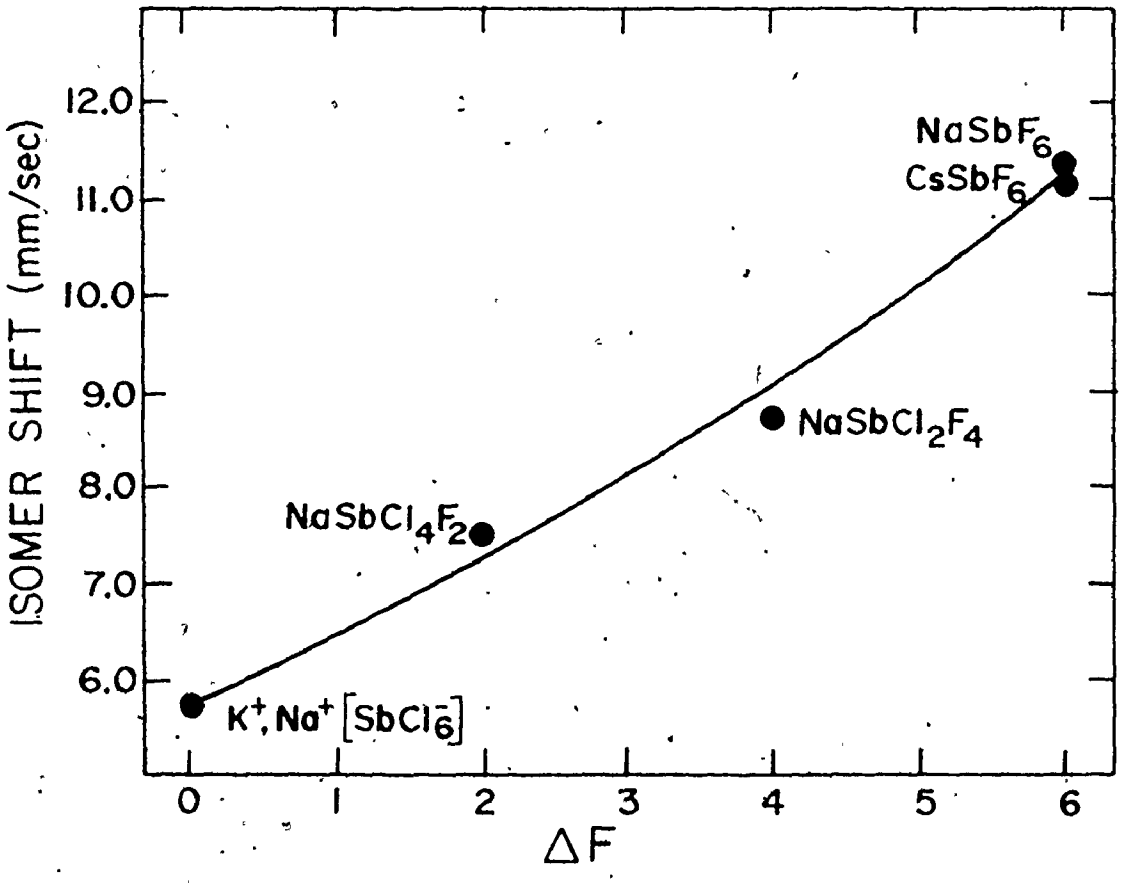

Figure 6.1. Graphical Representation of the Change in Isomer Shift of an Antimony Anionic Site Surrounded by Six Halogens as the Chlorines are replaced by Fluorines. (ΔF Represents the Change in the Number of Fluorines about the Antimony Site.)

shape. They concluded from comparisons of experimental line widths that there were no asymmetries in the resonance line shapes. This conclusion, however, contradicts the Mössbauer data for $K[SbF_6]$ reported by Ruby et al. in 1967,[77] who reported a slight quadrupole splitting. This quadrupole splitting was subsequently confirmed by Birchall et al.,[99] although they reported a much smaller value. In addition, the early crystal structure of $K[SbF_6]$ suggests a distorted octahedron.[152] As shown in Table 6.1, $Cs[SbF_6]$ also has a small quadrupole coupling constant of the same sign and magnitude as that observed for $K[SbF_6]$. Although this splitting is small, it suggests that the octahedron in this salt may be slightly distorted like that of $K[SbF_6]$.

The isomer shift value reported in Table 6.1 for $Na[SbCl_4F_2]$ is less positive than that of $Na[SbF_6]$ as a result of the increased number of chlorine atoms about the antimony nucleus of the former. Since the $\Delta R/R$ term for ^{121}Sb is negative, this trend reflects the steady augmentation of s electron density at the antimony nucleus when the Sb-F bonds are replaced by the more covalent Sb-Cl bonds (Figure 6.1). This trend is mirrored by the ^{119}Sn chemical isomer shifts of the $[SnX_nY_{6-n}^{=}]$ anions, (where X = Cl, Br, or I, and Y = F, Cl, Br, or I),[153] however, this trend is reversed since the $\Delta R/R$ term of ^{119}Sn is positive.

The isomer shift value quoted for $Na[SbCl_2F_4]$ in Table 6.1 is more positive than that of the $Na[SbCl_4F_2]$ salt. This increase in isomer shift results from the decrease in the number of Sb-Cl bonds, as opposed to Sb-F bonds, about the antimony nucleus. This material is not well-characterized since it could not be obtained as a pure sample.

Table 6.1. ^{121}Sb Mössbauer Data of the Antimony(V) Chloride Fluoride Anions

Compound	δ/mm sec^{-1}	eQV_{ZZ}/ mm sec^{-1}	Γ/mm sec^{-1}	m	$(CHI)^2$/deg. of freedom	Ref.
$Na[SbF_6]$	11.36	--- [a]	3.06	0.19	1.05	
$Na[SbF_6]$	11.42	---	---	---	---	103
$Cs[SbF_6]$	11.16	+4.57	3.12	0.13	1.10	
$Cs[SbF_6]$	11.16	---	---	---	---	103
$Na[SbCl_2F_4]$	8.73	--- [b]	3.25	---	0.93	
$Na[SbCl_4F_2]$	7.54	--- [b]	3.13	---	1.05	
$Na[SbCl_6]$	5.77	--- [a]	2.00	1.64	1.23	
$K[SbCl_6]$	5.71	--- [a]	3.09	0.21	1.11	
$Rb[SbCl_6]$	5.8 [c]	---	2.8	---	---	111

[a] eQV_{ZZ} values were too small to calculate.

[b] Lorentzian fit because salts could not be obtained pure.

[c] recorded at 80°K.

In each of the previously mentioned chloride fluoride antimonates(V), the isomer shift values were determined for a single line fit of Lorentzian shape. The Mössbauer spectrum of $Na[SbCl_4F_2]$ is shown in Figure 6.2. This material, obtained from a reaction of $SbCl_4F$ and NaCl in liquid SO_2 was never obtained pure. Although these impurities were not obvious from the Mössbauer spectrum (Figure 6.2), the Raman spectrum contained bands identical to those expected for $Na[SbCl_6]$ and possibly also $Na[SbCl_2F_4]$. For this reason, the quadrupole coupling constant was not determined since the peak representing $Na[SbCl_4F_2]$ would be broadened by these impurities and subsequently distort the value determined from the computer analysis. For example, as shown in Figure 6.2, a small impurity of $Na[SbCl_6]$ would produce an asymmetric peak tailing off to the left which would be interpreted as a positive quadrupole splitting. In all attempts at the reactions described by Kolditz et al.[51] (equation 6.1) and Müeller et al.[50] (equation 6.2), a mixture of chloride fluoride anions was always produced as indicated by the Mössbauer spectrum. One of the components in this spectrum had an isomer shift (δ = -7.54 mm sec^{-1}) identical to that identified separately as $Na[SbCl_4F_2]$ and the other major peak had an isomer shift value between that of $Na[SbF_6]$ and that assigned to $Na[SbCl_4F_2]$. Since the isomer shift of this peak coincided on the smooth curve (Figure 6.1) with an antimony(V) anionic site surrounded by two chlorines and four fluorines, it was assigned to $Na[SbCl_2F_4]$. Because this material could not be isolated, it was not possible to extract a reliable quadrupole coupling constant from the spectrum.

Figure 6.2. ^{121}Sb Mössbauer Spectra of

(a) Solid $Na[SbCl_6]$ and

(b) Solid $Na[SbCl_4F_2]$ at 4°K.

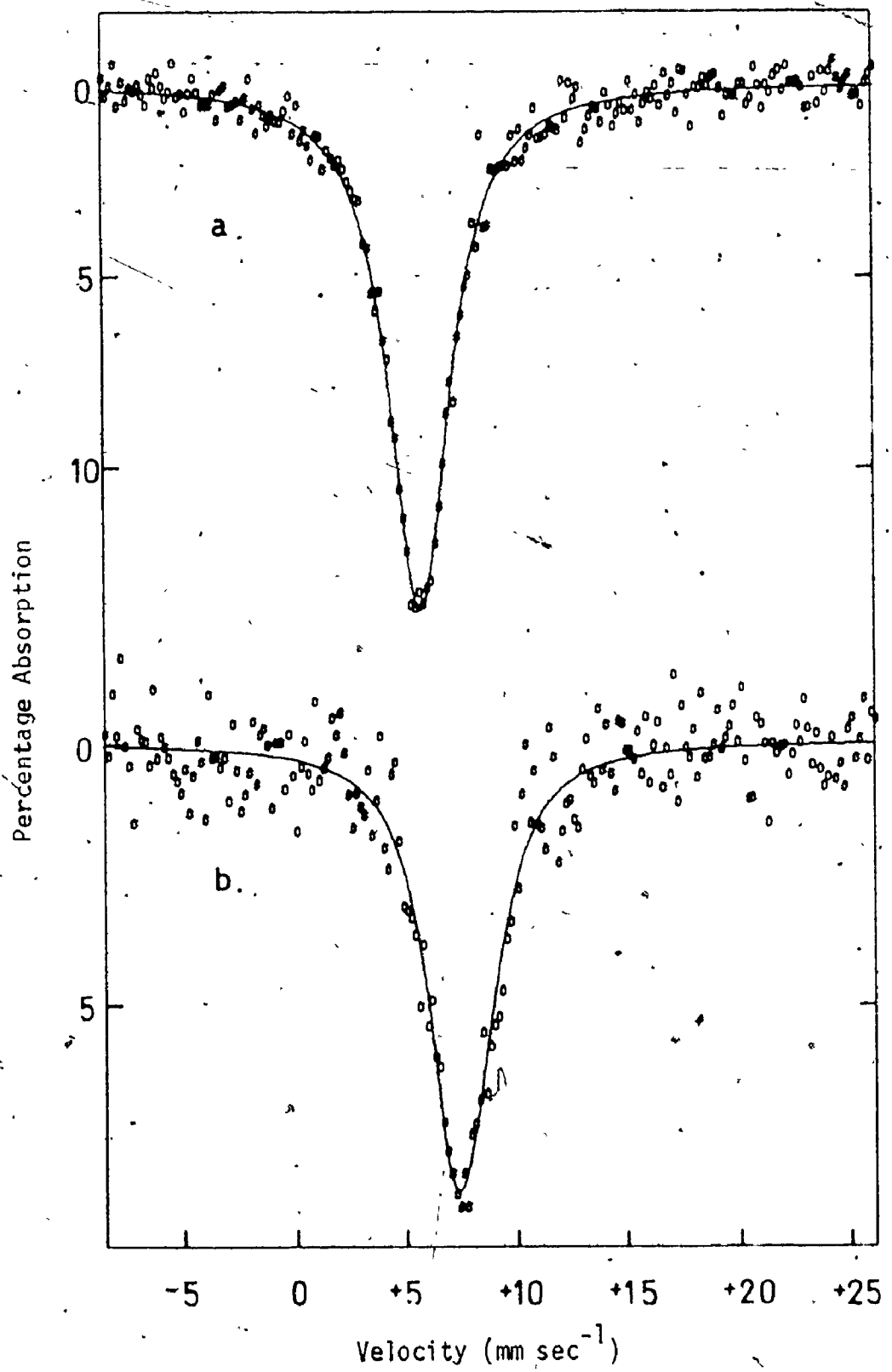
0
5
10
a.
0
5
b.
Percentage Absorption
-5
0
+5
+10
+15
+20
+25
Velocity (mm sec^{-1})

The quadrupole coupling constant is normally a valuable parameter for structure elucidation, particularly in these cases where the antimony anions can be present in either, or both of two possible isomeric forms, i.e., cis or trans. Parish and Johnson[154] used simple point charge calculations to develop an appropriate guide to the magnitude and sign of the quadrupole coupling constants of tin(IV) compounds in different geometries. This same guide should be applicable to antimony(V) compounds as well. In the case of the trans isomer for $[SbCl_2F_4^-]$, the quadrupole coupling constant should be large and positive whereas in the case of the cis isomer, the magnitude would be smaller and negative. It is likely that this ion would have cis-chlorines, hence a negative quadrupole coupling constant, and the line shape should tail off to more positive velocities. The $[SbCl_4F_2^-]$ ion would be expected to have the fluorines trans to one another, reducing the electron density along the z axis and again giving a negative coupling constant. Because these salts were not obtained pure it was not possible to determine either the magnitude or the sign of the quadrupole splitting.

The isomer shift data reported in Table 6.1 for the hexachloroantimonates(V) agree favourably with that reported for the rubidium salt by Birchall et al.[111] In each case, the quadrupole coupling constant was zero suggesting that the anions have O_h symmetry.

(ii) Raman Spectroscopy

The Raman frequencies and assignments for $NaSbCl_6$ are given in Table 6.2 along with the infrared and Raman frequencies of $KSbCl_6$ reported by Burgard and MacCordick.[148] The Raman frequencies of these anions are identical, and consistent with O_h symmetry.

The Raman frequencies and assignments of the $[SbCl_4F_2^-]$ anion are included in Table 6.3. The band at 332 cm^{-1} is identical to the $\nu_1(A_{1g})$

Table 6.2 Vibrational Spectra of $NaSbCl_6$ and $NaSbCl_4F_2$ Compared with that of $KSbCl_6$ [a]

$NaSbCl_6$	$\nu(cm^{-1})$ $KSbCl_6$ [a]		$NaSbCl_4F_2$		Assignments
Raman	I.R.	Raman	Raman	$[SbCl_6^-](O_h)$	$[SbCl_4F_2^-](D_{4h})$
			625(vw)		? ν_{as} Sb-F_{eq} [cis-$SbCl_4F_2^-$]
			529(w)		$\nu_1(A_{1g})$ Sb-F_{ax} sym str.
			390(wsh)		?[$SbCl_2F_4^-$]
			380(vs)		$\nu_3(B_{2g})$ $SbCl_4$ out-of-plane str.
			368(wsh)		
	346(s)			$\nu_3(T_{iu})$	
331(s)		340(s)	332(w)	$\nu_1(A_{1g})$	$\nu_1(A_{1g})$ [$SbCl_6^-$]
			312(m)		$\nu_2(A_{1g})$ $SbCl_4$ in-plane str.
283(m)		290(w)		$\nu_2(E_g)$	
			261(vw)		$\nu_4(E_g)$ F-Sb-Cl bend
	186(s)			$\nu_4(T_{1u})$	
184(wbr)		189(m)			
163(w)		180(m)		$\nu_5(T_{2g})$	
			172(w)		$\nu_5(B_{1g})$ $SbCl_4$ in-plane scissor
			142(m)		
		137(w)			
		119(w)			

[a] reference 148

band of the $[SbCl_6^-]$ anions and probably represents an impurity. The bands at 625 and 390 cm^{-1}, which varied in intensity depending upon the number of stages of purification, were assigned to other salt impurities. For example, the band at 625 cm^{-1} may be due to the presence of the $[SbCl_2F_4^-]$ anion or possibly the cis-$[SbCl_4F_2^-]$ isomer which should have a Raman active $\nu_{asymmetric}$ Sb-F equatorial stretch. The Raman bands remaining for the anion $[SbCl_4F_2^-]$ are consistent with a trans-$[SbCl_4F_2^-]$ anion having D_{4h} symmetry. Such an ion will have eleven fundamental modes with symmetry designations $2A_{1g}$, B_{1g}, B_{2g}, E_g, $2A_{2u}$, B_{2u}, and $3E_u$. The A_{1g}, B_{1g}, B_{2g}, and E_g modes are Raman active only, and therefore a maximum of five Raman lines are expected for this ion. Five bands should be observed in the infrared, $2A_{2u}$, and $3E_u$. We assign the band at 380 cm^{-1} with a shoulder at 368 cm^{-1} to the $\nu_3(B_{2g})$ Sb-Cl, symmetric out-of-plane stretch and the band at 312 cm^{-1} is assigned to the $\nu_2(A_{1g})$ mode which corresponds to the $SbCl_4$ in-plane stretching mode. In $[SbCl_6^-]$, the $\nu_1(A_{1g})$ mode is at 330-340 cm^{-1}. The band at 529 cm^{-1} was assigned to the $\nu_1(A_{1g})$ Sb-F_{ax} symmetric stretch. The symmetric stretch in the $[SbF_6^-]$ anion is found at 660 cm^{-1}. Partial substitution of fluorine atoms by chlorine atoms tend to weaken the remaining Sb-F bonds, while the Sb-Cl bonds are strengthened when the chlorine atoms are substituted by fluorine atoms. This results in a lower frequency in the former and a higher frequency in the latter case. The bands at 172 cm^{-1} and 142 cm^{-1} were assigned to the $\nu_5(B_{1g})$ Sb-Cl_4 in-plane scissor motion. These assignments must be considered tentative in view of the fact that the material was not pure, and that much more work must be done on this system in order that the salt can be completely characterized.

Müeller et al.[50] suggested, from an infrared analysis of the product of SbF_5 and NaCl, that the resultant salt, $Na[SbCl_4F_2]$, had a

cis-configuration. However, in light of the fact that this material was consistently found to be a mixture in this work, and since the two strongest bands in their spectrum coincided with the infrared spectrum of the $[SbCl_6^-]$ anion, their interpretations are viewed with some reservation. The Raman spectrum of the product obtained from this same reaction in this work was not assigned since the Mössbauer spectrum consistently indicated that it was a mixture of chloride fluoride salts.

(iii) Attempted Preparation of the $[SbCl_5F^-]$, $[SbCl_3F_3^-]$, and $[SbClF_5^-]$ Anions

Attempts were made to prepare the alkali metal salts containing the anions, $[SbCl_5F^-]$, $[SbCl_3F_3^-]$, and $[SbClF_5^-]$, from stoichiometric mixtures of antimony pentachloride, an antimony(V) chloride fluoride, or antimony pentafluoride and the appropriate alkali metal chloride or fluoride. In every case, the resultant Mössbauer spectrum indicated that a mixture of anions were present, which were identified as $[SbCl_6^-]$ and $[SbCl_4F_2^-]$, or $[SbCl_2F_4^-]$. In some instances, however, the Raman spectrum was recorded to determine if the mixture contained the $[SbCl_6^-]$ and $[SbCl_4F_2^-]$ anions, since in these cases the Mössbauer spectrum of the mixture did not allow a positive identification to be made between these two salts.

CHAPTER SEVEN

ANTIMONY PENTAFLUORIDE AND ANTIMONY PENTACHLORIDE ADDUCTS: THEIR CHARACTERIZATION BY ^{121}Sb MÖSSBAUER SPECTROSCOPY

(A) INTRODUCTION

Layered compounds of graphite with antimony pentafluoride and antimony pentachloride have recently drawn some attention in the literature.[55,155-157] In each of these experiments, it was reported that the highly reactive liquids, SbF_5 and $SbCl_5$, did not interact with the graphite. For example, wide line n.m.r. experiments have shown that the graphite is best viewed as a solvent, which does not radically affect the chemistry of the intercalated molecules.[157] In view of these conclusions, this procedure appeared to be an excellent way to obtain the ^{121}Sb Mössbauer parameters of these very reactive materials. Mössbauer data for frozen liquid SbF_5 and $SbCl_5$ have previously been reported,[56,57] but only at 80°K with resultant low percentage absorption. It, therefore, seemed advisable to reinvestigate these compounds at 4°K. ^{121}Sb Mössbauer data are presented for SbF_5 and $SbCl_5$ as pure frozen liquids as well as intercalated in a graphite lattice.

Antimony pentafluoride, as a strong Lewis acid, forms a variety of SbF_5-X type adducts, where X represents a donor compound. In addition, SbF_5 has been shown to form a number of adducts with SbF_3. Ruff and Plato[158] were the first to report the preparation of these adducts, which they identified as $SbF_5 \cdot nSbF_3$ (n = 2,5 and possibly 3,4). The

Mössbauer and Raman data of two of these adducts in the solid state. $SbF_5 \cdot SbF_3$ (type A) and $SbF_5 \cdot SbF_3$ (type B), were reported by Birchall et al.[60] Recently, one of these forms (type B) was shown by X-ray crystallography,[61] to have the composition $5SbF_5 \cdot 6SbF_3$ or $Sb_{11}F_{43}$. Since this time, a third form was identified by Edwards and Slim[62] as $SbF_5 \cdot 2SbF_3$ and for clarity shall be termed (type C). Very recently, Gillespie et al.[63] reported the X-ray crystal structure of a 1:1 adduct of $SbF_5 \cdot SbF_3$ which they claim, from Raman data, to be identical to that previously labelled $SbF_5 \cdot SbF_3$ (type A). Hewitt et al.[159] obtained two adducts on fluorination of antimony metal in a flow system. They inferred, from the Raman data, that one was $Sb_{11}F_{43}$, and the other contained an $[Sb_2F_{11}^-]$ ion. Since none of the known structures contain $[Sb_2F_{11}^-]$ ions, the nature of this compounds remains uncertain and indeed may represent another $SbF_5 \cdot SbF_3$ adduct. ^{121}Sb Mössbauer spectra at 4°K are reported in this chapter on the 1:1 $SbF_5 \cdot SbF_3$ adduct reported by Gillespie et al.,[63] and the $SbF_5 \cdot SbF_3$ (type A) adduct.

AsF_3 forms a well-defined complex with antimony pentafluoride. This complex was first reported by Woolf and Greenwood.[59] The structure was determined by Edwards and Sills[58] and the Raman spectrum of this material was reported in a later paper by Gillespie et al.[60] $SbF_5 \cdot SO_2$ was first prepared in 1951 by Aynsley et al.[65] The crystal structure, reported in 1968 by Moore et al.,[66] showed that it was an O-donor complex. During the time the work was being done on this thesis, the Raman spectrum of $SbF_5 \cdot SO_2$ was reported by Byler and Shriver[160] and the Mössbauer spectrum was reported by Carter et al.[161] In this chapter we examine the ^{121}Sb Mössbauer spectra of each of these adducts.

Recently, a number of mixed Sb(III), Sb(V) anions have been prepared in conjunction with interchalcogen cations such as $[Te_2Se_2^{2+}]$, and $[Te_{3.3}Se_{0.7}^{2+}]$.[64] These mixed anions are formulated as $[Sb_3F_{14}^-]$. These compounds have also been shown to contain an $[SbF_6^-]$ anion. We report in this chapter the ^{121}Sb Mössbauer spectra of these anions.

(B) RESULTS AND DISCUSSION

(i) SbF_5 and $SbCl_5$

Both SbF_5 and $SbCl_5$ are intercalated rapidly into the graphite lattice.[55,155] The Mössbauer parameters of the resulting free flowing powders are listed in Table 7.1. Both powders gave spectra which showed two resonance absorptions. The stronger absorption is in the Sb(V) region of the spectrum while a much weaker absorption is present in the Sb(III) region, as is shown in the spectrum for the $SbCl_5$ case in Figure 7.1. Although the Sb(III) absorption was present in both of these intercalates, none was detected in the spectra of the pure compounds. Clearly, the pentahalides do not enter the lattice without some reaction occurring, contrary to what had been reported.[55,155] Lalancette and Lafontaine[55] found, by an elemental analysis of the intercalates, that the ratio of F:Sb was 5:1. From this, they assumed that there was no reaction of the SbF_5 with the graphite. Since we have established that there is reduction from Sb(V) to Sb(III), it seems reasonable to assume that C-halogen bond formation takes place on reaction of the SbF_5 or $SbCl_5$ with the graphite, thus preserving the 5:1 stoichiometry. A similar reduction-oxidation has been noted for arsenic pentafluoride intercalated into graphite.[162]

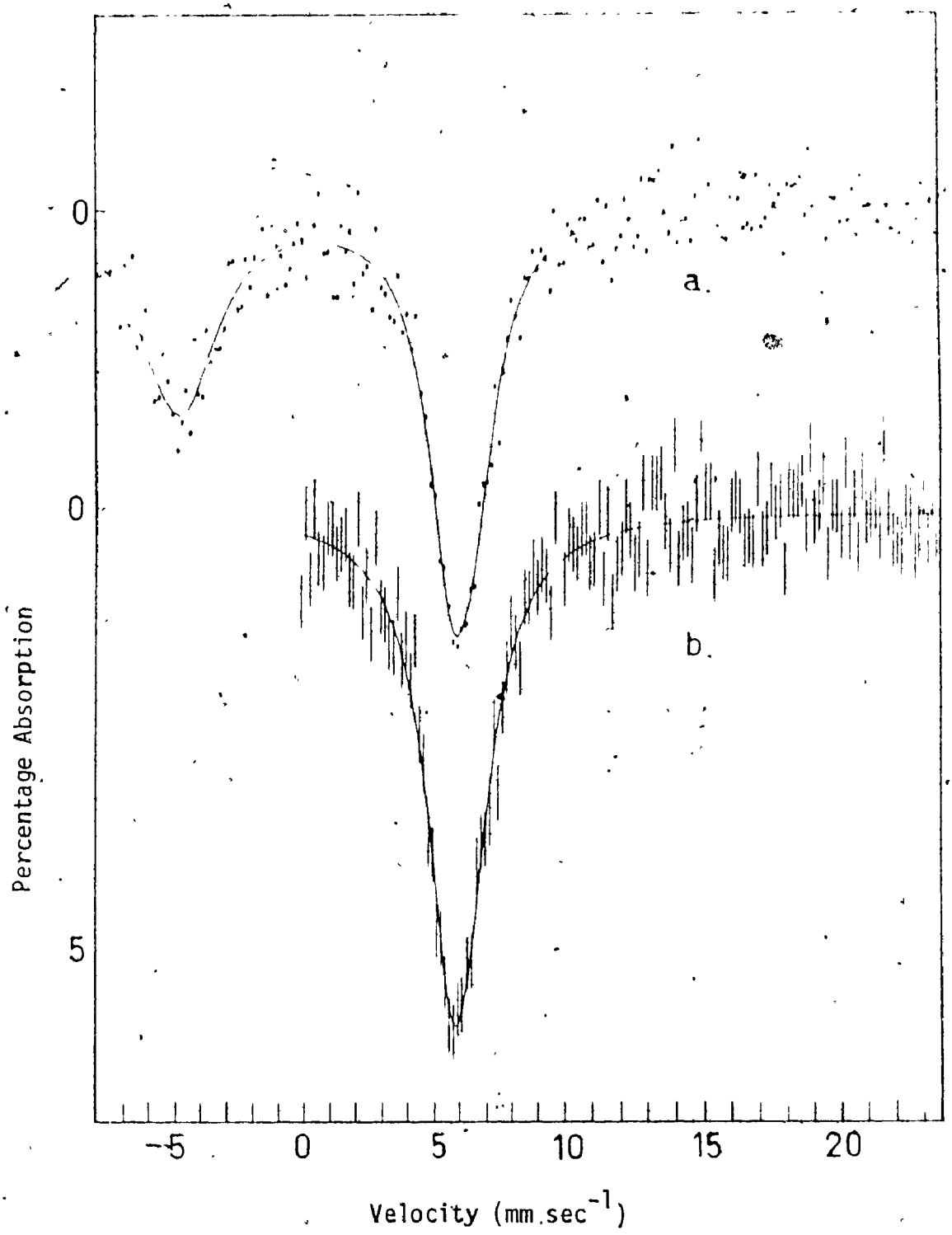

Figure 7.1. ^{121}Sb Mössbauer Spectrum at 4°K of $SbCl_5$ intercalated into graphite:

(a) Each Resonance Fitted to an Eight-Line Pattern

(b) Sb(V) Region only fitted to a Single Lorentzian.

Table 7.1 ^{121}Sb Mössbauer Parameters of SbF_5 and $SbCl_5$ at 4°K

Compound	Sample Preparation	δ/mm sec^{-1} ± 0.1	eQV_{ZZ}/ mm sec^{-1} ± 2.0	Γ/ mm/sec^{-1}	m	$(CHI)^2$/deg. of freedom	Type of Fit
SbF_5	intercalated into graphite	10.63 - 6.32	4.40 --	2.5 ---	0:03	1.03	eight-lines both Sb sites
		10.63	4.50	2.5	0.07	0.96	eight-lines Sb(V) site only
		10.48	--	2.9	--	0.98	one-line Sb(V) site only
	sublimed	10.26	8.74	2.2	0.72	1.05	eight-lines
		10.30	---	2.8	--	1.26	one-line
	Reference 57	10.79[a]	--	---	--	--	
SbF_3	sublimed	- 6.25	18.89	2.2	0.17	1.20	eight-lines
	Reference 57	- 6.04[a]	19.60	---	--	--	
$SbCl_5$	intercalated into graphite	5.90 - 5.02	- 5.02 --	2.2 ---	0.43	1.13	eight-lines both Sb sites
		5.92	- 3.90	2.3	0.80	1.25	eight-lines Sb(V) site only
		5.50	--	2.6	--	1.21	one-line Sb(V) site only
	sublimed	5.28	- 5.71	2.3	1.35	0.94	eight-lines
		5.20	--	2.4	--	1.06	one-line

Continued.....

Table 7.1 (Continued)

Compound	Sample Preparation	δ/mm sec^{-1} ± 0.1	eQV$_{ZZ}$/ mm/sec^{-1} ± 2.0	Γ/ mm/sec^{-1}	η	χ^2/deg. of freedom	Type of Fit
	Reference 57	5.44[a]	- 4.4	---	--	--	
$SbCl_3$	Reference 57	- 5.24[a]	12.20	---	--	--	

[a] Absorber temperature was 80°K.

The Mössbauer parameters obtained in this work for SbF_5 and $SbCl_5$ are similar to those previously reported (Table 7.1). Antimony pentafluoride gave a positive quadrupole coupling constant although, at first sight, the fitting to a single Lorentzian line was equally as good. However, according to the arguments developed in Chapter IV regarding line widths, the reduction in line width from the one-line Lorentzian fit to the eight-line fit confirms a finite quadrupole splitting. Such a splitting would be expected from a slightly distorted octahedral arrangement about the antimony. The structure and Mössbauer of SbF_5 were discussed in detail in Chapter V. This quadrupole coupling is evident in the spectra of both the intercalated and the frozen liquid SbF_5. Antimony pentachloride, whether intercalated or sublimed, consistently gave a small negative eQV_{ZZ} value no matter what the sign of the initial estimates for the computer fitting. The slight reduction in the line width, when the spectra are fitted to eight lines, is also observed in this case, confirming the presence of a finite eQV_{ZZ} value. This negative value is consistent with the trigonal bipyramidal structure reported by Ohlberg.[46] This rules out the possibility that $SbCl_5$ exists as $[SbCl_4^+]$-$[SbCl_6^-]$, at low temperatures, as discussed in Chapter V. The two halides, when intercalated, have slightly higher isomer shifts than when sublimed directly onto the Mössbauer probe. This suggests that the Lewis acids may be involved in a significant way with the C-X halogen. The weak absorptions in the Sb(III) regions of the spectra of the intercalated samples have isomer shifts which are close to those for SbF_3 and $SbCl_3$.[57] Unfortunately, the poor statistics of these resonances did not allow us

to abstract reliable quadrupole coupling data which would confirm these assignments.

The isomer shift for sublimed $SbCl_5$ agrees quite well with the literature value[57] at 80°K, but there is a significant difference between that found for SbF_5 in this work and that reported by Stevens and Bowen[57] at 80°K. Since the earlier workers gave no indication that the SbF_5 they used was distilled prior to sample preparation, and since the method of sample preparation was fairly crude, it is possible that their sample contained impurities (for example, antimony(V) oxyfluorides). Therefore, we believe that our lower value at 10.26 mm/sec is the correct isomer shift for pure SbF_5.

(ii) $SbF_5 \cdot X$ Adducts

Details of the ^{121}Sb Mössbauer spectra of the $SbF_5 \cdot SbF_3$ adducts are presented in Table 7.2 together with the data of some related SbF_5-X adducts. Each of the $SbF_5 \cdot SbF_3$ adducts have two antimony sites. As explained earlier, the Sb(III) site with a 5s electron pair would leave a relatively high s electron density at the antimony nucleus, whereas the Sb(V) site with no non-bonding electrons would have a much lower s electron density. Since the nuclear term, $\Delta R/R$, for the antimony nucleus is negative, the Sb(III) site will have a much lower isomer shift than the Sb(V) site. These sites are clearly shown for the 1:1 $SbF_5.SbF_3$ adduct in Figure 7.2. It is also worth noting that the stereochemically active lone pair in SbF_3 in each of these adducts gives rise to a large quadrupole coupling constant. The antimony(V) sites, however, have small quadrupole coupling constants.

Table 7.2. ^{121}Sb Mössbauer Parameters for $SbF_5 \cdot X$ Adducts and Related Anions at 4°K (X = SbF_3, AsF_3, etc.)

Compound	δ mm sec^{-1} ± 0.1	$eQV_{ZZ}/$ mm sec^{-1} ± 2.0	$\Gamma/$ mm sec^{-1}	η	T_a	m	$(CHI)^2$ deg. of freedom	References
SbF_5 SbF_3 (A)	10.96	2.09	3.1	-	--	0.29	1.42	
	- 8.23	19.98	3.3	-	--	-- [a]	-- [a]	
	11.3[b]	8.0	---	-	--	--	--	60
	- 8.3	18.2	---	-	--	--	--	
SbF_5 SbF_3 (B)	11.2[b]	5.4	---	-	--	--	--	60
	- 7.5	18.3	---	-	--	--	--	
$[SbF_4]_4$	11.03	4.57	3.0	-	--	0.05	1.07	
	- 7.85	14.12	3.9	-	--	-- [a]	-- [a]	
SbF_5 AsF_3	10.94	-- [c]	3.3	-	0.20	1.45	0.90	
SbF_5 SO_2	10.71	- 6.31	2.3	-	0.14	0.81	1.14	
	10.56[d]	--	---	-	--	--	--	161
$[Te_2Se_2][Sb_4F_{20}]$	11.04	-- [c]	3.0	-	--	0.41	1.09	
	- 6.53	15.2	3.8	-	--	-- [a]	-- [a]	
$[Te_{3.3}Se_{0.7}][Sb_4F_{20}]$	10.87	--	3.5	-	--	--	1.25	
	- 5.14	--	3.5	-	--	--	-- [a]	
	- 8.76	--	4.2	-	--	--	-- [a]	
$[Te_{3.3}Se_{0.7}][Sb_4F_{20}]$ eight-lines Sb(III) site only	- 7.25	18.94	3.0	0.99	--	--	1.51	

Continued.....

Table 7.2 (Continued)

[a] One value for "m" and "$(CHI)^2$/degree of freedom" calculated for each spectrum.

[b] Spectrum recorded at 80°K.

[c] Assumed close to zero since too small to calculate.

[d] Reported as +2.06 mm sec^{-1} from $Ba^{121}SnO_3$ (assumed δ InSb = -8.50 mm sec^{-1} relative to $Ba^{121}SnO_3$).

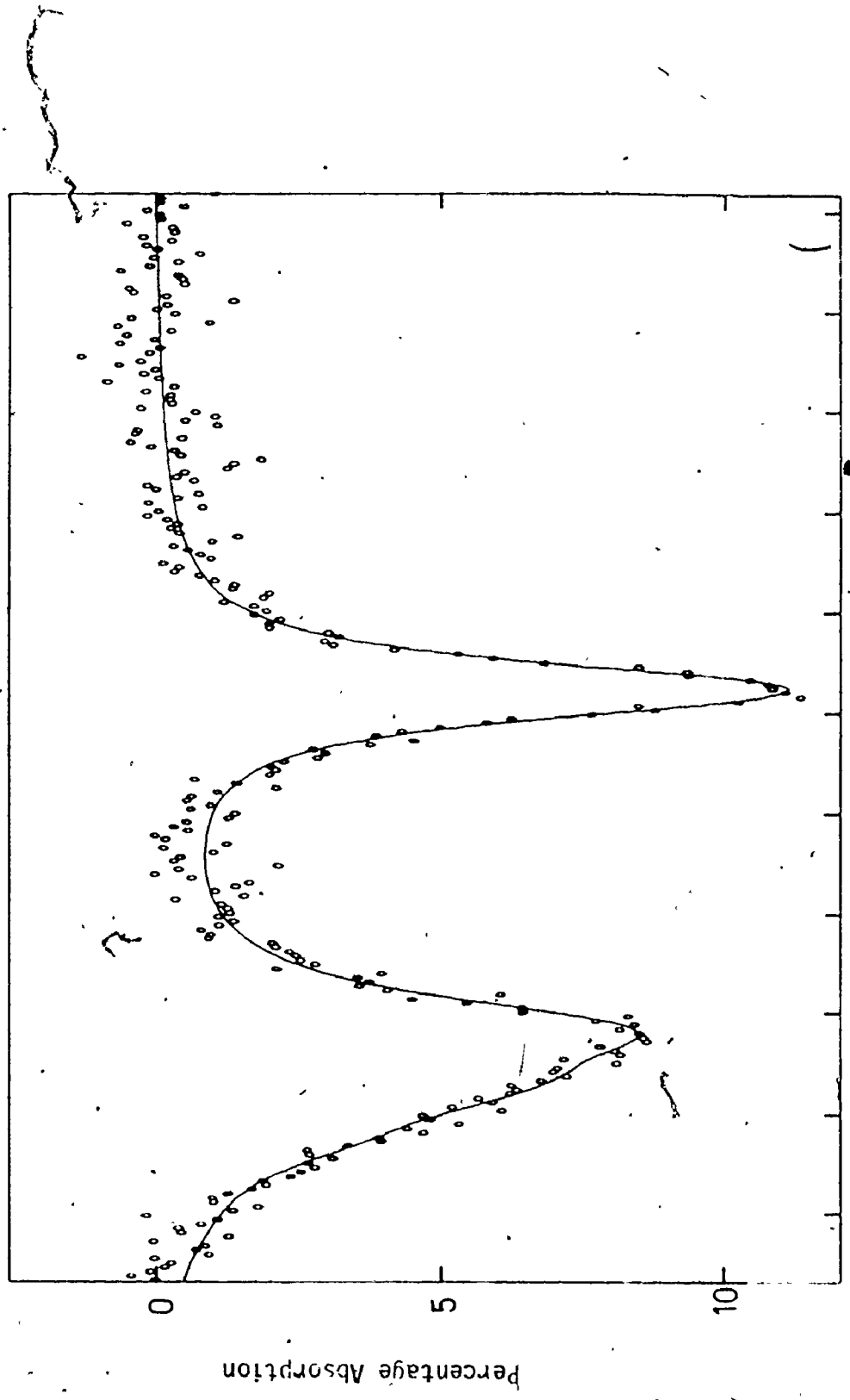

Figure 7.2 ^{121}Sb Mössbauer of $[Sb_2F_4^{2+}][SbF_6^-]_2$ at 4°K

The Mössbauer parameters for $SbF_5 \cdot SbF_3$ (type A) reported in this work at 4°K are similar to those reported earlier by Birchall et al.[60] for this same compound at 80°K. It may be worth noting, however, that the quadrupole coupling constant for $SbF_5 \cdot SbF_3$ (type A) (Table 7.2) is smaller than that previously reported.[60] These Mössbauer parameters have been discussed previously and will not be repeated here.

The Mössbauer parameters reported for the 1:1 $SbF_5 \cdot SbF_3$ adduct, $[Sb_2F_4^{2+}][SbF_6^-]$ are different from those reported for $SbF_5 \cdot SbF_3$ (type A). The isomer shift and quadrupole coupling constant of the Sb(V) site of both species are essentially identical, however, the parameters for the Sb(III) site are quite different. Although the Raman spectra of these two adducts were nearly the same,[61] this difference in the Mössbauer spectra indicates that the two adducts are probably not identical. This contradiction can probably only be resolved when an X-ray crystal structure is carried out on the (type A) adduct, i.e., the adduct prepared from SbF_3 and SbF_5 in liquid SO_2.[60]

The 1:1 $SbF_5 \cdot SbF_3$ ($[SbF_4]_4$) adduct has been shown by Gillespie et al.[61] to contain an $[Sb_2F_4^{2+}]$ cation and two slightly different $[SbF_6^-]$ octahedral anions. As indicated in Table 7.2, these two octahedral anions are not separately resolved in the Mössbauer spectrum, however, the presence of these two sites may account for the slight asymmetry which has been interpreted by the fitting procedure as a small positive quadrupole splitting. The $[Sb_2F_4^{2+}]$ cation consists of two Sb(III) sites as shown in Figure 7.3. The site depicted in Figure 7.3a has three shorter bonds, and with the lone pair, has pyramidal AX_3E coordination similar to that

Figure 7.3. The Two Antimony Sites of the $[Sb_2F_4^{2+}]$ Cation.

(a) Projection of the $[Sb(1)F_7]$ Unit down the c Axis.

(b) Projection of the $[Sb(2)F_6]$ Unit down the a Axis.

The Numbers on the Atoms are the Same as Those in Reference 63.

a.

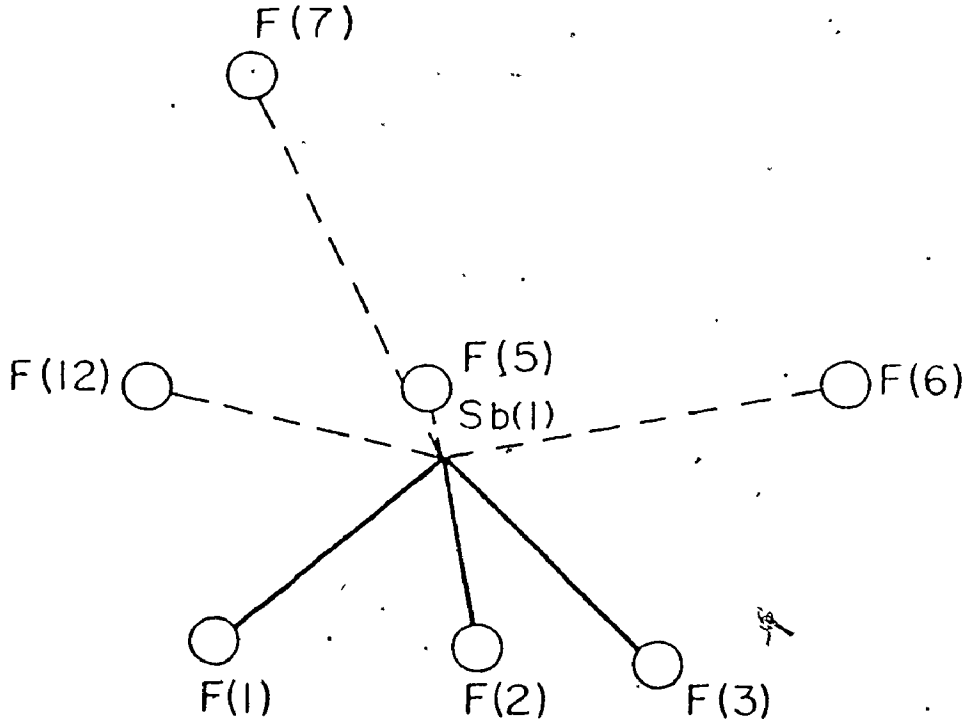

b.

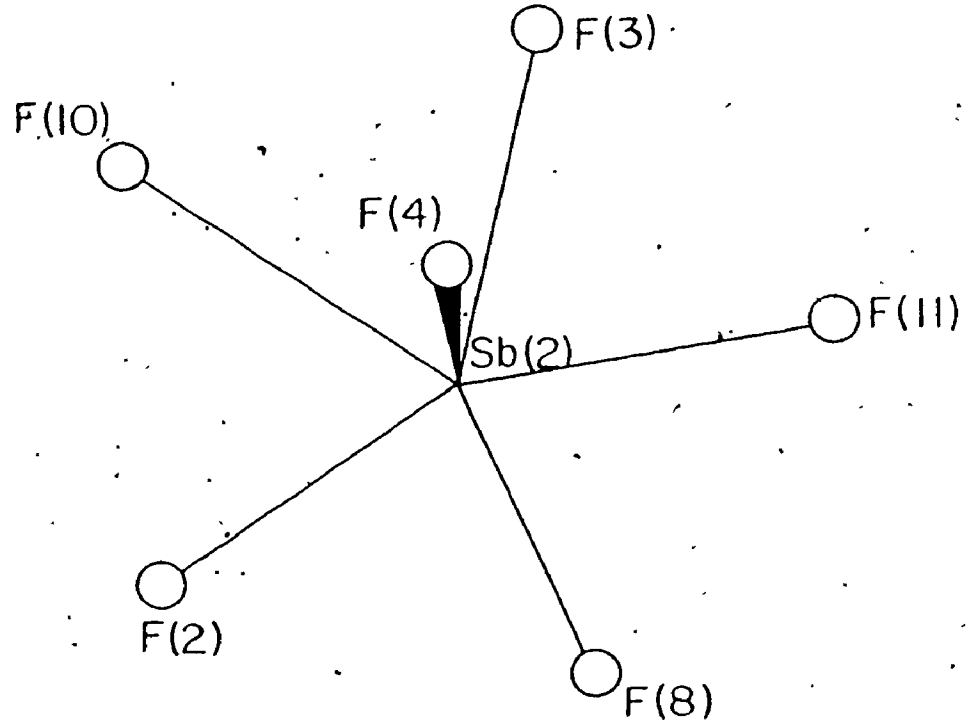

found in SbF_3.[18] The Sb(1)-F(1) bond length, 1.88 Å, is similar to that found in SbF_3, 1.90 Å, but the Sb(1)-F(2) and Sb(1)-F(3) bond lengths, 1.99 and 2.01 Å, respectively, are significantly longer due to bridging interactions. In addition to the short bonds to F(1), F(2), and F(3), four long contacts to neighbouring fluorines with bond lengths 2.54-2.87 Å are found. This site was regarded by Gillespie et al.[61] as having an AX_7E stereochemistry with the lone pair between the four long contacts. The Sb(1)F(1)F(2)F(3) group is linked by an angular asymmetric fluorine bridge to the Sb(2)F(4) group forming the $[Sb_2F_4^{2+}]$ cation. The Sb(2)-F(4) bond is similar to that found for Sb(1)-F(1). The second Sb(III) site, shown in Figure 7.3b, has, in addition to the short bond, five short contacts to neighbouring fluorines in the range of 2.10-2.42 Å. This site was regarded as having an AXY_5E stereochemistry in the form of a pentagonal bipyramid with a lone pair occupying one of the axial positions. The isomer shift of both of the Sb(III) sites of $[Sb_2F_4^{2+}][SbF_6^-]_2$ are more negative than that found for SbF_3 (Table 7.1). These lower values can be rationalized in terms of placing some positive charge on the Sb(III) sites, resulting in the contraction of the s orbitals, hence increasing the s electron density. This increase produces a shift to more negative values. In one of the sites of this cation, there are presumably three strong Sb(III)-F bonds and four weaker Sb(III)-F-Sb(V) bonds. In the second site, there is one strong Sb(III)-F bond and five weaker bridge bonds. Since the more weakly bound fluorines would be less effective at removing electron density that the stronger Sb(III)-F bonds, a more negative isomer shift would be expected for the latter site. However,

these two Sb(III) sites are not resolved in the Mössbauer spectrum (Figure 7.2). This suggests that the s electron density about each of these sites is comparable, in spite of the fact that the antimony nuclei have quite different environments. Since the broad asymmetric resonance at -7.85 mm/sec is the result of two Sb(III) sites with similar isomer shift values, the quadrupole coupling constant calculated for this peak cannot be realistically interpreted in terms of electric field gradients at the antimony sites.

The crystal structure of the $SbF_5 \cdot AsF_3$ adduct was reported by Edwards and Sills.[58] They showed that the antimony atom was coordinated by fluorine atoms in a distorted octahedron, with one bond slightly longer, 1.99 Å, than the others (mean 1.83 Å). The arsenic atom has two nearest fluorines at 1.64 Å, two intermediate neighbours at 2.01 and 2.39 Å, and two long contacts at 2.73 Å. Since the bridging fluorine atom of AsF_3 was associated more closely with the antimony than the arsenic, this structure was described as having some contribution from the ionic formulation $[AsF_2^+][SbF_6^-]$. The ^{121}Sb Mössbauer isomer shift is indeed consistent with this formulation. The isomer shift of the antimony(V) atom resembles that reported for the fluorine bridged octahedral anions of $[Sb_2F_4^{2+}][SbF_6^-]_2$. However, this small distortion in the octahedron observed by Edwards and Sills[58] for $SbF_5 \cdot AsF_3$ does not result in a measurable quadrupole coupling constant.

The structure of crystalline $SbF_5 \cdot SO_2$ was determined by Moore et al.[66] They found that five fluorine atoms and one oxygen atom of the SO_2 formed an octahedral arrangement which was elongated in the

direction of the F-Sb-O axis. All of the Sb-F bonds were essentially equal, 1.85 Å, and the Sb-O bond was 2.13 Å. The equatorial fluorines are bent toward the Sb-O bond, i.e., the Sb atom is displaced 0.14 Å from the plane made by the four equatorial fluorines toward the axial fluorine. The isomer shift value of the antimony site in this complex is slightly lower than those recorded for the analogous fluorine bridged adducts mentioned earlier. This suggests that the oxygen atom is less effective at removing s electron density than both the Sb(III)-F-Sb(V) or As(III)-F-Sb(V) bridging fluorines mentioned earlier, resulting in a higher s electron density at the Sb(V) site. The isomer shift value recorded in this work is slightly greater than that recorded by Carter et al.[161] The reason for this is not obvious.

$SbF_5 \cdot SO_2$ consistently gave a small negative quadrupole coupling constant regardless of the sign of the initial estimates for the computer fitting. A negative quadrupole splitting indicates a concentration of charge in the plane perpendicular to the principle axis. If the principle axis is through the F-Sb-O bonds, then the negative sign suggests a concentration of charge in the plane including the antimony and the four equatorial fluorines. Although the eQV_{ZZ} value is small, it may arise as a result of the distortions from O_h geometry observed by Moore et al.[66] Carter et al.[161] also reported that a small quadrupole coupling constant was present in the spectrum of $SbF_5 \cdot SO_2$. Although they reported the magnitude to be $\sim$ 5.3 mm/sec for the eQV_{ZZ} values for a number of compounds studied, including $SbF_5 \cdot SO_2$, they did not indicate the sign of this constant for $SbF_5 \cdot SO_2$.

(iii) $[Sb_3F_{14}^-]$ Anions

Each of the compounds $[Te_2Se_2][Sb_4F_{20}]$ and $[Te_{3.3}Se_{0.7}][Sb_4F_{20}]$ contain two anions namely $[Sb_3F_{14}^-]$, and $[SbF_6^-]$. The $[Sb_3F_{14}^-]$ ion consists of two $Sb(V)F_6$ octahedra linked by strong fluorine bridges to an $Sb(III)F_2$ group. The Sb(III) atom has been described by Gillespie et al.[64] as having the typical AX_4E environment. This site also forms four additional weak Sb-F bonds to other anions. The geometry of this unit is similar to the corresponding unit in $[AsF_2^+][SbF_6^-]$, where the lone pair occupies an equatorial position of a trigonal bipyramid and bridging fluorines occupy axial positions.

In $[Te_2Se_2][Sb_4F_{20}]$, the Sb(III) site of the $[Sb_3F_{14}^-]$ anion has two short bonds at 1.91 Å and two intermediate Sb-F bonds at 2.18 Å. This antimony atom also forms two long bonds with other fluorine atoms at 2.59 Å and two still longer ones at 2.94 and 3.07 Å, giving an overall eight coordination. In the case of $[Te_{3.3}Se_{0.7}][Sb_4F_{20}]$, the two short bonds are at 1.89 and 1.91 Å, the intermediate Sb-F bonds at 2.25 and 2.19 Å, and the two long bonds are at 2.63 and 2.77 Å. In addition, this antimony site forms two still longer bonds at 2.92 and 2.88 Å. In both of these cases, the antimony atom is surrounded by eight fluorines and the overall geometry can be described as a distorted monocapped square antiprism with the lone pair occupying the capped position.

In the $[Sb_3F_{14}^-]$ ion the bridging fluorine atoms were displaced towards the amtimony(V) atoms. Thus, $[Sb_3F_{14}^-]$ was approximately described as a $[SbF_2^+]$ ion bonded by fluorine bridges to two $[SbF_6^-]$ ions. In both compounds, these antimony(V) sites and that of the independent $[SbF_6^-]$ anion were slightly distorted from octahedral geometry. In $[Te_2Se_2][Sb_4F_{20}]$,

the mean Sb-F distance at these sites was 1.82 Å, whereas the analogous mean Sb-F distance in $[Te_{3.3}Se_{0.7}][Sb_4F_{20}]$ was 1.86 Å.

The ^{121}Sb Mössbauer spectra of these compounds each contain two resonances. In both cases, the resonance absorption at the more positive velocity is typical of Sb(V) in a six-coordinate environment, such as $[SbF_6^-]$. In both compounds, the resonance representing these sites appears to be symmetric. In the case of $[Te_2Se_2][Sb_4F_{20}]$, the quadrupole coupling constant of the Sb(V) site was found to be very close to zero using the eight line fit. The Sb(V) site in $[Te_{3.3}Se_{0.7}][Sb_4F_{20}]$ shown in Figure 7.4 was only fitted to a single line of Lorentzian shape. The slight distortion from octahedral geometry discovered by Gillespie et al.[64] for these anions are not obvious from the data reported here.

The other resonance absorption in each of these spectra occurs at negative velocities with respect to InSb. In the case of $[Te_2Se_2][Sb_4F_{20}]$, this resonance is broad and very asymmetric, which is typical of the very distorted environments found in adducts involving SbF_3. In previous cases, such as the $SbF_5 \cdot SbF_3$ adducts, this asymmetry is attributed to the influence of the stereochemically active 5s electron pair. The involvement of these electrons in the bonding scheme in this case is substantiated by the magnitude of the isomer shift. In the case of $[Te_{3.3}Se_{0.7}][Sb_4F_{20}]$, the Sb(III) resonance appears as a doublet as shown in Figure 7.4. This adduct was initially fitted to two peaks of Lorentzian shape, one at -5.14 mm/sec, and the other at -8.76 mm/sec. Such a fitting procedure would imply the presence of two antimony(III) sites with small or zero quadrupole coupling constants. Since this interpretation is not compatible

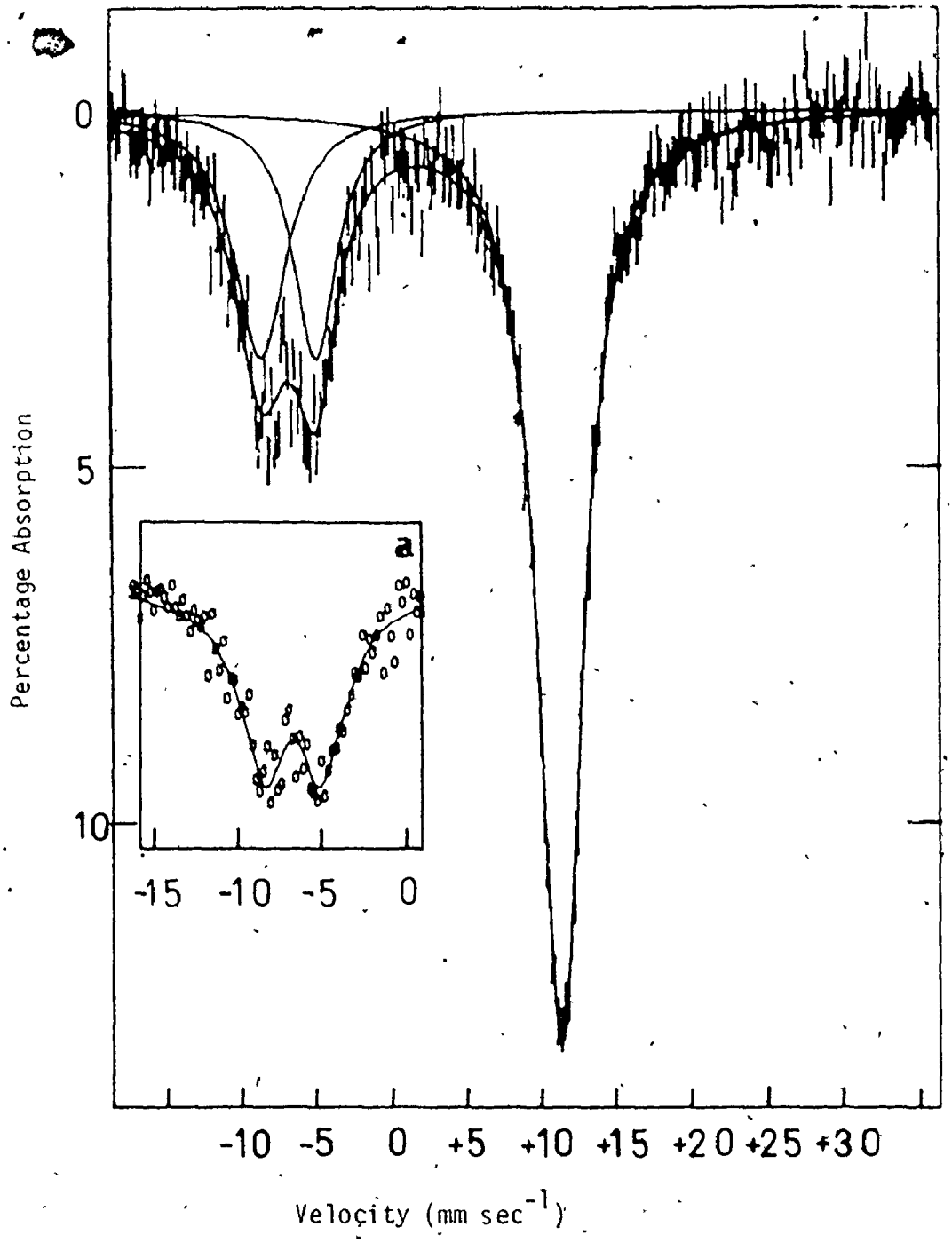

Figure 7.4. ^{121}Sb Mössbauer Spectrum of $[Te_{3.3}Se_{0.7}^{2+}][Sb_3F_{14}^-][SbF_6^-]$ Fitted to Three Lorentzians. (a = doublet fitted to eight-line pattern with asymmetry parameter > 0.)

with known Sb(III) fluorine environments, this portion of the spectrum was fitted using the transmission integral function and a variable value for the asymmetry parameter (η). Using this fitting procedure, the Sb(III) resonance was fitted to a single antimony site with a large quadrupole coupling constant, as observed for the other $[Sb_3F_{14}^-]$ ions as well as an η value near 1.0. This fit is shown in Figure 7.4a. The isomer shift value determined for this resonance is similar to that found for the Sb(III) site of $[Te_2Se_2^{2+}][Sb_4F_{20}]$. The large quadrupole coupling constant is consistent with an Sb(III) site with a stereochemically active lone pair as observed for SbF_3, other $SbF_5 \cdot SbF_3$ adducts, and the other $[Sb_3F_{14}^-]$ ion (Table 7.2). The large η value indicates that the Sb(III) site has considerable asymmetry about the principle axis. As described earlier, the principle axis, in the case of the Sb(III) site, is assumed to be through the stereochemically active lone pair. This conclusion appears to be consistent with the crystal structure of this compound, i.e., the immediate environment of the Sb(III) site appears to be more asymmetric than the analogous site in $[Te_2Se_2^{2+}][Sb_4F_{20}]$.

CHAPTER EIGHT

(A) SUMMARY

The antimony-121 Mössbauer parameters reported in this thesis for the complex anions derived from SbF_3 are consistent with the known stereochemistries of these anions. These data showed that in each case the 5s electrons are involved in the bonding scheme conformable with the presence of a stereochemically active lone pair. The predominant geometry of these anions is described as AX_6E, i.e., having a monocapped octahedral configuration (3.3.1). Previous investigators[99,106] had examined some of these antimony(III) fluoride anions and interpreted their data in terms of the antimony in these salts being six coordinate or lower, i.e., AX_5E or AX_4E.

The ^{121}Sb Mössbauer parameters reported here for some chloride, bromide, and iodide complexes of Sb(III) have been interpreted in terms of the 5s electron pair having no distorting effect on the antimony environment. In the majority of these cases, the ^{121}Sb Mössbauer data were consistent with an antimony atom surrounded by six ligands in a near octahedral configuration. The small quadrupole coupling constants found for some of these anions were interpreted in terms of either asymmetry in the bonds about the antimony nucleus, or lattice effects. Previous investigators[76,106] had interpreted the Mössbauer parameters of some of these complexes in terms of structures having AX_5E or AX_4E geometry. The results presented here are contrary to such an interpretation.

This thesis describes the first detailed study of the solid state

chemistry of the mixed antimony(V) chloride fluoride complexes. Prior to this work a number of these compounds had been suggested in the literature, but extensive spectroscopic evidence had only been reported for $SbCl_4F$.[41,97]

This work provides evidence for the existence of two structural types; a cis-fluorine bridged tetramer, and a cis-fluorine bridged trimer. X-ray crystallography has shown that $SbCl_3F_2$ is a cis-fluorine bridged tetramer similar to that reported earlier for $SbCl_4F$.[41] Each of the antimony sites of this tetramer has one additional fluorine per antimony replacing a terminal chlorine in the $SbCl_4F$ structure. The Sb-F bond is perpendicular to the plane of the tetramer or cis to the bridging fluorines. X-ray crystallography has also shown $Sb_3Cl_{10.75}F_{4.25}$ to be a cis-fluorine bridged trimer. This material in the solid state is a mixture of two trimers, namely $Sb_3Cl_{10}F_5$ and $Sb_3Cl_{11}F_4$. The former contains two sites similar to that found in $SbCl_4F$ and one similar to that of $SbCl_3F_2$, whereas, the latter contains one site resembling that found in $SbCl_4F$ and two resembling that of $SbCl_3F_2$. Preiss[44] recently reported that the structure of "$SbCl_2F_3$" was ionic, consisting of tetrahedral $[SbCl_4^+]$ cations and $[Sb_2Cl_2F_9^-]$ anions, with no interactions reported between the cation and the anion. The bond lengths and bond angles of this compound have been recalculated using Preiss' atomic coordinates and it is found that there are weak covalent interactions between these ions. Although these interactions are longer than the normal Sb-F covalent bonds, they are shorter than the sum of the van der Waals radii of antimony and fluorine. The tetrahedral $SbCl_4$ unit of this complex is preserved. However, four fluorines are observed about this antomony, one on each face

of the $[SbCl_4^+]$ tetrahedron. This antimony and the two antimony atoms of the $[Sb_2Cl_2F_9^-]$ unit are situated in the crystal such that a trimeric arrangement is formed similar to that observed for $Sb_3Cl_{10.75}F_{4.25}$. This same trimeric arrangement is implied for $[SbCl_4^+][Sb_2F_{11}^-]$. As the number of fluorines on the $Sb_2Cl_xF_{11-x}$ unit is decreased, the complex becomes less ionic as is evident from $Sb_3Cl_{10.75}F_{4.25}$.

The Mössbauer spectroscopic findings in this thesis were interpreted in terms of these structures. The Mössbauer data were consistent with the $SbCl_xF_{5-x}$ complexes containing two different antimony sites; one surrounded by six halogens in a pseudo-octahedral arrangement, observed in all of the complexes, and the other having tetrahedral geometry as observed for the $[SbCl_4^+]$ unit of $[SbCl_4^+][Sb_2Cl_2F_9^-]$ and $[SbCl_4^+][Sb_2F_{11}^-]$. It was discovered that the ^{121}Sb Mössbauer isomer shift parameters can be crudely related to the number of chlorines or fluorines about the pseudo-octahedral sites. This relationship proved valuable as an aid to elucidating structures. The trimeric structure alluded to earlier for $[SbCl_4^+][Sb_2F_{11}^-]$ was based upon a comparison of the Mössbauer data.

The vibrational spectra of these $SbCl_xF_{5-x}$ complexes have been studied by Raman spectroscopy. It has been demonstrated that the Raman spectra of the trimers and tetramers can be assigned by using the local symmetry approximation. In the case of $SbCl_3F_2$, the antimony site of the tetramer could be satisfactorily assigned as having C_s symmetry. The Raman spectrum of $Sb_3Cl_{10.75}F_{4.25}$ was assigned by comparison to those of $SbCl_3F_2$ and $SbCl_4F$, since the two trimers which were found in the solid contains antimony sites very similar to those observed in the tetramers. The $[SbCl_4^+]$ unit of $[SbCl_4^+][Sb_2Cl_2F_9^-]$ and $[SbCl_4^+][Sb_2F_{11}^-]$ were

satisfactorily assigned on the basis of T_d symmetry. Although the $[Sb_2Cl_2F_9^-]$ and $[Sb_2F_{11}^-]$ anions were distinguishable by Raman spectroscopy, their spectra were not assigned.

The mass spectroscopic data given in Table 5.8 for many of the $SbCl_xF_{5-x}$ complexes illustrated that the parent trimers and tetramers were not observed in the vapour phase. This data also showed that the fragments underwent rapid halogen exchange on the walls of the ionization chamber. Therefore, the spectra were generally representative of the relative abundances of atoms present rather than the fragmentation of the particular trimer or tetramer.

This thesis studied the reaction of $SbCl_4F$ with several Lewis acids. From the study of products of these reactions by Mössbauer and Raman spectroscopy, the nature of the reaction products were found to be dependent on the particular Lewis acid employed. In the case of AsF_5 and SbF_5, halogen exchange took place in solution resulting in the preparation of $[AsCl_4^+][SbF_6^-]$ and $[SbCl_4^+][Sb_2Cl_2F_9^-]$, respectively. However, when NbF_5 was reacted with $SbCl_4F$, a fluorine bridged $SbCl_4F{\cdot}NbF_5$ adduct was formed, which had little contribution from $[SbCl_4^+][NbF_6^-]$. As in the case of the $[SbCl_4^+]$ cation mentioned earlier, the Raman spectrum of the $[AsCl_4^+]$ cation of the $[AsCl_4^+][SbF_6^-]$ was assigned on the basis of T_d symmetry. The assignments of the latter adduct (Table 5.7) must be considered tentative since the final product was not completely characterized. From the data presented here, the $SbCl_4F{\cdot}(NbF_5)_2$ adduct could not be ruled out.

Prior to this work, very little spectroscopic evidence had been presented substantiating the existence of the $[SbCl_xF_{6-x}^-]$ anions of the

alkali metals. In this thesis, Mössbauer spectroscopy was used to identify both $[SbCl_4F_2^-]$ and $[SbCl_2F_4^-]$ anions. Although the latter chloride fluoride was not obtained pure, i.e., it was obtained as a mixture of chloride fluoride salts, it was identified from the isomer shift data. The Raman spectrum of $Na[SbCl_4F_2]$ was assigned on the basis of D_{4h} symmetry in contrast to the assignments made earlier by Müeller et al.[50] From the reactions studied in this thesis, the $[SbCl_4F_2^-]$ salt prepared earlier by Müeller et al.[50] was shown to be a mixture of alkali metal antimony(V) salts. Attempts to isolate the alkali metal salts of the $[SbCl_5F^-]$, $[SbCl_3F_3^-]$, and $[SbClF_5^-]$ were unsuccessful.

Previously, it had been reported that SbF_5 and $SbCl_5$ are intercalated into graphite unchanged[55,155] and it was suggested that this medium acted like a solvent which did not substantially affect the chemistry of the intercalated material. This medium was also thought to be an excellent means of examining the ^{121}Sb Mössbauer spectra of very easily hydrolysed compounds such as SbF_5 and $SbCl_5$. The Mössbauer data reported in this thesis showed that the SbF_5 and $SbCl_5$ do not enter the lattice without some reaction occurring, i.e., reduction to Sb(III). In addition, the Mössbauer isomer shift data were always slightly higher than those for the same material distilled onto the Mössbauer probe, indicating some interaction between the medium and the Lewis acid.

The Mössbauer parameters reported in this thesis for the $SbF_5 \cdot SbF_3$ adducts do not support the view that the complex formed from SbF_5 and SbF_3 in liquid SO_2, i.e., SbF_5-SbF_3 (type A),[60] was identical to the 1:1 SbF_5:SbF_3 adduct recently reported by Gillespie et al.[63] The Mössbauer spectra of $SbF_5 \cdot AsF_3$ and $SbF_5 \cdot SO_2$ were found to be consistent with the

known structures. However, the sign of the quadrupole coupling constant of the latter adduct was opposite to that previously reported.[161]

This thesis also includes the ^{121}Sb Mössbauer data for some recently reported compounds[64], which contain a mixed Sb(III)-Sb(V) anions, namely $[Te_2Se_2^{2+}][Sb_3F_{14}^-][SbF_6^-]$ and $[Te_{3.3}Se_{0.7}^{2+}][Sb_3F_{14}^-][SbF_6^-]$. The antimony(III) site of the latter compound was fitted with an η value of 0.99, whereas the same site in the former compound was fitted with a much smaller η value. These observations were consistent with the known crystal structures of the anions.

REFERENCES

1. A. Byström, S. Backlund and K. A. Wilhelmi, Ark. Kemi., 4, 175 (1951).
2. A. Byström, S. Backlund and K. A. Wilhelmi, Ark. Kemi., 6, 77 (1952).
3. A. Byström and K. A. Wilhelmi, Ark. Kemi., 3, 17 (1951a).
4. A. Byström and K. A. Wilhelmi, Ark. Kemi., 3, 373 (1951b).
5. A. Byström and K. A. Wilhelmi, Ark. Kemi., 3, 461 (1951c).
6. B. Ducourant, R. Fourcade, E. Philippot and G. Mascherpa, Rev. Chim. Min., 12, 553 (1975).
7. R. Fourcade, G. Mascherpa and E. Philippot, Acta. Cryst., B31, 2322 (1975).
8. S. H. Martin and R. R. Ryan, Inorg. Chem., 10, 1757 (1971).
9. R. R. Ryan, S. H. Mastin and H. C. Larson, Inorg. Chem., 10, 2793 (1971).
10. R. Fourcade, Ph.D. Thesis, Université des Sciences et Techniques du Languedoc, Montpellier, France (1975).
11. R. Fourcade, G. Mascherpa, E. Philippot and M. Maurin, Rev. Chim. Min., 11, 481 (1974).
12. R. R. Ryan and D. T. Cromer, Inorg. Chem., 11, 2322 (1972).
13. J. G. Ballard, T. Birchall and (in part) J. B. Milne and W. D. Moffett, Can. J. Chem., 52, 2375 (1974).
14. D. R. Schroader and R. A. Jacobson, Inorg. Chem., 12, 515 (1973).
15. B. Ducourant, R. Fourcade, B. Bonnet and G. Mascherpa, Rev. Chim. Min., Bull. Soc. Chim., 7-8, 1471 (1975).
16. E. A. Kravchenko, R. L. Davidovich, L. A. Zemnukhova and Y. A. Buslaev, Doklady Academii. Nauk. SSSR, 214, (3), 611 (1974).
17. B. Ducourant, R. Fourcade, G. Mascherpa and E. Philippot, Rev. Chim. Min., 12, 485 (1975).

18. A. J. Edwards, J. Chem. Soc. (A), 2757 (1970).

19. S. K. Porter and R. A. Jacobson, J. Chem. Soc. (A), 1356 (1970).

20. C. Y. Ahlijah and M. Goldstein, J. Chem. Soc. (A), 326 (1970).

21. R. K. Wismer and R. A. Jacobson, Inorg. Chem., 13, (7), 1678 (1974).

22. R. D. Whealy and R. L. Yeakley, J. Inorg. Nucl. Chem., 25, 365 (1963).

23. R. D. Whealy and J. B. Blackstock Jr., J. Inorg. Nucl. Chem., 26, 243 (1964).

24. T. Barrowcliffe, I. R. Beattie, P. Day and K. Livingston, J. Chem. Soc. (A), 1810 (1967).

25. S. K. Porter and R. A. Jacobson, J. Chem. Soc. (A), 1359 (1970).

26. C. R. Hubbard and R. A. Jacobson, Inorg. Chem., 11, (9), 2247 (1972).

27. W. Pflaum and R. A. Jacobson, in D. R. Schroader and R. A. Jacobson, Inorg. Chem., 12, 515 (1973).

28. R. J. Gillespie, "Molecular Geometry", Van Nostrand Reinhold, London (1972).

29. D. R. Schroader and R. A. Jacobson, Inorg. Chem., 12, 210 (1973).

30. S. L. Lawton and R. A. Jacobson, Inorg. Chem., 5, 743 (1966).

31. E. Edstrand, M. Inge and N. Ingri, Acta. Chem. Scand., 9, 122 (1955).

32. R. K. Wismer and R. A. Jacobson, Inorg. Chem., 13, 7, 1678 (1974).

33. S. K. Porter and R. A. Jacobson, J. Chem. Soc., Chem. Comm., 23, 1244 (1967).

34. F. Swartz, Bull. Acad. roy-Belgique [3], 29, 874 (1895).

35. O. Ruff, J. Zedzer, M. Knoch and H. Graf, Ber. Dtsch. Chem. Ges., 42, 4021 (1909).

36. A. L. Henne and P. Trott, J. Amer. Chem. Soc., 69, 1820 (1947).

37. L. Kolditz, Z. Anorg. Allg. Chem., 289, 128 (1957).

38. L. Kolditz and W. Lieth, Z. Anorg. Allg. Chem., 310, 237 (1961).

39. K. Dehnicke and J. Weidlein, Z. Anorg. Allg. Chem., 323, 267 (1963).

40. K. Dehnicke and J. Weidlein, Chem. Ber., 98, 1087 (1965).

41. H. Preiss, Z. Chem., 6, 350 (1966).

42. R. R. Holmes, Accounts Chem. Res., 5, 296 (1972).

43. E. L. Muetterties, W. Mahler, K. J. Packer and R. Schmutzler, Inorg. Chem., 3, 1298 (1964).

44. H. Preiss, Z. Anorg. Allg. Chem., 389, 254 (1972).

45. H. B. Miller, H. W. Baird, C. L. Bramlett and W. K. Templeton, J. Chem. Soc., Chem. Comm., 262 (1972).

46. S. M. Ohlberg, J. Amer. Soc., 81, 811 (1959).

47. R. W. G. Wyckoff, "Crystal Structures", Vol. 3, Interscience, New York, 324 (1965).

48. I. R. Beattie, T. R. Gibson, K. Livingston, V. Fawcett and G. A. Ozin, J. Chem. Soc. (A), 712 (1967).

49. G. Barnikow and W. Abraham, Z. Chem., 10, 194 (1970).

50. U. Müeller; K. Dehnicke and K. S. Vorres, J. Inorg. Nucl. Chem., 30, 1719 (1968).

51. L. Kolditz, D. Weisz and U. Calov, Z. Anorg. Allg. Chem., 316, 261 (1962).

52. A. J. Edwards and P. Taylor, J. Chem. Soc., Chem. Comm., 1376 (1971).

53. K. Olie, C. C. Smitskamp and H. Gerding, Inorg. Nucl. Chem. Lett., 4, 129 (1968).

54. R. F. Schneider and J. V. Dilorenzo, J. Chem. Phys., 47, 2343 (1967).

55. J. M. Lalancette and J. Lafontaine, J. Chem. Soc., Chem. Comm., 815 (1973).

56. V. S. Shpinel, V. A. Bryukhanov, V. Kothekar, B. Z. Iofa and S. I. Semenov, Farraday Soc. Symposia, 1, 69 (1967).

57. J. G. Stevens and L. H. Bowen, Möss. Effect. Method., Plenum Press, New York, 5, 27 (1970).

58. A. J. Edwards and R. J. C. Sills, J. Chem. Soc. (A), 942 (1971).

59. A. A. Woolf and N. N. Greenwood, J. Chem. Soc., 2201 (1950).

60. T. Birchall, P. A. W. Dean, B. Della Valle and R. J. Gillespie, Can. J. Chem., 51(5), 667 (1973).

61. A. J. Edwards and D. R. Slim, J. Chem. Soc., Chem. Comm., 178 (1974).

62. A. J. Edwards and D. R. Slim, private communication.

63. R. J. Gillespie, D. R. Slim and J. E. Vekris, J. Chem. Soc., in press.

64. P. Boldrini, I. D. Brown, R. J. Gillespie, D. R. Slim and E. Maharajh, private communication.

65. E. E. Aynsley, R. D. Peacock and P. L. Robinson, Chem. and Ind., 1117 (1951).

66. J. W. Moore, H. W. Baird and H. B. Miller, J. Amer. Chem. Soc., 90, 1358 (1968).

67. R. L. Mössbauer, Z. Physik, 151, 124 (1958).

68. F. R. Metzer, Prog. Nucl. Phys., 7, 54 (1959).

69. C. Kittel, "Introduction to Solid State Physics", Wiles, New York, Chapt. 5 and 6 (1956).

70. J. Petzold, Z. Physik, 163, 71 (1961).

71. W. M. Wisscher, Ann. Phys., 9, 194 (1960).

72. H. Frauenfelder, "The Mössbauer Effect", W. A. Benjamin, Inc., New York (1962).

73. T. C. Gibb, "Principles of Mössbauer Spectroscopy", Chapman and Hall, London, Chapt. 6 (1976).

74. N. N. Greenwood and T. C. Gibb, "Mössbauer Spectroscopy", Chapman and Hall, London (1971).

75. R. L. Collins and J. C. Travis, in "Mössbauer Effect Methodology", I. J. Gruverman, Ed., Plenum Press, New York, New York, 3 (1967).

76. J. D. Donaldson, M. J. Tricker and B. W. Dale, J. Chem. Soc. (Dalton), 893 (1972).

77. S. L. Ruby, G. M. Kalvius, G. B. Beard and R. E. Snyder, Phys. Rev., 159, 239 (1967).

78. J. G. Stevens and S. L. Ruby, Phys. Lett. (A), 32, 91 (1970).

79. J. R. Gabriel and S. L. Ruby, Nucl. Instr. Meth., 36, 23 (1964).

80. S. Margulies and J. R. Ehrman, Nucl. Instr. Meth., 12, 131 (1961).

81. V. I. Gol'danskii and E. F. Makarov in "Chemical Applications of Mössbauer Spectroscopy", V. I. Gol'danskii and R. H. Herber, Eds., Academic Press, New York, New York (1968).

82. S. L. Ruby and J. M. Hicks, Rev. Sci. Instr., 33, (1), 27 (1962).

83. G. K. Shenoy and J. M. Friedt, Nucl. Instr. Meth., 116, 573 (1974).

84. G. K. Shenoy and J. M. Friedt, Phys. Rev. Letts., 31, 419 (1973).

85. G. J. Schrobilgen, Ph.D. Thesis, McMaster (1973).

86. G. M. Bancroft, A. G. Maddock, W. H. Ong, R. H. Price and A. J. Stone, Appendix by A. J. Stone, J. Chem. Soc. (A), 1966 (1967).

87. G. K. Shenoy and B. D. Dunlap, Nucl. Instr. Methods, 71, 285 (1969).

88. A. Messiah, "Quantum Mechanics", Vol. II, J. O. Potter transl., John Wiley and Sons, Inc., New York, New York, p. 560 (1964).

89. J. G. Stevens and S. L. Ruby, Phys. Lett. (A), 32, 91 (1970).

90. L. H. Bowen, G. L. Heimback and B. D. Dunlap, J. Chem. Phys., 59, 1390 (1973).

91. T. E. Cranshaw, J. Phys. (E), 7, 1 (1974).

92. M. Celia Dibar Ure and P. A. Flinn, "Möss. Methodology", Vol. 7, Ed. I. J. Gruverman, Plenum Press, New York, New York, 247 (1971).

93. J. P. Krasznai, Ph.D. Thesis, McMaster (1975).

94. A. I. Vogel, "A Textbook of Quantitative Inorganic Analysis", Third Ed., Longman Group Ltd., London (1961).

95. Dr. F. Pascher/E. Pascher, "Mikroanalytiches Laboratorium", 5300 Buschstr. 54, West Germany.

96. R. C. Thompson, Ph.D. Thesis, McMaster (1962).

97. I. R. Beattie, K. M. S. Livingston, G. A. Ozin and D. J. Reynolds, J. Chem. Soc. (A), 958 (1969).

98. C. J. Adams and A. J. Downs, J. Chem. Soc. (A), 1534 (1971); L. E. Alexander and I. R. Beattie, J. Chem. Soc. (Dalton Trans.), 1745 (1972).

99. T. Birchall and B. Della Valle, Can. J. Chem., 49, (17), 2808 (1971).

100. H. Yamatera and K. Nakatsu, Bull. Chem. Soc. J., 27, 244 (1954).

101. W. H. Wheller, J. Amer. Sci., 46, 269 (1893).

102. D. Ras, S. N. Thaker, P. R. Rai, Proc. Indian Acad. Sci. Sect. A, 71, (1), 42 (1970).

103. J. P. Dévort and J. M. Friedt, Chem. Phys. Lett., 35, 423 (1975).

104. M. Merhain, B. Ducourant, R. Fourcade and G. Mascherpa, Bull. Soc. Chim., 5-6, 757 (1974).

105. N. Habibi, B. Ducourant, R. Fourcade and G. Mascherpa, Rev. Chim. Min., 11, 2320 (1974).

106. J. D. Donaldson, J. T. Southern and M. J. Tricker, J. Chem. Soc., Dalton, 2637 (1972).

107. J. D. Donaldson and B. J. Senior, J. Chem. Soc. (A), 1798 (1966).

108. S. L. Ruby, "Mössbauer Effect Methodology", Proc. of the Eight Symposium, Ed. I. J. Gruverman, 8, 263 (1973).

109. J. Lindquist and A. Niggli, J. Inorg. Nucl. Chem., 2, 345 (1956).

110. I. D. Brown, Can. J. Chem., 42, 2758 (1964).

111. T. Birchall, B. Della Valle, E. Martineau and J. B. Milne, J. Chem. Soc. (A), 1855 (1971).

112. T. B. Brill, P. E. Garrou and G. G. Long Jr., Inorg. Nucl. Chem., 33, 3285 (1964).

113. S. K. Porter and R. A. Jacobson, J. Chem. Soc. (A), 1356 (1970).

114. L. Pauling, "Nature of the Chemical Bond", 3rd Ed., Cornell University Press, Ithaca, New York (1960).

115. S. M. Swingle, a private communication quoted by P. W. Allen and L. E. Sutton, Acta. Cryst., 3, 46 (1950).

116. S. L. Lawton, R. A. Jacobson and F. S. Frye, Inorg. Chem., 10, 701 (1971).

117. R. A. Davies, U.S. 3,240,826, March 15 (1966).

118. Md. O. Ali, M, F. A. Dove, Fluorine Conference Durham (1971).

119. M. F. A. Dove and Md. O. Ali, J. Inorg. Nucl. Chem. (Supplement 1976), Pergamon Press, Great Britain (1977).

120. J. Weidlein and K. Dehnicke, Z. Anorg. Allg. Chem., 337, 113 (1965).

121. J. G. Ballard, T. Birchall and D. R. Slim, Can. J. Chem., 55(5), 743 (1977).

122. A. J. Edwards and G. R. Jones, private communication.

123. W. Hasse, Acta. Cryst., B30, 2465 (1974).

124. International Tables for X-Ray Crystallography, Vol. 1, Kynoch Press, Birmingham, U.K. (1962).

125. J. G. Ballard, T. Birchall and D. R. Slim, J. Chem. Soc., Chem. Comm., 653 (1976).

126. A. J. Edwards and R. J. C. Sills, J. Chem. Soc., Dalton Trans., 1726 (1974).

127. A. J. Edwards and R. J. C. Sills, J. Chem. Soc. (A), 2697 (1970).

128. A. J. Edwards and P. Taylor, Chem. Comm., 1376 (1971).

129. H. Preiss, Z. Anorg. Allg. Chem., 346, 272 (1966).

130. H. Preiss, Z. Anorg. Allg. Chem., 362, 13 (1968).

131. F. A. Cotton and G. Wilkinson, "Advanced Inorganic Chemistry", Interscience Publ., Third Edition (1972).

132. W. Bues, F. Derneray and W. Brocker, Spectrochim. Acta., 30A, 1709 (1974).

133. R. F. Schneider and J. V. Dilorenzo, J. Chem. Phys., 47, 2343 (1967).

134. G. K. Shenoy, J. M. Friedt, H. Maletta and S. L. Ruby, "Mössbauer Effect Methodology", 9, 277 (1974).

135. A. J. Edwards and G. R. Jones, J. Chem. Soc. (A), 1467 (1969).

136. A. J. Edwards and G. R. Jones, J. Chem. Soc. (A), 1891 (1970).

137. A. J. Edwards, J. Chem. Soc. (A), 2325 (1972).

138. A. J. Edwards, J. Chem. Soc. (A), 3714 (1964).

139. G. L. Carlson, Spectrochemica Acta., 19, 1291 (1963).

140. P. Reich and H. Preiss, Z. Chem., 7(3), 115 (1967).

141. J. Weidlein and K. Dehnicke, Z. Anorg. Allg. Chem., 337, 113 (1965).

142. R. J. Gillespie and B. Landa, Inorg. Chem., 12, 1383 (1973).

143. B. Landa, Ph.D. Thesis, McMaster University (1974).

144. J. M. Miller, Brock University, private communication.

145. M. J. Vasile and N. E. Falconer, Inorg. Chem., 11(9), 2282 (1972).

146. E. W. Lawless, Inorg. Chem., 10(9), 2084 (1971).

147. A. M. Qureshi and F. Aubke, Can. J. Chem., 48, 3117 (1970).

148. M. Burgard and J. MacCordick, Inorg. Nucl. Chem. Lett., 6, 599 (1970).

149. F. J. Brinkman, Inorg. Nucl. Chem. Lett., 6, 453 (1970).

150. G. Rockstroh, F. Wolf and G. Schwachader, Z. Chem., 10, 11 (1970).

151. H. McBee and H. Hass, 2nd. Engng. Chem., 39, 384 (1947).

152. H. Bode and E. Voss, Z. Anorg. Chem., 264, 144 (1951).

153. C. A. Clausen and M. L. Good, Inorg. Chem., 9(4), 817 (1970).

154. R. V. Parish and C. E. Johnson, J. Chem. Soc. (A), 1906 (1971).

155. J. Mélin and A. Hérold, C. R. Acad. Sci. Paris, Series C, 269, 877 (1969).

156. J. Mélin and A. Hérold, C. R. Acad. Sci. Paris, Series C, 280, 641 (1975).

157. L. B. Ebert, R. A. Huggins and J. I. Braumann, J. Chem. Soc., Chem. Comm., 924 (1974).

158. O. Ruff and Plato, Ber., 37, 674 (1904).

159. A. J. Hewitt, J. H. Holloway and B. Frlec, J. Fluorine Chem., 5, 169 (1975).

160. D. M. Byler and D. F. Shriver, Inorg. Chem., 15(1), 32 (1976).

161. H. A. Carter, J. N. Ruddick, J. R. Sams and F. Aubke, Inorg. Nucl. Chem. Lett., 11, 29 (1975).

162. L. Chun-Hsu, H. Selig, M. Rabinovitz, I. Agranat and S. Sarig, Inorg. Nucl. Chem. Lett., 11, 9 (1975).